Missouri S&T Library and Learning Resources

Scholars' Mine

Doctoral Dissertations | Student Theses and Dissertations

1970

Voids in neutron irradiated aluminum

Nicholas H. Packan

Follow this and additional works at: https://scholarsmine.mst.edu/doctoral_dissertations

 Part of the Metallurgy Commons

Department: Materials Science and Engineering

Recommended Citation

Packan, Nicholas H., "Voids in neutron irradiated aluminum" (1970). *Doctoral Dissertations*. 2069.
https://scholarsmine.mst.edu/doctoral_dissertations/2069

This thesis is brought to you by Scholars' Mine, a service of the Missouri S&T Library and Learning Resources. This work is protected by U. S. Copyright Law. Unauthorized use including reproduction for redistribution requires the permission of the copyright holder. For more information, please contact scholarsmine@mst.edu.

VOIDS IN NEUTRON IRRADIATED ALUMINUM

by

NICOLAS HAYES PACKAN, 1942-

A DISSERTATION

Presented to the Faculty of the Graduate School of the

UNIVERSITY OF MISSOURI - ROLLA

In Partial Fulfillment of the Requirements for the Degree

DOCTOR OF PHILOSOPHY

in in

METALLURGICAL ENGINEERING

1970

Albert E. Bolon
Advisor

H. L. Leighly Jr

William A. Frad

Robert Gesson

R. E. Moore

PLEASE NOTE:

Some pages have small
and indistinct type.
Filmed as received.

University Microfilms

ABSTRACT

Void formation in high purity aluminum resulting from irradiation to fluences between 1.5×10^{19} and 1.6×10^{22} neutrons/cm^2 ($E > 0.1$ MeV) at a temperature of 55 ± 5°C was studied, primarily by means of transmission electron microscopy. In particular the effects of neutron fluence and flux were examined, as well as the possible influences of both preexisting and transmutation-produced impurities.

A very low concentration of voids (about 10^{12}/cm^3) resulted from irradiation to 1.5×10^{19} neutrons/cm^2; they averaged about 150 Å in diameter. Void concentrations and sizes increased with fluence, reaching values of 6×10^{14} voids/cm^3 averaging 500 Å in diameter at 1.6×10^{22} neutrons/cm^2. Void formation initially was nonuniform in distribution, but tended to be homogeneous at higher fluences. The void shapes were always consistent with those of octahedra bounded by {111} planes, sometimes with the vertices truncated by {100} planes.

Void size distribution curves were obtained for all fluences, and from these the mean void size was found to increase in proportion to the fluence raised to the one-sixth power.

The void concentration displayed a fluence dependence best described by a power law, $N \sim (\phi t)^a$, in which the exponent decreased from 2 at 1.5×10^{19} neutrons/cm^2 ($E > 0.1$ MeV) down to only 0.1 at 1.6×10^{22} neutrons/cm^2. Treating the swelling with a similar power law, $\Delta V/V \sim (\phi t)^b$, a similar saturation effect was observed, with the fluence exponent b decreasing roughly from 2.5 to 0.5 over the range of fluence studied.

At 1.6×10^{22} neutrons/cm^2 the total void volume or swelling amounted to 7.4%.

Microhardness increases in the irradiated specimens can be explained on the basis of void contributions to the impeding of dislocation motions.

Irradiation at a factor-of-ten lower flux produced effects upon the void morphology (e.g., half as many but larger and more elongated voids) much like those resulting from irradiation at a higher temperature. In each case, the lowering of the vacancy supersaturation during irradiation is a consequence.

Irradiation, annealing to remove damage, and reirradiation of a specimen, each exposure to a fluence of 5×10^{20} neutrons/cm^2 ($E > 0.1$ MeV), yielded twice as many voids of smaller maximum size, having the same total void volume as those produced by the first irradiation alone. The effect is attributed to submicroscopic remnants of the original voids surviving the anneal and serving as preexisting nuclei in the second irradiation.

In postirradiation void annealing experiments performed inside a high vacuum electron microscope, the rate at which void radius changed, dr/dt, varied considerably from void to void. A transient effect in dr/dt was observed upon abrupt changes in the annealing temperature. Both effects are ascribed to the actions of local vacancy sinks near the voids, such as a suggested population of submicroscopic gas bubbles.

The experimental observations are compared with the current models for void formation. The two models most consistent with the experimental evidence both involve transmutation-produced helium playing a crucial

role in void nucleation--one involving helium-stabilized spikes and the other small helium bubbles as the nuclei of voids. Throughout this work effects were found which demonstrate a strong influence of impurities upon void formation in high purity aluminum.

ACKNOWLEDGMENTS

The author would like to express his sincere appreciation to his advisor, Dr. A. E. Bolon, for initially introducing him to the radiation damage field and subsequently for his professional guidance and sustained encouragement during the course of this work.

This research was carried out in the Metals and Ceramics Division of the Oak Ridge National Laboratory, operated by the Union Carbide Corporation for the U. S. Atomic Energy Commission. The author is grateful for the opportunity to perform this investigation at the Laboratory, where the necessary expertise and facilities were available. Special appreciation is expressed to Dr. J. H. Frye, Jr., Division Director, and to the many members of the Metals and Ceramics Division who have made this experience a pleasant and rewarding one.

In particular, gratitude is expressed to J. R. Weir, Jr., Dr. H. E. McCoy, Jr., Dr. R. T. King, J. O. Stiegler, Dr. K. Farrell, Dr. F. W. Wiffen, and Dr. E. E. Bloom for their many helpful discussions, suggestions, and continued support. The author gratefully acknowledges the assistance given in various phases of the experimental work by E. Bolling, J. T. Houston, C. Jones, C. E. Zachary, C. K. H. DuBose, B. L. Corbett, A. F. Zulliger, W. T. Mullins, A. A. Walls, and E. L. Long, Jr. Gratitude is extended to Dr. D. L. Kinosz of the Alcoa Research Laboratories and to J. R. Sites, Dr. J. E. Bigelow, and Dr. J. P. Moore of the Oak Ridge National Laboratory for performing various analyses to characterize the purity of the specimen material. The *in situ* void annealing experiments were carried out in collaboration with, and using the apparatus of,

D. N. Braski of the Isotopes Division, Oak Ridge National Laboratory, to whom thanks are due. Typing assistancy by the author's wife, Karen, is very greatly appreciated.

During the period of this research, the author held a National Science Foundation Graduate Traineeship, except for the summers 1968-70 when he was employed by the Oak Ridge National Laboratory as a summer Research Associate. The financial assistance provided by the Traineeship and the employment is gratefully acknowledged.

Finally, the author would like to express his deepest thanks to his stepfather and mother, Dr. Paul E. Thompson and Mrs. Charlotte H. Thompson, and especially to his wife, Karen, for their understanding and patience during the past five years of graduate work.

TABLE OF CONTENTS

	Page
ABSTRACT	ii
ACKNOWLEDGMENTS	v
LIST OF ILLUSTRATIONS	ix
LIST OF TABLES	xii
I. INTRODUCTION	1
II. REVIEW OF THE LITERATURE	5
A. Early Observations of Radiation Damage in Aluminum	5
B. Voids in Neutron-Irradiated Metals	8
C. Proposed Mechanisms for Void Formation	27
III. EXPERIMENTAL DETAILS	37
A. Material Characterization	37
B. Irradiation Procedures	41
C. Electron Microscopy	47
D. Obtaining Void Size Distributions	52
E. Immersion Density Measurements	53
F. Unirradiated Control Specimens	54
G. Microhardness Testing	54
H. Electron Microscope In Situ Void Annealing	55
I. Flux-Effect Experiments in the ORR	57
J. Experimental Errors	61
IV. RESULTS	63
A. Fluence Effects	63
B. Flux Effects	76
C. Reirradiation Experiment	79

Page

D. Impurity Influences 84

E. Void Annealing Studies 89

V. DISCUSSION 98

A. Discussion of the Observations 98

1. Effects of Neutron Fluence 98

2. Effects of Neutron Flux 113

3. Reirradiation and Degassed Aluminum Experiments 115

4. Void Annealing Studies 117

B. Evaluation of Proposed Void Nucleation and Growth Models 120

1. Nucleation Models 120

2. Growth Models 124

3. Swelling Models 125

4. Preferred Models for High Purity Aluminum . . . 126

VI. CONCLUSIONS 127

VII. APPENDICES 131

A. Determination of Fast Neutron Flux and Fluence Values 132

B. Establishment of the Void Morphology by Transmission Electron Microscopy and Electron Diffraction Techniques 134

VIII. LIST OF REFERENCES 139

IX. VITA 147

LIST OF ILLUSTRATIONS

Figures Page

1. Schematic of High Flux Isotope Reactor core 42
2. Views of a HFIR hydraulic tube capsule and specimen rods . . 43
3. Lower portion of specimen holder used in void annealing studies 56
4. Examples of voids produced over the range of fluence studied 64
5. Possible void-pairs after irradiation to 10^{19} neutrons/cm^2 . 66
6. Differing views of an octahedral void bounded by {111} planes 68
7. Example of a void size distribution histogram 70
8. Void size distribution curves for all except the lowest fluence 72
9. Void size distribution curves for the lower three fluences . 73
10. Dislocation loops and segments after irradiation to 10^{21} neutrons/cm^2 75
11. Voids resulting from irradiation at a temperature of $\approx$ 100°C 78
12. Voids resulting from irradiation to 10^{20} neutrons/cm^2 at (a) high flux and (b) low flux 80
13. Void size distributions for the high and low flux irradiations 81
14. Voids resulting from (a) original irradiation and (b) reirradiation (striations visible are polishing effects on the foil surface) 82

Figures Page

15. Void size distributions for original irradiation and reirradiation 83

16. Size distributions of voids produced by irradiation in as-received and degassed high purity aluminum 88

17. Sequence of micrographs depicting void annealing at 150°C . 90

18. Examples of void annealing curves, including all data points 91

19. Voids and "pits" after a 3-hr anneal at 150°C 92

20. Annealing curves for 16 voids in the specimen material irradiated to 3 x 10^{20} neutrons/cm^2 (E > 0.82 MeV) 93

21. Void annealing behavior upon raising the temperature from 150° to 170°C in the middle of the run 95

22. Void annealing behavior upon dropping the temperature in midrun from 150° to 100°C 96

23. Void size distributions in type 304 stainless steel irradiated at (a) 370-380°C and (b) 460-470°C 99

24. Fluence dependence of the maximum and the mean void sizes in high purity aluminum 101

25. Fluence dependence of the maximum void size in type 304 stainless steel 102

26. Void concentration as a function of neutron fluence in high purity aluminum 103

27. Void concentration as a function of neutron fluence in type 304 stainless steel 105

28. Variation of the total void volume with fluence in high purity aluminum 107

Figures Page

29. Density decrease (void volume) versus neutron fluence for type 304 stainless steel 109

30. Density decrease versus fluence for high purity aluminum (this study) and for two aluminum alloys (reference 100) . 111

31. Hardness increase ΔH versus $(Nd)^{1/2}$, with N the void concentration and d the average void diameter 114

32. Octahedral voids in irradiated high purity aluminum 135

33. Indexed selected area diffraction pattern corresponding to the region shown in Figure 32 136

LIST OF TABLES

Tables		Page
I.	Characteristics of Voids in Irradiated Metals	13
II.	Current Void Models	36
III.	Solid Impurities Found in As-Received Cominco Grade 69 Aluminum	38
IV.	Resistivity Ratios of As-Received Cominco Grade 69 Aluminum	39
V.	Hydrogen Content of As-Received Cominco Grade 69 Aluminum	39
VI.	Details of the Irradiations	46
VII.	Comparison of the HFIR and the ORR Neutron Spectra	60
VIII.	Collected Statistics on the Observed Void Populations	65
IX.	Variation of the Microhardness with Fluence	77
X.	Calculated Concentrations of Transmutation-Produced Impurities	86
XI.	Comparison of Irradiation-Produced Voids in As-Received Versus Degassed Cominco Grade 69 Aluminum (Lot 5719)	87

I. INTRODUCTION

A major research effort is proceeding in the United States, Great Britain, Germany, France, the Soviet Union, and several other nations directed toward development of a breeder reactor within this decade. Nuclear reactions in such a reactor will convert fertile into fissile nuclides (e.g., U^{238} into Pu^{239}) while in the process consuming some of the fissile nuclides thus formed. The reactor will therefore incur small, or even negative, fuel costs (i.e., produce more nuclear fuel than it consumes) and also conserve the world's limited supply of naturally fissile nuclear material.

The several distinct types of breeder reactors under development differ in their method of cooling (liquid metals, molten salts, or gases) but all currently share one vital problem--the potential of severe irradiation damage to core components which are exposed to the very high density of fast neutrons. Several high flux reactors are already being employed to study this problem of irradiation damage, among them the Experimental Breeder Reactor-II (EBR-II) in the U.S., the Dounreay Fast Reactor (DFR) in Great Britain, the Rhapsodie reactor of France, and the High Flux Isotope Reactor (HFIR) of Oak Ridge National Laboratory (ORNL), U.S.A. The first three reactors are constructed chiefly of stainless steel, which is the major candidate for use in Liquid Metal Fast Breeder Reactors (LMFBR's), while the water-cooled HFIR is made of aluminum.

Components of these reactors have already exhibited deleterious irradiation-induced effects, including significant amounts of swelling

and sharp reductions in ductility. One of the underlying causes of these effects has been found to be the presence of large numbers of voids in the microstructure. These features may act to harden the metal and their collective volume corresponds to the observed swelling. The voids, only visible in the electron microscope, were first found by Cawthorne and Fulton[1] in cladding from the DFR reactor. Shortly thereafter, cladding on several "target rods" in the HFIR reactor split open, releasing actinide elements into the cooling water and causing a shutdown of the reactor. Examination[2] of irradiated HFIR components also revealed voids, on the order of several hundred Angstrom units in diameter and over $10^{15}/cm^3$ in concentration. A program at ORNL was initiated to investigate void formation and other irradiation effects in aluminum. This study is a part of that program.

At the time this work was begun, it was clear that void formation in a number of metals was strongly dependent upon both the irradiation temperature and the fast neutron fluence. An investigation in nickel[3] has since examined the influence of the irradiation temperature, but no controlled study of voids in any metal had been reported concerning the effect of fast neutron fluence (keeping the temperature constant). Such a study was undertaken to examine voids produced at a number of fluences in 99.9999% (6-9's) aluminum. This material was chosen for several reasons. Previous studies[4,5] had revealed that void formation (visible in the electron microscope) commences sooner in high purity metals than in alloys; thus a more complete inspection of void formation could be accomplished within reasonable irradiation times. It was also felt

that the results obtained in studying a high purity material might be more readily interpreted and perhaps possess broader implications than any that might develop from using a particular alloy. Another advantage in the selection of high purity aluminum came to light during post-irradiation handling and sample preparation, when the high purity material was found to be considerably less radioactive than any aluminum alloys or impure aluminum exposed to comparable fluences.

In the published literature on irradiation-produced voids in metals, a number of terms have been used with varying meanings. For the purposes of this study, they will be considered to signify the following. A void is a three-dimensional vacancy cluster, which may contain some gas, but at a pressure significantly less than that which would be required to balance the surface tension. Although it may resemble a void, a bubble contains gas such that the internal pressure does approximately balance the surface tension (as expressed by the relation $p = 2\gamma/r$, where γ is the surface tension and r is the bubble radius). The words cavity and pore will be considered general terms including both voids and bubbles and making no distinction between them. The term loop will be used sometimes, for brevity, to refer to the dislocation loop, either vacancy or interstitial in character and usually perfect (unfaulted) in aluminum. It is another kind of defect cluster resulting from irradiation.

The words flux and fluence will be employed very frequently. Unless otherwise indicated, the term flux will be taken to mean the flux of fast neutrons having energy > 0.1 MeV or some similarly high energy.

The term fluence (the product of flux and irradiation time, formerly called dose, exposure, or integrated flux) will in the same fashion refer to the fast neutron fluence.

II. REVIEW OF THE LITERATURE

Radiation damage effects are discernable in the electron microscope only when the individual defect species (vacancies, interstitial atoms, and possible impurity atoms resulting from transmutation reactions) produced by irradiation form defect clusters which either are visible themselves or influence other observable phenomena (e.g., in the impeding of dislocation movements). Three basic types of defect clusters have been observed in most irradiated metals, including aluminum: vacancy or interstitial dislocation loops, gas-stabilized bubbles, and voids. Each is stable within a certain range of irradiation temperature (expressed as a fraction of the metal's melting point on the Kelvin temperature scale, T_m): loops alone below 0.3 T_m, loops and voids between roughly 0.3 and 0.5 T_m, and bubbles at irradiation temperatures greater than $\approx$ 0.5 T_m. In the first part of this chapter, early observations of loops or "displacement damage" in aluminum will be briefly reviewed. In the second part, the literature dealing with voids in all metals will be examined in greater detail.

A. Early Observations of Radiation Damage in Aluminum

The first direct observation (by transmission electron microscopy) of neutron irradiation damage effects in metals was made by Smallman and Westmacott.[6] In 99.99% aluminum irradiated at -196°C to a fluence of 10^{18} neutrons/cm^2, they observed jogged and spiral dislocations and scattered dislocation loops. Shortly thereafter, Silcox and Hirsch[7] reported detailed observations of neutron damage in copper, noting the presence of a relatively high density ($\approx 3 \times 10^{15}$/cm^3) of "small regions

of strain," some of which could be resolved as dislocation loops. These features have since been frequently noted and referred to as black spots, black dots, or black death.

However several subsequent studies of neutron-irradiated aluminum failed to find the same structural effects noted by Smallman and Westmacott. Silcox[8] could see no damage effects in Johnson-Matthey "specpure" aluminum irradiated to fluences ranging from 7×10^{17} to 1×10^{20} neutrons $/cm^2$ at temperatures from 35 to < 100°C. Thomas and Whitton,[9] who irradiated "super-pure" aluminum in both thin foil and bulk form to 7×10^{19} neutrons/cm^2 ($E > 0.5$ keV), observed no loops but did note the impeding of dislocation motions, presumably by vacancies or small vacancy clusters.

Several types of defects were found by Barnes and Mazey[10] after bombarding Johnson-Matthey spectroscopically standardized copper and aluminum with 1.4×10^{17} alpha particles/cm^2. In the layers where the alpha particles had come to rest, large dislocation loops (radius $r \approx 200$ Å) were observable against a background of small black dots ($r \approx 20$ Å). Postirradiation annealing at 350 and 450°C caused the loops to enlarge and become entangled, while the black dots disappeared and small bubbles ($r \approx 40$ Å) became visible near the grain boundaries. The authors interpreted these results to indicate that the large loops were of interstitial character, while the black dots were vacancy clusters and possible nuclei of the bubbles which grew to visibility upon annealing. More recent analysis[11] of the contrast expected from small defect clusters has made it theoretically possible to distinguish between vacancy and interstitial clusters from their black-white images under dynamical conditions, if the defect depths within the foil are known (as from stereo

microscopy). Conflicting results have resulted from such analyses[11-14] however, and apparently other factors such as the dot size must be considered; a recent review is given by Wilkins[15] (see also Norris[14]).

Further observations of neutron irradiation damage in aluminum were reported by Piercy and Whitton,[16] and by Bierlein and Mastel.[17] The former investigators observed dislocation loops, but only in specimens which had been deformed or quenched prior to irradiation to a fluence of 4×10^{19} neutrons/cm^2 at 50°C. They proposed that both deformation and quenching must have produced submicroscopic loops which were enlarged by the radiation-induced vacancies. In the latter study, 5-9's (99.999%) aluminum showed small prismatic dislocation loops and larger dislocation rings when irradiated in bulk, but not in thin foil, form. The fluences which produced loops ranged from 3×10^{18} to 1.6×10^{20} neutrons/cm^2 ($E > 1$ MeV), and the irradiation temperature was less than 60°C. More recent reexamination[4] indicated that the loops were of both interstitial and vacancy type, and also revealed the presence of a very low concentration of voids in material irradiated to 3×10^{19} neutrons/cm^2.

From this brief outline of the early electron microscopy studies of fast-neutron irradiation damage in aluminum, it is clear that the observations have not been completely consistent. Of the experiments cited above, two observed dislocation loops after irradiations in the 10^{18} neutrons/cm^2 range, and two failed to observe loops even after irradiation in the 10^{19} range. Stiegler et al.[5] have suggested that variations in specimen purity may have an important influence upon the nature of irradiation damage, and may therefore provide a rationale for the discrepancies among earlier studies.

B. Voids in Neutron-Irradiated Metals

The existence of voids in metals was postulated at least as early as 1959,[18] the presence of voids was directly observed in quenched metals in 1961[21] and in neutron-irradiated metals in 1966,[1] and theories pertaining to their formation during irradiation arose shortly thereafter. Of the predictions and quenching studies, a brief and incomplete survey will be given here. Void observations, and theories pertaining to the nucleation and growth of voids, will be covered more extensively.

In a study of dislocation loops produced by quenching 5-9's aluminum, the presence of both loop pairs and loops of unexpected shapes and orientations was noted by Kuhlmann-Wilsdorf and Wilsdorf.[18] The authors explained such occurrences by postulating the formation of voids which later flattened and collapsed into loops. They noted previous dilatometric experiments which lent support to this theory, and also showed that the formation of voids prior to loops was necessary on energetic grounds.

Later calculations were made by Johnson[19] on the stability of voids relative to those of stacking fault tetrahedra and dislocation loops in nickel. He showed that voids were the most stable defect cluster up to very large sizes, after which dislocation loops became slightly favored energetically.

Other comparative stability calculations, for five defect configurations in six f.c.c. metals, were made by Sigler and Kuhlmann-Wilsdorf.[20] They found that for clusters smaller than about 10^3 vacancies, either the void (in Al and Ni, which have relatively high stacking fault energies)

or the stacking fault tetrahedron (in the cases of Pt, Cu, Au, and Ag, with lower stacking fault energies) was the most stable form. For larger clusters, perfect dislocation loops became generally more stable. However, they pointed out that a rather appreciable energy barrier may have to be overcome in the conversion from voids (or tetrahedra) to loops. Since the energy barrier increases with the size of voids, the initially stable void may often continue to grow as a metastable form instead of converting to a loop.

Ruedl et al.[21] apparently were the first to actually observe "cavities," which they produced by quenching very thin platinum foils. The features observed were circular or polygonal in cross section, smaller than 100 Å in diameter, and exhibited a different contrast from that of dislocation loops. They were considered to be within the foil, as opposed to being surface pits, because some could be seen interacting with (presumably pinning) the midsections of dislocations which connected the top and bottom surfaces of the foil. In annealing studies, the cavities disappeared only after anneals at about 800°C.

Similar small (20-100 Å) voids were observed by Kiritani and co-workers[22-25] in quenched 99.999% or zone-refined aluminum. Void concentrations ranging from 10^{12} to $10^{16}/cm^3$ were observed and their shape was found to be that of octahedra bounded by {111} planes. Loops were formed in addition to voids and the spatial distribution of both defect types was nonhomogeneous; where there was a high local concentration of one type, the other was often sparce in number.[23] Both loops and voids were absent from a region or "denuded zone" along grain

boundaries, but the denuded zone for voids, 0.3-0.5 μ wide, was generally narrower than that for loops. Annealing studies[26] of bulk material revealed that quenched-in voids require a higher temperature to begin to shrink appreciably than do loops also formed by quenching. The polyhedral voids became spherical as they shrank during an anneal, and a temperature of 180°C was required to remove them completely in 1 hr. Many of these voids were up to 200 Å in diameter.

Still larger voids, up to 500 Å in diameter, were found by Das and Washburn[27] in quenching studies on 99.999% aluminum. The voids were again octahedral and as in the Japanese studies discussed above, void formation was favored over loop formation by a slow quenching rate and by a higher aging temperature following the quench. Loops, on the other hand, were generated in greater numbers by rapid quenching.

In a work which is of considerable significance to current interpretations of irradiation-produced voids, Shimomura and Yoshida[28] demonstrated that all quenched voids may be nucleated heterogeneously by the aid of dissolved hydrogen atoms. Experimenting with different quenching atmospheres, they obtained voids readily in hydrogen or wet air atmospheres, but saw little or no void formation when vacuum, dry air, or carbon monoxide was employed. Moreover they produced more voids with specimens of increasing purity (99.995%, 99.999%, and zone refined aluminum); this was interpreted as showing the ability of metallic impurities to getter hydrogen and thus reduce the number of potential void nuclei. Similar results in quenched copper, silver, and gold were reported by Clarebrough et al.[29] but they found that oxygen (as well as hydrogen) affected the void numbers in silver and the void shapes in both copper and silver.

Void formation in gold was less affected, but the solubility of both hydrogen and oxygen in gold is much less than in copper and silver.

Before proceeding with a chronological survey of void studies in neutron-irradiated metals, mention should be made of voids which have been found for some time in ionic solids such as LiF,[30] KI,[31] and MgO.[32,33] The voids in ionic solids are distinguished from those discussed below in that these were not present in the as-irradiated specimens, but only came into existence upon postirradiation annealing. In the case of the MgO studies (given fast-neutron fluences greater than 10^{20} neutrons/cm^2), annealing at temperatures above 1500°C was required to develop voids; apparently below this temperature the vacancy mobility was too low for voids to form.

In 1966 Cawthorne and Fulton reported[1] the observation of voids in austenitic stainless steel specimens irradiated as either cladding or tensile test specimens in the Dounreay Fast Reactor between temperatures of 270°C and 650°C at fluences up to 6×10^{22} neutrons/cm^2. For irradiation temperatures up to about 350°C, only black spot defects were formed, but for the cladding material at the "hot end" of the fuel pins, voids were observed. The higher the temperature, the fewer but larger were the voids. At 450°C, voids up to 240 Å numbered about 4×10^{15}/cm^3, while at 560°C, 2×10^{14} voids/cm^3 were found with sizes up to 500 Å. Stereo pairs of electron micrographs proved that the features lay within the material, and their aggregate volume amounted to 1-2% (up to 7% in a later report[34]). Had these objects all been gas-stabilized bubbles, a total of 4000 atomic ppm of helium would have been required to fill them--yet only an estimated 10 ppm He was actually produced in the steel by (n,α) transmutation reactions. It was therefore concluded that the

features were voids and not gas bubbles, a conclusion reinforced by the fact that they could be almost completely removed by a one hour, 900°C anneal. The authors suggested that the voids in the cladding could have been formed from the stress-assisted expansion of small gas bubbles; however the tensile specimens which also developed voids were unstressed during irradiation. Alternatively the authors felt that such voids could arise from the condensation of vacancies out of the high vacancy supersaturation present during irradiation, perhaps upon transmutation-produced helium nuclei.

A short time later Bloom et al.[35] noted black dot defects and also "small white dots" in neutron-irradiated AISI type 304 stainless steel. They suggested the latter were either bubbles of transmutation-produced helium or sites where precipitates had been lost during thinning, but in retrospect it seems probable that they also were voids.

Holmes et al.[36] investigated the annealing behavior and hardening effects of voids produced in type 304 stainless steel irradiated to 1.4×10^{22} neutrons/cm^2 ($E > 0.18$ MeV) at the relatively high irradiation temperature of 540°C (about 0.49 T_m). The voids were octahedra bounded by {111} planes, averaging 160 Å in projected diameter--see Table I for additional statistics from this and the other void studies. Void annealing at progressively increasing temperatures resulted in both a steady decrease in void numbers and occasionally an increase in the average void size, attributed to the preferential annealing of smaller voids first. Frank sessile loops were also formed by irradiation, but they annealed out at lower temperatures than did the voids. The measured increases in yield strength could be attributed either to loops alone

Table I. Characteristics of Voids in Irradiated Metals

Material	$T_{irrad.}$ (°C)	$\frac{T}{T_m}$	Quoted Fluence (neutrons/cm^2)	Void Concentration (Voids/cm^3)	Void Size Avg.,or Max (M)	Swelling (% $\Delta\rho/\rho$)	Homogeneous Void Distrib.	Ref. No.
Austenitic s.s.	350-560	0.38-0.51	5-6 x 10^{22}	2-40 x 10^{15}	500 (M)	1-2	Yes	1
316 stainless steel	500	0.47	7.8 x 10^{22}		1100 (M)	7.	N.D.	34
304 stainless steel	532	0.49	1.4 x 10^{22}	5 x 10^{14}	160	0.11	N.D.	36
304 stainless steel	290	0.34	6 x 10^{21}	N.D.	N.D.	N.D.	Yes	39
99.997 Ni	380	0.38	5 x 10^{19}	4 x 10^{15}	83	0.11	N.D.	41
99.997 Ni	260	0.31	12 x 10^{19}	4 x 10^{16}	55	0.30	N.D.	4
99.999 Cu	260	0.39	12 x 10^{19}	3 x 10^{14}	230	0.17	N.D.	
99.999 Al	50	0.35	3.2 x 10^{19}	very few	270	N.D.	No	
304L stainless steel	422	0.42	4.8 x 10^{22}	N.D.	N.D.	1.15	N.D.	43
1100 Aluminum	60	0.36	1.5 x 10^{22}	N.D.	N.D.	1.5	N.D.	44
Commercial Vanadium	630	0.41	1.7 x 10^{22}	> 1 x 10^{15}	100	0.05	Yes	45,46
304 stainless steel	660	0.56	3.4 x 10^{22}	1 x 10^{15}	260	1.2	Yes	47
347 stainless steel	660	0.56	3.4	2	75	0.5	Yes	
Incoloy 800	660	0.48	3.4	7	175	2.5	Yes	
304L stainless steel	370	0.38	0.8 x 10^{22}	1.4 x 10^{15}	70	0.07	Yes	48
	398	0.40	1.2	1.3	100	0.15	Yes	
	430	0.42	1.4	1.3	125	0.17	Yes	
	460	0.44	1.3	0.9	100	0.16	Yes	
	472	0.45	0.9	0.4	100	0.08	Yes	

Table I (continued)

Material	$T_{irrad.}$ (°C)	$\frac{T}{T_m}$	Quoted Fluence (neutrons/cm^2)	Void Concentration (Voids/cm^3)	Void Size Avg.,or Max (M)	Swelling (% $\Delta\rho/\rho$)	Homogeneous Void Distrib.	Ref. No.
99.997 Ni	50	0.19	4.0×10^{19}	none	---	---	---	3,59
	380	0.38	5.7	4×10^{15}	83	0.11	Yes	
	500	0.45	5.7	8×10^{14}	165	0.16	Yes	
	575	0.49	6.2	2.5×10^{14}	245	0.17	Yes	
	640	0.53	5.2	8×10^{13}	270	0.07	N.D.	
	750	0.59	5.2	$\approx 10^{11}$	≈400	< 0.001	N.D.	
99.992 W	1000	0.35	1.5×10^{20}	2×10^{16}	37	0.04	yes	51,52
	1300	0.43	1.6	1×10^{15}	100	0.05	yes	
99.97 Mo	700	0.34	1.4	3×10^{16}	40	0.10	yes	51,52
	1000	0.44	1.3	5×10^{14}	200	0.19	yes	
304 stainless steel	375	0.39	2.4×10^{22}	1.06×10^{15}	101	0.53	N.D.	56
	410	0.41	4.5	2.16	101	1.26		
	450	0.43	4.1	4.08	118	1.67		
	463	0.44	3.1	1.71	198	1.15		
	470	0.44	2.4	2.0	160	0.39		
	462	0.44	1.3	2.5	117	N.D.		
	465	0.44	1.4	4.0	105	N.D.		
	492	0.46	1.1	1.5	140	N.D.		
99.9999 Al	50	0.35	3.5×10^{20}	1.3×10^{14}	400 (M)	N.D.	No	5
1100 Al	45	0.34	1.5×10^{22}	N.D.	800 (M)	N.D.	No	
99.999 Fe	450	0.40	3×10^{21}	1×10^{14}	280	0.12	Yes	57

Table I (continued)

Material	$T_{irrad.}$ (°C)	$\frac{T}{T_m}$	Quoted Fluence (neutrons/cm^2)	Void Concentration (Voids/cm^3)	Void Size Avg.,or Max (M)	Swelling (% $\Delta\rho/\rho$)	Homogeneous Void Distrib.	Ref. No.
8001 Al	60	0.36	1×10^{22}	1×10^{15}	210	0.8	N.D.	61
8001 Al, preirradiated	60	0.36	1×10^{22}	2×10^{15}	150	0.4	N.D.	
99.99 Fe, recrystal.	415	0.38	1.5×10^{21}	1.4×10^{14}	350	N.D.	No	63
Nonrecrystal. regions	415	0.38	1.5×10^{21}	4.3×10^{14}	125	N.D.	Yes	
99.9999 Al	125	0.43	4×10^{20}	N.D.	3000 (length)	N.D.	No	64
	150	0.45	4×10^{20}	N.D.	30,000 (length)	N.D.	No	
304 s.s. without He	390	0.40	7.4×10^{21}	2.4×10^{15}	130 (M)	0.10	N.D.	65
304 s.s. with He	390	0.40	7.4×10^{21}	5.2×10^{15}	75 (M)	0.06	N.D.	
99.99 Mo	1050	0.45	1×10^{21}	1.2×10^{14}	290	0.17	N.D.	68
	1150	0.49		0.5	470	0.28		
99.97 Re	1050	0.38		7.0	110	0.07		
	1150	0.41		5.0	140	0.10		

or to loops plus voids when both were present; after the loops had annealed out, the remaining strengthening could be accounted for by the voids alone, based on Coulomb's theory of cavity strengthening.[37] Later tensile testing studies[38] indicated that deformation alone below 600°C could not eliminate the voids from the microstructure, although higher temperature deformation did eliminate them.

Cavities which behaved like gas-stabilized bubbles upon annealing were reported by Brager and Robbins.[39] The material was type 304 stainless steel, irradiated to the rather low fluence of 6×10^{21} neutrons/cm^2 at 290°C (0.34 T_m) in the ETR, a reactor having a high thermal flux. The voids were distributed uniformly throughout the material, including the grain boundary regions. Also, during annealing, their average size increased while their numbers decreased in such a way that the total cavity volume increased but the total surface area did not change. The authors felt such behavior was more typical of gas-filled bubbles than voids. The estimated helium concentration produced by the irradiation was more than an order of magnitude too small to stabilize all the cavities. However the measured helium content published later[40] was much higher (237 ± 45 ppm) and in fact nearly sufficient to stabilize the cavities as bubbles. Besides indicating that the value taken for the cross section of the B^{10} (n,α) reaction may have been incorrect, these results warn that cavity studies in thermal reactors may be difficult to interpret because of transmutation-produced gases.

As reported by Brimhall and Mastel,[41] 99.999% pure Ni was the first high purity material to exhibit voids, and at fluences much lower than those of the stainless steel studies--only 4-5 $\times 10^{19}$ neutrons/cm^2

(E > 1 MeV) at 380-450°C (≈ 0.4 T_m). Yet high densities (2-4 x 10^{15}/cm^3) of octahedral voids ranging in size from 50 to 150 Å were produced. In addition to showing that too few transmuted helium atoms were present to stabilize the cavities as bubbles, the authors also calculated that the total quantity of irradiation-produced vacancies was 50 times greater than the number represented in the aggregate void volume. Therefore the voids could indeed be clusters of those irradiation-produced vacancies which were not annihilated with the self-interstitials or at sinks. Values for the void sizes and numbers consistent with the above electron microscopy results were also obtained by small-angle x-ray scattering studies.[42] Shortly thereafter, the same authors submitted some further results for nickel together with the first information on voids in pure (99.999%) copper and aluminum.[4] The voids in the latter material were relatively large (≈ 270 Å diam.) but extremely few in number. However the fluence was the lowest yet shown to have yielded voids (3.2 x 10^{19} neutrons/cm^2, E > 1 MeV), and of the three materials the aluminum had the highest density of dislocation loops, some of which were vacancy loops. The average void sizes were shown to be proportional to the vacancy mobilities in the three materials.

Immersion density measurements by Holmes[43] of the volume change of type 304L stainless steel irradiated up to 4.8 x 10^{22} neutrons/cm^2 (E > 0.1 MeV) yielded change in density values up to 1.15% and a plot of swelling vs. fluence which was roughly linear. A density decrease or swelling of 1.5% was found by King and Long[44] in 1100 (commercial purity) aluminum, after irradiation to 1.5 x 10^{22} neutrons/cm^2 (E > 0.8 MeV).

The first voids reported in a b.c.c. metal were found by Wiffen and Stiegler[45] in commercial purity vanadium irradiated to a fluence of 1.7 x 10^{22} neutrons/cm^2 at 630°C; the voids were greater than $10^{15}/cm^3$ in concentration and averaged 100 Å in diameter.

Octahedral voids were found in type 347 stainless steel and Incoloy 800 as well as type 304 austenitic stainless steel by Lauritzen et al.[47] and the bulk volume increases ranged from 0.5 to 2.5% (see Table I). Several interesting findings were noted by Stiegler and Bloom[48] in a detailed paper on voids in type 304L stainless steel. For a fixed fluence and increasing irradiation temperature, the void concentration decreased while the average and maximum void sizes increased (confirming Cawthorne and Fulton's observations). They also noted that the width of the zone denuded of voids near grain boundaries first decreased (from 1300 Å to 100-200 Å) and finally increased (to 500 Å) with constantly increasing irradiation temperature. The denuded zone width presumably depends upon temperature-dependent vacancy diffusion processes.

In addition, they calculated that there were approximately equal numbers of point defects in the dislocation loops as in the void population, leading the authors to suggest that the loops were composed of the irradiation-produced interstitial atoms. The voids had a variety of shapes, many being quite irregular.

Further investigations, especially annealing studies, were made on voids in 99.997% nickel by Brimhall and Mastel.[3] Over a rather wide range of irradiation temperatures--260° to 575°C (0.31-0.49 T_m)--the void volume fraction changed relatively little (Table I). An irradiation

of Ni at the much lower temperature of 50°C, where vacancies are not mobile, failed to produce voids. The authors attempted to "develop" voids in this material by postirradiation annealing at 550°C. The result was a depletion of the small dislocation loops initially present and the generation of very small ($\approx$ 50 Å) black spots much like those which Bourret and Dautreppe[49] had termed "tetrahedral voids." Brimhall and Mastel argued convincingly that these defects were really stacking fault tetrahedra, and that voids in irradiated metals apparently cannot be produced by irradiating below some "critical temperature" for void formation (probably about 0.3 T_m) and subsequently annealing at a higher temperature. (Note the contrast with just such experiments done earlier in neutron-irradiated ionic solids.[30-33]) The observed increase in average void size upon postirradiation annealing was interpreted as due to void coarsening (small voids yielding their vacancies by diffusion to larger voids). A similar conclusion was reached by Straalsund et al.[50] studying void annealing in type 304L stainless steel. However the same observation had been made in several previous annealing studies[36,39,41] and the explanation then offered was that the preferential annealing out of small voids by itself shifted the average void size to larger values. As in the previous study, the width of grain boundary denuding was found to be temperature-dependent; in the current work it increased continuously with increasing irradiation temperature.

Voids were seen in body-centered cubic tungsten and molybdenum by Rau et al.[51,52] Their shape was dodecahedral, with main {110} faces truncated by smaller {100} facets; these are the planes of lowest surface energy in the b.c.c. system. For irradiation at similar

homologous temperatures, tungsten exhibited both smaller voids and a lower total void volume. This was explained as due to the fewer vacancies produced per fast neutron collision in tungsten, and also to the greater production of transmutation impurities, acting as vacancy sinks in tungsten. Noting that voids have been found in cubic metals only for irradiation temperatures higher than the Stage IV recovery temperature, $\approx 0.31\ T_m$, the authors felt this lent support to the contention that the free migration of vacancies first becomes possible in Stage IV (the "two-interstitial theory"--see Corbett[53] for a lucid if somewhat partisan review of this controversy).

At the International Atomic Energy Agency symposium held in Vienna in 1969, Nelson and Mazey[54] described how they created voids in type 316 stainless steel by bombarding specimens with C, Fe, O, or H ions in an ion accelerator. Displacement damage equivalent to 10^{22} neutrons/cm^2 (which would take up to a year or more of irradiation in a reactor) could be generated in a few hours bombardment. Since there were no neutrons employed there were no impurity atoms (especially helium) created by transmutation--although implanted ions did contaminate the specimens. However when helium was deliberately injected by the accelerator prior to the main damage-producing bombardment with carbon ions, an order of magnitude greater void concentration and total void volume resulted, compared with a specimen given the same bombardment without prior helium injection. Clearly the nucleation and growth of voids was strongly influenced by the presence of helium, although voids also formed to a lesser degree in the apparent absence of helium.

At the same symposium, Claudson et al.[55] presented experimental results and a theoretical interpretation of swelling in type 304 stainless steel irradiated to fluences as high as 9×10^{22} neutrons/cm^2 ($E > 0.1$ MeV) in the EBR-II reactor. Their swelling data plotted versus fluence (on logarithmic paper) showed a nearly linear relation though with a slight upward concavity. The voids were roughly spherical at lower irradiation temperatures, but they became faceted at higher temperatures. Details of the theoretical treatment will be discussed in the last section of this chapter. Harkness and Li[56] also presented a model for void formation (to be discussed later) and similar experimental findings in type 304 stainless steel. They observed that void formation in this material was restricted to the 350-650°C temperature range, with the maximum swelling occurring at an irradiation temperature of about 500°C. Finally, Stiegler et al.[5] described apparent impurity effects strongly influencing void formation in 99.9999% and 99% aluminum. The former material developed nonhomogeneously distributed voids at fluences as low as 4×10^{20} neutrons/cm^2. Linear and planar arrays of voids were observed, as well as patches containing high concentrations of voids and few loops, adjacent to regions where the reverse was true. The impure material, irradiated to 1.0×10^{22} neutrons/cm^2, contained a more uniform distribution of cubic voids, vacancy and interstitial loops, and a fine silicon precipitate. From surface energy considerations, a cubic void shape should be less favorable than an octahedral shape in an f.c.c. material. Annealing the 99% pure aluminum above 230°C removed the voids, coarsened the precipitate, and at 455°C gas bubbles grew on grain boundaries and dislocations to visible size.

Voids were found in 99.999% iron by Kulcinski et al.[57]; see Table I for details. They were described as truncated octahedra bounded by various sets of {110} planes, but they actually were presumably truncated dodecahedra.

A study of swelling in three nickel alloys was reported by Holmes.[58] The three materials each displayed a linear relation between swelling and fluence but with greatly differing slopes. (In stainless steel, by contrast, the relation is apparently a power law.) For Nickel-270 (99.98% Ni), the swelling increased steeply with fluence, for Nickel-200 (99.6% Ni), the slope was much more moderate, and for Inconel-600 (73% Ni-17%Cr-8% Fe) there was no swelling at all; the fluence range was from 1.0 to 5.0 x 10^{21} neutrons/cm^2 (E > 1 MeV). Brimhall and Mastel extended their study of the influence of irradiation temperature at constant fluence on voids in 99.997% nickel.[59] They found that the swelling is nearly independent of temperature between 400° and 600°C and falls to a negligible value both at 250° and 750°C (0.30 and 0.59 T_m).

Continued studies by Bloom and Stiegler[60] of void formation in type 304L stainless steel produced further understanding of void formation in alloys. They showed that while the concentration of voids produced during irradiation at 460°C was lower than that produced at 370°C, the void concentration at 460°C increased more rapidly with increasing fluence. The rates of increase with fluence were such that a void concentration > 10^{16} voids/cm^3 might result from irradiation at either temperature for fluences somewhat in excess of 10^{23} neutrons/cm^2. The authors also found that although the <u>mean</u> void diameters did continue to increase with increasing fluence, the <u>maximum</u> void diameters did <u>not</u>

increase, for irradiations beyond about 1 x 10^{22} neutrons/cm^2. The limiting void size depended on the irradiation temperature, increasing from about 220 Å diam. at 370°C to about 300 Å at 460°C. The overall swelling increased more rapidly with increasing fluence at 460°C than at 370°C. The observation of a limiting size for voids was explained on the basis of the varying mobilities of the different constituents of this alloy. These results will be treated further in the discussion section.

Combined electron microscopy and mechanical properties studies were recently performed on the 8001 aluminum alloy (Al - 1 wt% Ni) by King et al.[61] Irradiation to 10^{22} neutrons/cm^2 at 60°C produced about 10^{15} voids/cm^3 and a fine solid precipitate of silicon from transmutation reactions. Prior to this irradiation some of the specimens had received a high thermal-neutron exposure; the voids in these specimens were smaller and more numerous than those in specimens which were not pre-irradiated. The effect may be linked to the extra quantities of transmutation-produced silicon or gases generated during the preirradiation. Bulk annealing achieved results similar to those of Stiegler et al.[5] already mentioned: the voids disappeared, the silicon precipitate coarsened, and finally gas bubbles became visible. Thin-foil in situ annealing studies of this material and high purity aluminum were performed by Packan and Braski[62] using an ultrahigh-vacuum electron microscope. They noted a considerable diversity in the annealing behavior of individual voids and an initial rapid-shrinkage effect apparently related to vacancy sinks other than the foil surfaces.

Farrell and Houston,[63] investigating Johnson-Matthey spectrographic iron irradiated at 415°C to a fluence of 1.5 x 10^{21} neutrons/cm^2 (E > 0.1 MeV), found significant heterogeneities in the spatial distributions of the voids formed. The voids were frequently arranged in clusters or lines (which may have been sections of planar arrays), and they were larger and more numerous in recrystallized regions than in recovered regions. By contrast, Kulcinski et al.[57] found a uniform void distribution, but his otherwise similar material was irradiated in the fully recrystallized condition, whereas Farrell's material was in the warm-worked condition prior to irradiation. Impurity effects were suggested as the explanation for the nonhomogeneities.

By far the largest voids yet reported were found by Farrell and King[64] in high purity aluminum irradiated to only 4 x 10^{20} neutrons/cm^2 at relatively high homologous temperatures (125 and 150°C, 0.43 and 0.45 T_m). Void shapes included ribbons, cylinders, plates, and equiaxed polyhedra. At the lower temperature, some of the elongated voids were as long as 3000 Å, and at the higher temperature, up to 30,000 Å. A low vacancy supersaturation resulting from the high irradiation temperatures was the suggested cause of these peculiar effects.

Several quite recent studies have dealt further with the effects of helium on void formation. Bloom and Stiegler[65] and Farrell et al.[66] preinjected helium into 304 stainless steel and aluminum, respectively, prior to fast neutron irradiation. In each case, voids which formed in the helium-bearing specimens were found to be smaller but more numerous than those in material not preinjected. The apparent effect of the helium was thus to increase the void nucleation rate early in the irradiation.

Using both electron microscopy and small-angle x-ray scattering to study the annealing of voids in nickel, Kulcinski et al.[67] found no coarsening, but rather a constant average void size of 400 Å through increasing annealing temperatures (up to 1050°C, which removed them entirely). Void annealing progressed into the grains from the grain boundary denuded zones. A correlation between hardness increase and void sizes and numbers, in good agreement with earlier theoretical considerations,[37] was also obtained.

Finally, voids have been discovered in the h.c.p. metal rhenium by Kulcinski et al.[68] after irradiation to 1 x 10^{21} neutrons/cm^2 (E > 0.1 MeV) at 1050 and 1150°C (0.38 and 0.41 T_m). They appeared to be bounded by prism planes. Thus void formation has been seen in all three common metal structures (although irradiation of the h.c.p. metals zirconium and titanium to even higher fluences at similar values of T_m have not yet produced observable voids).

Summarizing the experimental observations on voids, it appears that voids observable by electron microscopy can be formed in metals of the common crystal structures, after sufficient fast-neutron irradiation at a homologous irradiation temperature between 0.3 and 0.5 T_m. For increasing irradiation temperatures within this range, the void concentration tends to decrease but their sizes increase. The threshold fast-neutron fluence required to produce voids seems to depend upon the purity of the material, being much lower for high-purity materials than for impure materials and alloys.

The amounts of transmutation-produced gases (H and He) generated during fast-neutron irradiations are generally found to be far less than

the quantities that would be required to fill and stabilize all the voids as gas bubbles. Also, voids have not been seen within denuded zones adjacent to grain boundaries or on grain boundaries--both preferred nucleation sites for gas bubbles. These reasons, coupled with their shrinking and disappearing behavior rather than growth upon postirradiation annealing, have caused these features to be called "voids" and considered to be distinct from bubbles. However, most investigators have admitted the possibility that the voids may contain some gas, and some have suggested that gas atoms or tiny gas bubbles may be the actual nuclei for void formation. In several studies gaseous impurities such as helium[54,65,66] or hydrogen[66] have been injected by cyclotron bombardment prior to fast-neutron irradiation; in one other case extra silicon and helium were produced in a prior thermal-neutron irradiation before the aluminum sample was exposed to fast neutrons.[61] The results each time were the same: generation of smaller but more numerous voids as a result of adding these impurities. It appears, therefore, that the nucleation of voids is indeed influenced in some way by the presence of impurities, particularly helium. Some studies, in aluminum[4,5,61] and iron[63] have found void clustering, void walls, and other nonhomogeneities which also were attributed to the influence of impurities.

There remain unresolved questions such as the mechanism by which voids are removed upon annealing, and the character of dislocation loops formed along with voids. Some[3,50] have interpreted void annealing as a coarsening process with larger voids first growing at the expense of smaller voids, while others[36,48,62,67] have concluded that <u>all</u> voids shrink but smaller ones shrink at more rapid rates. Both interpretations

may actually be correct, under different circumstances. In several cases the dislocation loops have been identified or interpreted as primarily interstitial in composition,[48,52] while other results indicate a major proportion of vacancy loops.[4,5] The character of the loops probably varies from case to case, depending upon the material, temperature, or irradiation conditions.

C. Proposed Mechanisms for Void Formation

A number of possible mechanisms have been proposed to explain the nucleation and the growth of voids. It is known that under continuing exposure to a high flux of fast neutrons, atoms are continually displaced from lattice sites to form interstitial atoms while leaving behind vacancies. Taking into account recombination of most of these vacancies with interstitials as well as the loss of both species to point defect sinks (grain boundaries, impurity particles, dislocations, etc.), there remain quasi-steady-state concentrations of interstitials and vacancies. It is thus quite reasonable for a vacancy supersaturation (above the thermal equilibrium vacancy concentration) to develop, and if it is sufficiently large one can envision the simple homogeneous nucleation of void-type vacancy clusters. However nucleation by means of other mechanisms which have been proposed would probably take place sooner.

Looking at the basic collision event in greater detail, it is generally accepted that displacement spikes are briefly formed, consisting of vacancy-rich cores surrounded by regions of self-interstitials. This initial separation of point-defect types leads to a temporary statistical clustering of each species, as demonstrated by Lück and

Sizmann.[69] While it is not felt that such clusters occurring in a single spike are stable, the coalescence of the cores of several nearly coincident spikes might be. The computer simulations of radiation damage by Beeler[70] do show that if three or four of these short-lived spike cores happen to occur close together in space and time (and if the temperature is greater than $T_m/3$), they can coalesce to form a faceted void nucleus which should be stable. The simulations further show that such faceted void nuclei should attract mobile vacancy configurations (single, di-, trivacancies, etc.) significantly more readily than they attract mobile interstitial configurations and the nuclei should therefore grow.

Harkness and Li[56] have combined these approaches in a model which assumes the displacement spike to be the predominant void nucleation site, but calculates the void nucleation rate using classical nucleation and growth theory (i.e., the homogeneous nucleation process first described). The model especially treats the temperature dependence of void formation, though the fluence dependence is of primary interest here. After showing the dominance of the vacancy supersaturation (chemical potential) term using reasonable values of the neutron flux and irradiation temperature, the authors obtain an expression for the nucleation rate I:

$$I = k\phi \exp(-16\pi\gamma^3/3RT\ \Delta F_v^2)(-\Delta F_a/RT) \qquad (1)$$

where

ΔF_v = $RT\rho/M \ln(N_v/N_{vo}) + P_g + \sigma$,

ρ,M = density, molecular weight of metal,

N_v = steady state vacancy concentration during irradiation,

N_{vo} = thermal equilibrium vacancy concentration,

P_g = gas pressure inside void (if any),

σ = applied stress (if any),

ϕ = neutron flux,

γ = surface energy of metal, and

ΔF_a = energy for vacancy diffusion.

The quantity N_v is obtained from the analysis of Greenwood,[71] and in deriving the nucleation rate expression, the assumption must be made that void nuclei of critical size grow sufficiently slowly that their steady state and equilibrium numbers are the same. This is difficult to justify for nucleation within spikes.

Harkness and Li consider void growth to be limited by the diffusion of vacancies to the void, and give the growth rate as:

$$dr/dt = \alpha D_v N_v / r \qquad (2)$$

where r = void radius, D_v = vacancy diffusion coefficient, and α, a constant with value less than one, is a screening parameter expressing the prescribed greater flux of vacancies than interstitials to the void. The growth and nucleation rates are combined by means of the approach of Johnson and Mehl[72] after assuming that the nucleation rate is time independent and that the total void volume is low enough to prevent impingement. The result for the void volume fraction is:

$$F = 1 - \exp[-KI(D_v N_v)^{3/2} t^{5/2}] \; . \qquad (3)$$

In this empirical model the constant K is an adjustable parameter with a value taken to best fit the data available. Among the predictions of this model are that certain material properties (the vacancy energies of formation and motion, and the surface energy) have an important influence on void formation, but that the neutron flux is not itself a significant variable.

Claudson et al.[55] have proposed a swelling vs. fluence relation by setting down a variety of potential nucleation and growth mechanisms together with their expected dependence on flux and time. They then select the most plausible combination which also agrees with the large collection of swelling data on stainless steel that they have compiled.

The five prospective nucleation models considered are: homogeneous nucleation with the vacancy concentration limited by either recombination or annealing at dislocation sinks, spike nucleation, spike nucleation stabilized by helium atoms, and preexisting nuclei only. For the void growth mechanism they choose from seven possibilities: diffusion limited, surface absorption limited with absorption over the whole void surface, surface limited with absorption allowed only at the tips of faceted voids--each of the above with either recombination- or dislocation sink-controlled vacancy concentration--and lastly rapid void growth to a limiting size with negligible growth thereafter. The resulting flux and time swelling parameters, $\underline{x}$ and $\underline{y}$ in $\frac{\Delta V}{\Delta} \sim \phi^{x} t^{y}$, are then calculated for each nucleation mechanism with each growth mechanism. Multiple linear regression analysis values for $\underline{x}$ and $\underline{y}$ of 1.59 ± 0.46 and 1.96 ± 0.52 respectively have been determined from experimental data. Since they also found no significant evidence for a flux dependence (where flux

differences up to about 40% existed) they include the criterion that $\underline{x}$ should be nearly equal to $\underline{y}$. The void formation model in best agreement with experimental results is, they feel, that of spike nucleation followed by void growth with vacancy absorption only on void tips and the vacancy concentration controlled by "linear annealing" (at dislocations, second phase particles). This model yields a swelling equation (including the assumed Arrhenius temperature dependence) of:

$$\text{Nucleation: } N \sim \phi t \quad ; \quad \text{Growth: } v \sim \phi t$$

$$\text{Combined: } \Delta V = A(\phi t)^2 \exp(-\Delta H/RT) \quad . \qquad (4)$$

In assessing the fact that this model gives a higher fluence exponent than the experimentally determined value of 1.65 (for x = y), the authors propose that void-loop interactions may impose saturation effects on the swelling which lower the net fluence dependence from 2.0 to the observed value. The model also predicts an unrealistic void size distribution (peaking at the maximum void size) and void-loop interactions are again invoked, to reduce the number of larger voids.

Shively[73] has presented a void formation theory which features nucleation in helium-stabilized spikes and projects a decreasing rate of both void nucleation and swelling as irradiation proceeds. Because spikes and helium are produced at a constant rate, nucleation should vary linearly with both flux (affecting spikes) and fluence (building up the helium concentration through transmutation), and initially then: $\dot{N} \sim \phi(\phi t)$. However, when the voids reach a size estimated to be on the order of 100 Å in stainless steel, they begin to act as significant helium sinks. The rate of helium influx into voids approximates the

helium production rate, the helium concentration in the lattice no longer increases, and the nucleation rate becomes constant. A second saturation effect occurs when the voids have grown to perhaps 200 Å; nearly all helium drains into the voids and further nucleation essentially ceases.

While the nucleation rate is changing, void growth continues following a single mechanism: that of diffusion-controlled migration of vacancies to the voids, while interstitials go preferentially to interstitial loops. The form is the same as in the Harkness model (see Eq. 2), and shares the latter's doubtful assumption of a vacancy supersaturation not dependent upon irradiation time. Combining these mechanisms yields a changing dependence of swelling with fluence as the irradiation progresses: $\Delta V/V \sim (\phi t)^{7/2}$ initially, $\sim (\phi t)^{5/2}$ after the first saturation effect takes hold, and $\sim (\phi t)^{3/2}$ later when nucleation has ceased and void growth alone continues. The authors feel that this variation in mechanism at successive stages of void formation is substantiated by the available swelling results.

A recent analytical treatment of void formation by Murley[74] consists of a set of coupled nonlinear equations describing the time rate of change of the vacancy, interstitial, interstitial cluster, gas atom, and void concentrations and the void volume. Assuming normal void size distributions, the model predicts for the mean void radius $\bar{r} \sim t^{1/2}$, while the swelling is proportional to $\phi t^{5/2}$ in the early stages of void formation--the same dependence that Harkness predicts. In the later stages, void coalescence dominates and the total void volume is conserved (contrary to all experiments so far). The void volume saturation level

is proportional to the square root of the flux.

Bullough et al.[75,76] and Gulden and Kaae[77] have both obtained similar expressions for void growth. Each explicitly treats the interstitial flux to the void instead of invoking a constant screening factor, and their common expression for dr/dt can be either positive or negative depending upon a balance between void radius, surface energy, and internal gas content. Gulden and Kaae also provide for an external stress, if any. In the terminology of Bullough:

$$\frac{dr}{dt} = \frac{1}{4b}\left(D_v C_v - D_i C_i\right) - \frac{D_s}{4b}\exp(F_m b^3/kT) \qquad (5)$$

with

$$F_m = \frac{2\gamma}{r} - \frac{3NkT}{4r^3}$$

where

C_v, C_i = vacancy and interstitial concentrations near the void,

D_v, D_i = vacancy and interstitial diffusion constants,

D_s = vacancy self-diffusion constant,

b = lattice spacing,

F_m = mechanical force acting on the void,

γ = surface energy,

r = void radius, and

N = number of gas atoms inside the void.

For purely empty voids, F_m is positive and increases as $r \to 0$, so that dr/dt becomes negative and small voids must shrink. However even a very small amount of gas (N) inside a small void causes F_m to become negative and makes the void stable; it can then grow in proportion to the net

vacancy flux, the first term in Eq. (5). For larger voids the second term in Eq. (5) becomes less important and the integrated equation yields $r \sim t$. In Gulden and Kaae's work, $r \sim t^{1/2}$ since they have $1/r$ instead of $1/b$ in the first term.

Bullough et al.[76] suggest that while gas bubbles are always stable against collapse, there exists an equilibrium size for voids, determined by the vacancy concentration, such that larger voids must tend to grow, and smaller voids must shrink (to disappearance if they contain no gas at all). Therefore under irradiation conditions where a certain vacancy supersaturation can be maintained (a highly questionable situation as irradiation proceeds), larger voids will grow at the expense of small voids, eventually leaving a few large voids. However such a prediction seems to be in conflict with observations, and does not necessarily follow. If the equilibrium void size were relatively small, and all voids larger than it were stable, then such voids would not grow at each others expense and one might indeed obtain many voids in a range of sizes.

Finally Bloom and Stiegler[65] have argued that the role of impurities, particularly helium, should be given great attention in the formulation of any void theory, rather than being ignored or included as only a possible minor factor. Numerous results have been reported recently which are most easily explained as impurity effects.[5,54,61,63,65,66] That the major quantitative theories proposed to date, such as those of Harkness and Claudson, have omitted any real treatment of impurity effects, especially with respect to void nucleation, is probably an indication of the difficulty in formulating such a model.

In Table II the nucleation and growth mechanisms and their dependence on fluence are summarized for each model. At this point there is little unanimity in the understanding of either the nucleation or the growth of voids. As Holmes[78] has recently noted, the attempts to develop "mechanistic models" for void formation have so far met with little success. In the meantime, until a satisfactory theoretical model arises, empirical models which contain parameters adjustable to the data are serving as reactor design guides.

Table II. Current Void Models

Model	Void Nucleation (N = void concentration)		Void Growth (r = void radius)		Overall Swelling
	Mechanism	Fluence Dependence	Mechanism	Fluence Dependence	
Beeler[70]	Overlapping Spikes	---	---	---	---
Harkness[56]	Spikes; homogeneous	$N \sim \phi t$	Diffusion-limited	$r \sim t^{1/2}$	$\frac{\Delta V}{V} \sim \phi t^{5/2}$
Claudson[55]	Spikes	$\sim \phi t$	Surface absorption-limited; only on void tips	$\sim (\phi t)^{1/3}$	$\sim (\phi t)^2$
Shively[73]	Spikes, He-stabilized	$\sim (\phi t)^a$, $a = 2 \rightarrow 0$	Diffusion-limited	$\sim t^{1/2}$	$\sim (\phi t)^b$, $b = \frac{7}{2} \rightarrow \frac{3}{2}$
Murley[74]	Spikes, He-stabilized	---	Diffusion-limited (?)	$\sim t^{1/2}$	$\sim \phi t^{5/2}$
Bullough, et al.[75,76]	---	---	Surface absorption-limited; on whole void surfaces	$\sim t$	---
Gulden and Kaae[77]	---	---	Diffusion-limited (?)	$\sim t^{1/2}$	---

III. EXPERIMENTAL DETAILS

A. Material Characterization

The material used in this study was high purity aluminum, Grade 69 sold by Cominco American, Inc., Electronic Materials Division, Spokane, Washington. The manufacturer specifies this material to be zone-refined 99.9999 + % Al, which would allow a total of 1.0 atomic ppm of metallic impurities. However the assay certificates supplied with each lot of material indicate impurity contents ranging from 1.2 ppm to 5.3 ppm. Precision analyses conducted by the ORNL Analytical Chemistry Division, Spectrochemical Laboratory, indicate total impurity contents ranging from 6 to 12 ppm. The results of the analyses are shown in Table III. Three lots of Cominco Grade 69 Aluminum were used in this work: lots 5719 and 6353 were received in the form of 0.125 in. diam. wire which had been drawn by the vendor, while the third, lot 7767, was supplied as 3/4 in. diam. as-zone-refined rod stock. The lot 5719 wire had been swaged at this laboratory to 0.10 in. diam. for use in other experiments, and the lot 7767 bar was swaged to 0.125 in. diam. for these studies. No annealing treatment was given the material prior to irradiation, to avoid possibly increasing the gaseous or solid impurity content. Normally, 50% cold-worked 6-9's purity aluminum recrystallizes at room temperature.

For an independent check on the purity of the material, the resistivity ratio of each lot was measured by the Physical Properties Group of the Metals and Ceramics Division. The results, in Table IV, indicate that the material was of quite high purity. This effort to characterize the purity of each lot was undertaken because the lot 6353 material

Table III. Solid Impurities Found in As-Received Cominco Grade 69 Aluminum

Lot No.	Element															
	B	Ca	Cr	Cu	Fe	In	K	Mg	Mn	Na	Ni	Si	Ta	Ti	Zn	Total
5719																
Cominco anal.		0.5		0.1				0.5				0.1				1.2
ORNL anal.	0.2	0.5	0.4	<0.06	0.2	<0.04	0.4	0.2	<0.04	2.0	<0.07	≈2.	<0.04	0.2	0.2	6.3
7767																
Cominco anal.								<0.1								<0.1
ORNL anal.	1.0	0.6	<0.08	<0.06	0.3	<0.04	0.5	0.3	<0.04	0.1	<0.07	≈4.	<0.04	0.1	0.4	7.3
6353																
Cominco anal.		1.0		0.1	1.0	2.0		0.5				0.2		0.5		5.3
ORNL anal.	0.5	0.4	2.0	<0.06	0.5	<0.04	0.3	0.1	0.2	0.5	1.0	≈6.	0.3	0.2	0.2	12.2

Table IV. Resistivity Ratios of As-Received Cominco Grade 69 Aluminum

Resistivity Ratio	Lot 7767	Lot 5719	Lot 6353
$\frac{\rho_{300\ K}}{\rho_{4.2\ K}}$	8.5×10^3 (highest purity)	2.9×10^3	2.7×10^3 (lowest purity)

Table V. Hydrogen Content of As-Received Cominco Grade 69 Aluminum

Hydrogen Content	Lot 7767	Lot 5719	Lot 6353
$\frac{\text{ml } H_2 \text{ (STP)}}{\text{100 gm Al}}$	0.82	0.61	0.80 to 3. +
Concentration of H (atomic ppm)	19.5	14.5	19 to 70 +

proved exceedingly difficult to thin for electron microscopy. This material consistently yielded unusable foils due to either the presence of some solid precipitate or of internal porosity.

To investigate the gaseous impurity content of the materials, wire samples of each lot about three feet long and weighing about 20 gm were sent to the Alcoa Research Laboratory, Physical Chemistry Division, for measurement of the internal gas content (mainly hydrogen) using a solid state extraction technique developed by Alcoa. After surface cleaning the procedure involved an initial 5 to 6 hr. gas extraction at about 40°C below the melting point at diffusion pump pressure, the readmission of air into the specimen chamber, and finally a second extraction like the first. The first extraction removed the internal H_2, in addition to H_2 from the surface and system outgassing. The second extraction served as a correction factor, removing again surface H_2 and outgassing. Subtracting the second quantity from the first yielded the internal hydrogen content. The rate of gas removal decreased from an initial rapid rate to a comparatively slow rate, indicating that essentially all of the internal gas had been removed from the specimen. Results of these tests are shown in Table V. According to Kinosz,[79] these hydrogen amounts are three to four times greater than the values commonly found in aluminum, and such high levels of gas are usually associated with internal porosity. The difficulties sometimes encountered in attempting to make electron-transparent thin foils may then have been caused by the intersection of pores with the specimen surface.

B. Irradiation Procedures

The fluence dependence of void formation was studied for specimens irradiated in the High Flux Isotope Reactor (HFIR) of the Oak Ridge National Laboratory. This reactor has fuel in two annular assemblies surrounding a central flux trap in which removable target rods are arranged in an hexagonal array (Fig. 1). There is also a hydraulic or "rabbit" tube currently occupying the centerline location of the flux trap. Nine hydraulic tube capsules 2.5 in. long x 0.5 in. diam. are inserted in a vertical stack, irradiated, and are removed at any time by reversing the flow of cooling water (which normally flows down the tube). Position No. 5 in the stack is roughly at the midplane of the reactor core and therefore receives the highest neutron flux. To a close approximation, the flux along the centerline follows a cosine profile centered on the reactor midplane. At the beginning of these experiments, the cosine relation and the best available value for the midplane-centerline neutron flux (7.5×10^{14} n/cm^2/sec, E > 0.82 MeV) were employed to calculate values for the flux in each of the other hydraulic tube positions. From these values the time required for a particular capsule to reach its intended fluence was calculated. The absolute flux value was investigated by the inclusion of a flux monitor wire in one of the final capsules. These considerations are discussed in detail in Appendix A. Briefly the results confirmed the validity of the cosine approximation for the axial flux profile, but suggested a lower value of about $6.5 \pm 0.8 \times 10^{14}$ n/cm^{2}sec (E > 0.82 MeV) for the peak flux value.

The perforated irradiation capsules kept the specimens in contact with the reactor cooling water (see Fig. 2). For these experiments,

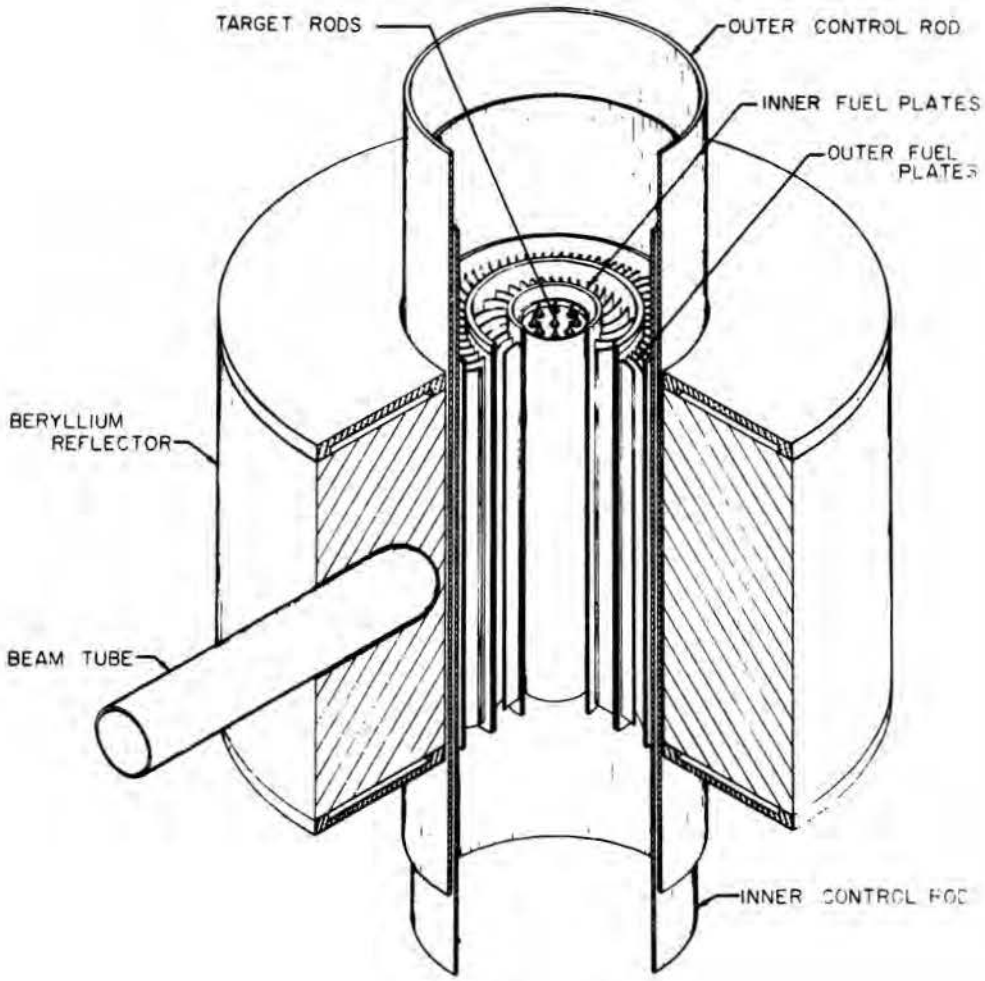

Fig. 1. Schematic of High Flux Isotope Reactor core.

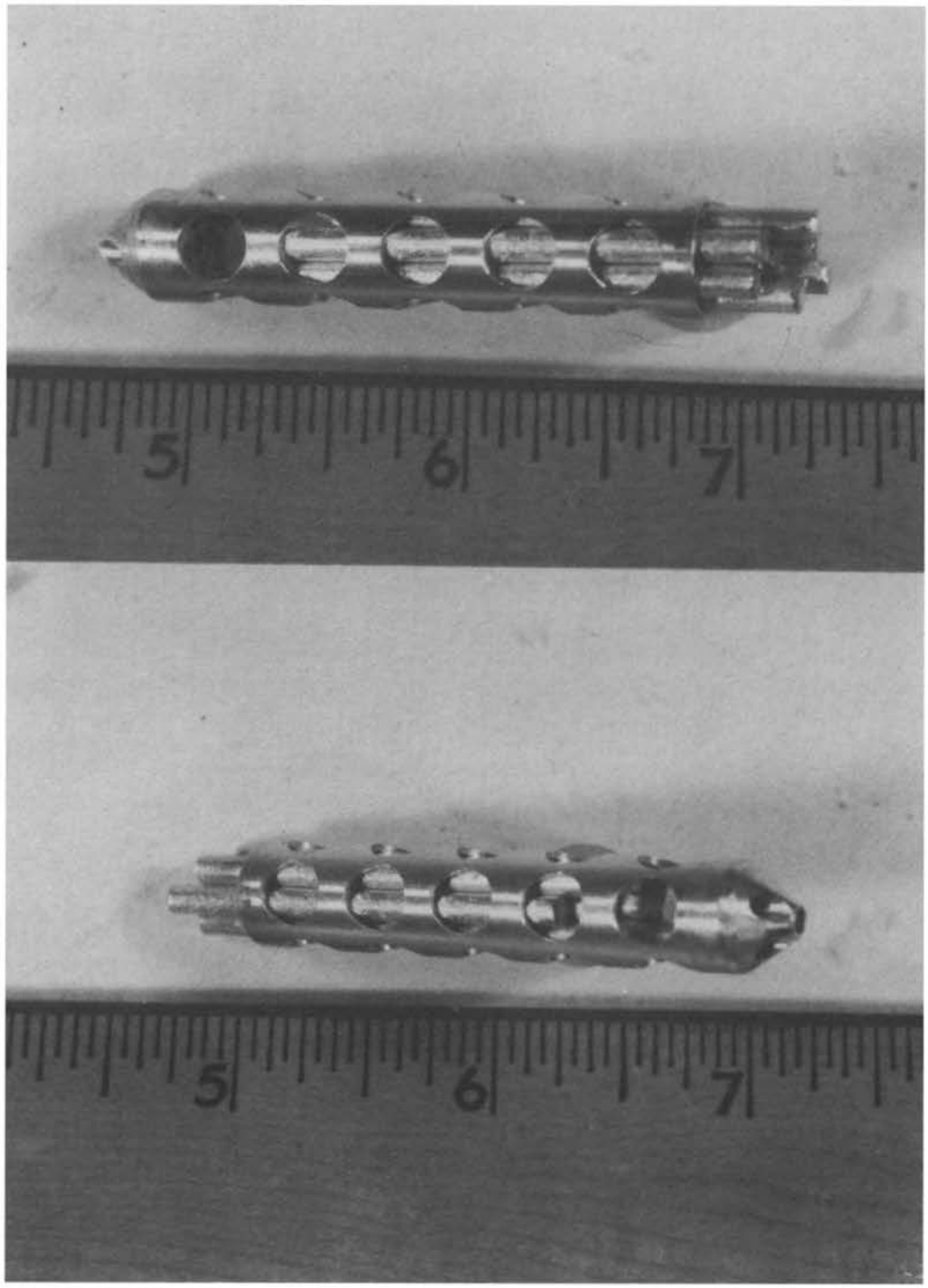

Fig. 2. Views of a HFIR hydraulic tube capsule and specimen rods.

typical contents of a capsule consisted of five to seven rods of Cominco Grade 69 aluminum, either 0.125 or 0.100 in. diam. and 1.75 in. long. These rods were carefully cut to length using a jeweler's saw with very-fine-tooth blade. Specimen rods for most irradiations were individually electropolished prior to loading into capsules, in an effort to reduce their postirradiation activity.

An irradiation capsule was assembled by welding on the end caps, using heliarc welding and a chill block to minimize thermal effects to the rods. The Reactor Operations Division conducted the irradiation, noting the date and time of all removals and reinsertions and the position the capsule occupied whenever it was in the core. For the longer irradiations there were many intervening removals and reinsertions. At the end of every 23-day cycle, the reactor was down for one to two days for refueling.

Upon completing the irradiation, a capsule was removed from the core and held in an underwater storage rack for two weeks or more to allow for decay of short-lived activity. It was then transferred to the hot cell facility. Capsules from long-term irradiations were disassembled in a hot cell; however, many capsules were of sufficiently low activity that they could be opened using a tubing cutter in a contamination zone instead of in a hot cell.

The next operation was sectioning the irradiated specimen rods into electron microscopy specimen disks. Unfortunately the equipment available for cutting contaminated material was restricted to handling only specimens with activity less than 75 mr/hr. The activity of a single specimen rod, measured about a month after the end of irradiation with

a "Cutie Pie" detector, ranged from about 50 mr/hr for the specimens irradiated to only 10^{19} neutron/cm^2 up to about 7.5 r/hr for the material irradiated to 10^{22} neutrons/cm^2. Although several cleaning methods were tried, the greatest reduction of postirradiation activity was achieved by electropolishing the surface. A later experimenter[80] found that electropolishing specimen rods of this material prior to irradiation reduced the postirradiation activity by up to an order of magnitude. This practice was also adopted. A gamma-ray spectral analysis of the postirradiation activity yielded important contributions from Cr^{51}, Fe^{59}, Co^{60} (all contaminants known to be in the HFIR cooling water) and Au^{198}. The latter element is apparently a residue from processing since other high purity metals, including gold, are drawn through the same dies that formed this aluminum wire. Therefore nearly all the high postirradiation activity could be traced to activated surface contaminants.

General information on the irradiations is compiled in Table VI; it includes special irradiations to be discussed later. Fast neutron fluences greater than 0.82 and 0.1 MeV are shown. The 0.82 MeV cutoff is the cutoff level closest to 1.0 MeV in an available multi-group diffusion theory calculation. It has been increasingly common in the literature to regard neutrons of energy > 0.1 MeV as capable of causing radiation damage structural effects, so the fluence for E > 0.1 MeV is given also.

To isolate the effect of fast neutron fluence on void formation, similar specimens were irradiated in identical capsules in the same irradiation facility and in contact with a temperature-controlled coolant flow. Thus the irradiation temperature was nearly constant. Determining the actual value of the temperature during irradiation was difficult.

Table VI. Details of the Irradiations

Capsule Ident.	Intended Fluence (neutrons/cm^2 E > 0.82 MeV)	Cominco Lot No.	Total Irradiation Time	Position(s) Occupied	Actual Fluence Received (neutrons/cm^2) E > 0.82 MeV	E > 0.1 MeV
RA	1×10^{17}	6353	134 sec	5	0.84×10^{17}	1.5×10^{17}
RB	1×10^{18}	6353	22.2 min	5	0.83×10^{18}	1.5×10^{18}
RC	1×10^{19}	6353	3.7 hr	5	0.84×10^{19}	1.5×10^{19}
RJ	5×10^{19}	7767	18.5 hr	5	0.42×10^{20}	7.7×10^{19}
RD	1×10^{20}	7767	38.7 hr	4	0.85×10^{20}	1.6×10^{20}
RE	3×10^{20}	5719	146.0 hr	6,7	2.8×10^{20}	5.2×10^{20}
RF	1×10^{21}	6353	22.1 days	7,8	0.87×10^{21}	1.6×10^{21}
RH	1×10^{22}	5719	201.3 days	2,6 mainly	0.88×10^{22}	1.6×10^{22}
RRE-2	3×10^{20}	5719	146.0 hr	6,7	2.8×10^{20}	5.1×10^{20}
DG-E	3×10^{20}	5719	146.0 hr	6,7	2.8×10^{20}	5.3×10^{20}
ORR L939	5×10^{19}	7767	13.7 days	F-8 Tube #12, Bottom	0.77×10^{20}	1.3×10^{20}
ORR 209	2×10^{19}	7767	43.2 days	P5	0.64×10^{20}	1.1×10^{20}

Gamma self-heating of specimen material at the rate of 33.7 watts/gram[81] generated about 30 watts of power in a typical 0.9 g specimen rod. Cooling water flowed through the hydraulic tube at a rate of about 5 gal/min. Its inlet temperature at the top of the tube was about 48°C, while its outlet temperature was 3-5°C higher.[82] With assistance of the Engineering Division, calculations were made to estimate the equilibrium specimen temperature in this environment. Assuming water flow through the capsule of 0.5 gal/min., one-tenth the total flow, and calculating the film coefficient for forced convection under these conditions, the temperature in the rod's interior was calculated to be about 5.5°C above the temperature of the cooling water. The irradiation temperature was therefore estimated to be about 55 ± 5°C.

C. Electron Microscopy

After de-encapsulation and any necessary surface cleaning, a specimen rod was sectioned into slices approximately 0.020 in. thick using a water-cooled cutoff wheel with an 0.010-in.-thick blade. Disk thickness was controlled to within ± 0.002 in. by a dial gauge mounted on the saw and the manual feed allowed the cutting speed to be kept as slow as desired. About a dozen disks were usually cut from a specimen rod and the excess was retained. The remaining rod was sometimes utilized in measurements of the macroscopic density change.

Thinning the specimen disks for electron microscopy was accomplished by a two-stage process which has been described by Dubose and Stiegler.[83] The technique consisted of first jet-polishing a flat-bottomed dimple into each face of the specimen disk such that about 0.004 in. of material remained between the dimples. The disk was then installed in a

conventional electropolishing cell equipped with a detection system to halt the current when penetration of the disk first occurred.

In the first-stage or "jetting" apparatus, an electrolyte of 700 ml ethanol, 120 ml distilled H_2O, 100 ml Butyl cellusolve, and 78 ml $HClO_4$ was used at a temperature of 25-30°C. Varying the jetting current and voltage changed the profile of the dimple from hemispherical through flat-bottomed to quasi-annular. A 75 ma current at 200-300v usually produced the desired flat-bottomed dimple which, when electropolished to penetration, yielded the largest amount of thin area.

The dimpled specimen disk, gripped by platinum-tipped tweezers, served as the anode in an electropolishing cell containing an electrolyte of nominally 1% $HClO_4$ in ethanol. The electrolyte temperature was held at about 0-5°C by an outer bath of methanol and dry ice. The electropolishing current was in the range 50-75 ma, and 10-30 min were required to achieve penetration. Two ports projecting into the cell contained lenses and fiber optics which lead, respectively, from a strong light source and a photo transistor-relay circuit. When a small penetration first appeared, allowing light to pass through, the circuit switched off the polishing current.

Thinned specimens were examined first in an optical microscope at 500x and those found suitable were examined in the electron microscope to obtain data. Three faults were very often found in the thinned specimens. Accidental rough handling of a specimen was likely to induce in the electron image a great number of bend contours which often obscured the features of interest. Some samples (especially of lot 6353) were found to have penetrated prematurely, presumably at a flaw in the

material, yielding only thick-edged holes with no electron-transparent region. The third and most common problem was the occurrence of pitting over part or all of the thin area. The presence of pitting in only one region of a foil did not render it useless, but care had to be taken to identify stray pits and not confuse them with voids. The occurrence of pitting was found to be reduced by prompt bathing of a freshly penetrated foil in distilled water and ethanol; however the problem recurred sporadically for unknown reasons.

The specimen configuration resulting from the preparation described above had several important advantages. The thin foil region was well protected by the thick outer ring which remained after dimpling. Also the specimen was self-supporting in the electron microscope specimen holder, eliminating the need for support grids. The foil was directly connected to a good heat sink, minimizing any effects of electron beam heating during electron microscope examination. Finally, the initial dimpling step removed the material most affected by the cutting of a specimen disk, exposing undeformed inner material for the final polish. As a result there was seldom any evidence of material deformed during preparation.

Most of the electron microscopy was conducted using a 100 kV Hitachi HU-11 transmission electron microscope which was equipped with a tilting stage and a liquid nitrogen cold finger. Occasionally a newer Hitachi HU-200 electron microscope operated at 200 kV was employed, and for the in situ void annealing studies an Hitachi HU-11B modified for ultrahigh vacuum operation was used.

In the taking of data micrographs, a standardized magnification of 21,000x on the photographic plates was nearly always employed. Printed at a 2.5x enlargement, or 52,500x total, this value was a compromise between resolution sufficiently high to detect the smallest voids likely to be present, and the coverage of enough area to encompass a representative population of voids. Typically, 8 to 24 micrographs were taken over a time span of 1 to 2 hours in gathering data from one foil, and at least two foils were examined from every irradiation. Such data would generally include several stereo pairs of micrographs for foil thickness determinations, in different sectors but at about the same radial distance from the hole. Micrographs would then be taken of areas adjacent to each stereo pair. Other data sometimes included micrographs of a representative dislocation loop population, or selected-area electron diffraction patterns to provide crystallographic information on the orientations or facets of voids.

Early stereo micrographs were obtained by tilting the specimen through some desired angle ϕ, often 7°, photographing, rotating the specimen 180°, and rephotographing. However it was found[84] that when the tilting stage registered zero tilt, it could in actuality be tilted at an angle δ up to $\pm$ 1°. The above procedure then introduces an error of 2δ into the desired tilt angle 2ϕ. Thus an alternative procedure was adopted consisting of taking the stereo pictures without rotation at zero and 10° tilt (the maximum obtainable). The actual tilt angles would then be $0° + \delta$ and $10° + \delta$, for a net tilt angle of 10°.

Stereo pairs of electron micrographs were analyzed by measuring the parallax between adjacent high and low features (usually voids) in the

foil, using a Hilger & Watts stereo viewer. In the viewer the features were visible in stereo (the voids distributed in three dimensions looking much like air bubbles inside an ice cube) together with a "floating" light spot which appeared to rise or fall through the foil as a micrometer knob, measuring parallax, was turned. The light spot was first brought level with very low voids several times, then with adjacent high voids and the readings of the micrometer recorded. Their average difference was the parallax Δx. (Before viewing, the pair of micrographs was oriented so that the maximum parallax lay parallel to the horizontal or $\underline{x}$ direction.) By use of the expression:

$$\Delta z = \frac{\Delta x}{M \sin(2\phi)}$$

where

M = magnification of print, and

2ϕ = net angle of tilt,

a value for the separation in depth Δz of the chosen voids was obtained. Several such measurements were made on a stereo pair and the local foil thickness $\underline{t}$ was assumed to be equal to the largest Δz measured. Unlike the customary method of marking the foil surfaces with islands of evaporated metal and measuring their depth separation, the current technique measured only the approximate thickness of the void-containing layer. This value was the most appropriate for use in calculating the concentration of voids, since it did not include the transparent oxide layer of unknown thickness on the foil surfaces. For various foils, thickness values ranging from 1200 Å to 3750 Å were measured; the mean

value for all stereo pairs was about 2250 Å. The uncertainty involved is treated in the discussion of experimental errors at the end of this chapter.

D. Obtaining Void Size Distributions

The Zeiss Particle Size Analyzer is a comparator device in which the size of a light spot is matched to the feature to be measured; activating a foot switch then registers a count for that size into a bank of counters. The counter sizes were calibrated against a millimeter scale. For use with the machine, special 10x enlargements were prepared on single weight, 16 x 20 in. photographic paper; these covered about one-fourth the area of an original plate at a total magnification of 210,000x.

In measuring a particular void, the light spot was opened wide and then smoothly closed down until it just encompassed the outer dark fringe of the void's image, this outer diameter being taken as the closest measure of the void's true size. Such a representation is in accord with the findings of Levy[85] who investigated the electron microscopic contrast effects of inert gas bubbles in metals, and it has also been employed by Claudson et al.[55] Others (e.g., Brimhall and Mastel[3]) have chosen the midpoint of the black fringe as the best diametral measure, but without justification. In attempting to measure nonequiaxed voids, particularly the elongated ones often seen after low fluence or low flux irradiations, an equivalent circular area was estimated and its diameter taken as the effective linear size.

E. Immersion Density Measurements

Measurements of the macroscopic density change of irradiated specimen material were performed using an immersion technique. Samples submitted were either whole or partial specimen rods remaining after the cutting of electron microscopy specimen disks. They weighed from 0.5 to 1.0 g. All density determinations were carried out in a hot cell using remote manipulators and a Torbal model EA-1 balance.

The procedure consisted of weighing the specimen both dry and immersed in n-octal alcohol. Rather than estimate the density of the liquid using temperature-density tables, this quantity was determined directly before and after each specimen density measurement using a stainless steel ball whose volume approximated that of the specimen. The density ρ_s of the stainless ball standard was in turn determined by the same two-stage procedure, using as a standard this time a tungsten carbide sphere of very accurately known weight and dimensions. The following two relations were then utilized:

$$\rho = \frac{w \cdot \rho_l - w^* \cdot \rho_a}{w - w^*}$$

and

$$\rho_l = \rho_s - \frac{w_s^*}{w_s} (\rho_s - \rho_a)$$

where

w, w_s = dry weight of specimen, standard,

w^*, w_s^* = immersed weight of specimen, standard, and

ρ_a = density of air (taken as 0.0012 g/cm^3).

The weights in grams were measured to four decimal places. A discussion

of the estimated errors is given in the last part of this chapter.

F. Unirradiated Control Specimens

Several specimen rods from each of the three lots of material were annealed for ten days in HFIR-type deionized water at 60°C to simulate the thermal and water exposure experienced by irradiated specimens. These rods then served as unirradiated control specimens for the immersion density and the microhardness measurements; some were sectioned to provide electron microscopy specimens.

No voids were observed by electron microscopy of the unirradiated control material, as expected. However a very few, scattered, presumably "grown-in" dislocation loops were observed. Little difference could be detected between the three lots, except that the lot 6353 material contained more frequent impurity bodies and it almost always exhibited a peculiar diffuse form of surface pitting. Whether irradiated or unirradiated, this lot of material proved quite difficult to thin.

G. Microhardness Testing

Microhardness testing was performed on all irradiated and control materials, using a Kentron model AK microhardness tester equipped with a Filar eyepiece and a 50x objective lens. The optimum load was found to be 50 g. A certain waviness in the sides of some indentations was noted, but a 25 g load only yielded smaller indentations possessing similar irregularities. Slices of each specimen rod were mounted to present a transverse section for testing and six measurements were made, commencing from the center of a section radially outward in two orthogonal directions. However, no significant influence of interior location upon the

hardness was found. In a section of the material irradiated to 10^{18} neutrons/cm^2, an anomalously high, but reproducible, hardness was measured at the central location. Since this material came from the #6353 "bad lot," it is thought that the high value may have been due to the presence of an impurity body.

H. Electron Microscope In Situ Void Annealing

The void annealing experiments were performed using an Hitachi HU-11B electron microscope which had been modified for operation under very high vacuum (10^{-7} to 10^{-8} torr). The modifications, described by Braski et al.,[86] essentially consisted of replacing the original diffusion pumps with ion pumps and titanium sublimator booster pumps. Entirely new high-vacuum feedthroughs were also designed and fitted for most of the controls on the microscope column. This instrument provided a very low contamination environment and permitted continuous monitoring of the void annealing behavior for long times at elevated temperature.

A standard Hitachi tilting hot stage with a modified specimen holder was used to heat the specimens; the lower portion of the specimen holder is shown in Fig. 3. The specimen was held in contact with a coil-heated hearth plate by the stainless steel spacers. A Chromel-P versus Alumel thermocouple, attached to the specimen holder as shown, was used to monitor specimen temperature. During each specimen insertion the thermocouple leads were manually connected to leads from an accurate potentiometer. This thermocouple was calibrated to read the specimen temperature by the use of a dummy specimen containing a similar thermocouple. The absolute accuracy of this apparatus for sensing specimen

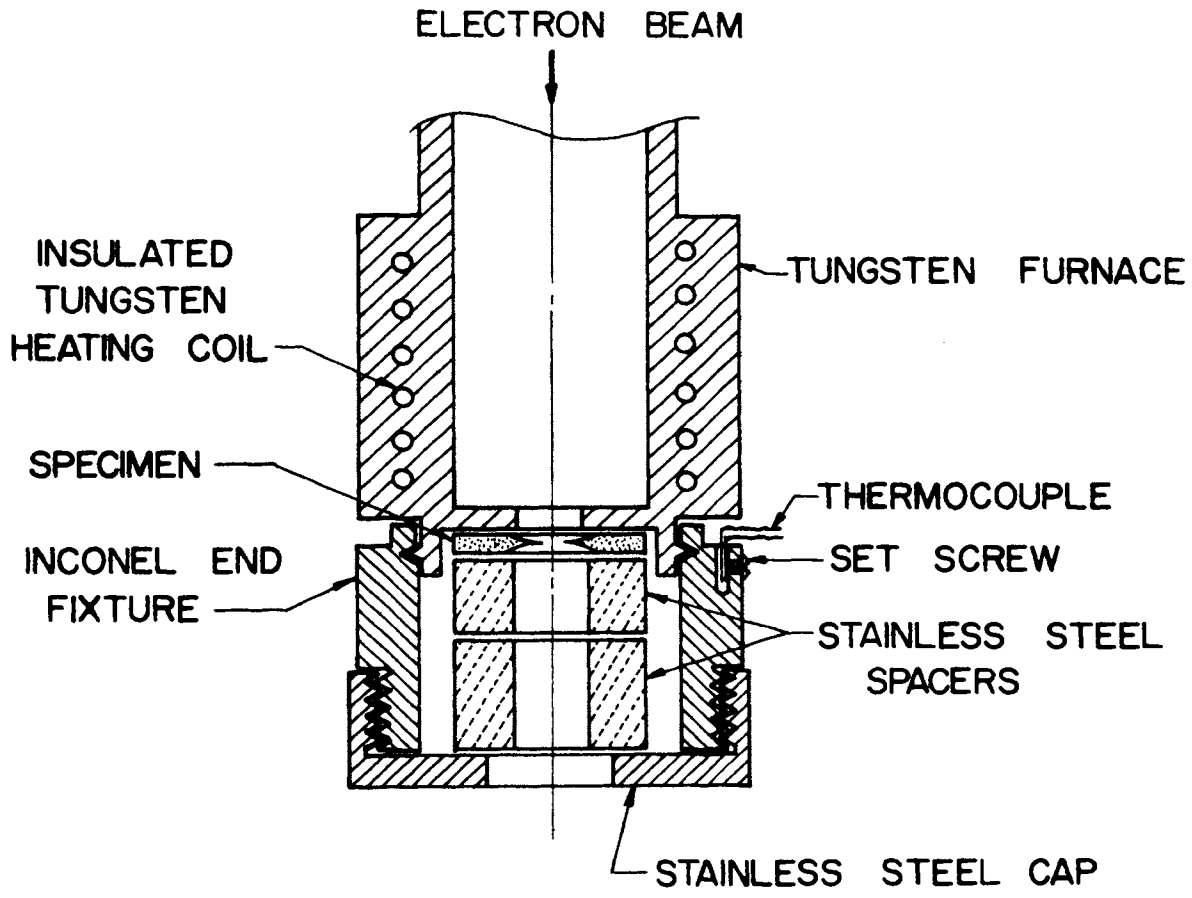

Fig. 3. Lower portion of specimen holder used in void annealing studies.

temperature was within ± 10 to 15°C. However, the relative accuracy from one specimen to another was within ± 5°C, and during any single annealing run, measured temperature variations could be held to within ± 1°C. A specimen was raised to the annealing temperature (generally 150°C) in approximately 5 min., after which from 14 to 18 electron micrographs of the voids were taken at various times during the anneal.

Changing void sizes were measured directly on the photographic plates by a boom-mounted zoom microscope, a light box, and a 0.1 mm-calibrated reticle. A Bausch & Lomb 7x measuring magnifier was later found to be equally effective. This method, though somewhat tedious, eliminated size errors which might have resulted from enlarging or print shrinkage. The estimated maximum error in the void-diameter measurements was ± 0.05 mm, which corresponds to ± 19 Å at the standardized plate magnification of 26,000x used throughout. The sizes of about 30 voids were followed through each annealing sequence, out of a total of 100 or more present in the field of view at the start of each run (for fluences of 3×10^{20} neutrons/cm^2 or higher).

I. Flux-Effect Experiments in the ORR

Experiments were undertaken to assess the influence of fast neutron flux upon void formation by irradiating samples of the material to fluences matching one or more of the HFIR irradiations in the Oak Ridge Research reactor (ORR) which has a flux about an order of magnitude lower than that of HFIR.

The first such experiment involved attaching three specimen rods to the bottom end-plate of a large experimental assembly (no. ORR 209)

which was to occupy a "poolside" location with a flux about 40 times lower than that of the HFIR irradiations. Removed at the end of one ORR cycle (43 days), it received a fluence of 1.1 x 10^{20} neutrons/cm^2 (E > 0.1 MeV). The resulting voids were of unusual shape and inexplicably large. The experiment was therefore repeated, this time with specimen rods and a thermocouple similarly mounted inside an identical assembly, no. ORR 213. The thermocouple indicated a temperature of 103°C inside the experiment can (which housed in-pile creep units with heaters) at the location of the specimen rods; clearly the irradiation temperature was not the 35°C of the pool water surrounding the can, as had been supposed. It is clear that these experiments did not yield evidence for an effect of flux, which should be a far more subtle influence than is the irradiation temperature.

A second type of experiment was therefore attempted. Specimen rods and a flux monitor wire were encapsulated and irradiated in the ORR hydraulic tube at core location F-8, tube #12, bottom position. The capsule was somewhat larger than, but essentially similar to, the HFIR capsules, and it also had side and end holes to permit the cooling water at 48-54°C, essentially the same temperature as in HFIR, to contact the specimen rods. The use of a flux monitor wire was especially important here because unlike the HFIR, the ORR core configuration (location of fuel, moderator, absorbers, etc.) is changed from time to time, changing the flux and fluence levels at any given location. The initial flux estimate, upon which was based the calculation of irradiation time required to attain the intended fluence, was thus subject to considerable error; a fluence of 5 x 10^{19} neutrons/cm^2 (E > 0.82 MeV) was desired but

the actual value attained was 7.7×10^{19} neutrons/cm^2. This latter value did not differ greatly, however, from the 8.5×10^{19} neutrons/cm^2 fluence received by the HFIR "RD" capsule, so an examination of the effect of varying neutron flux, at fixed fluence and temperature, was finally made possible.

Variations in the neutron energy spectrum must be considered whenever irradiation results from different reactors are to be compared. A number of important processes often are going on simultaneously during irradiation, and each can depend quite differently upon neutron energy. In most metals, defect clusters including voids can result from lattice-fast neutron collisions in which the incident neutron energy is greater than about 0.1 MeV, as already noted. However the generation of helium in fast neutron transmutation reactions is only effected by even more energetic incident neutrons (greater than about 8 MeV in aluminum), while on the other hand the production of silicon by transmutation of aluminum is a thermal neutron reaction.

There does seem to be a general similarity between the neutron spectra of the HFIR and ORR reactors (for the core locations utilized in this flux-effect experiment), as is evident in the data presented in Table VII. If only energies in the fast neutron range (the first three columns) are considered, the spectra are quite similar, and even if thermal fluxes are included, the ORR-HFIR flux ratio still varies by less than a factor of two over nearly the entire range of neutron energies.

Table VII. Comparison of the HFIR and the ORR Neutron Spectra

Reactor; Core Location	Neutron Flux (neutrons/cm^2/sec) E > 8 MeV (x 10^{12})	E > 0.82 MeV (x 10^{14})	E > 0.1 MeV (x 10^{14})	E > thermal energy (x 10^{15})
ORR ; F-8	0.5 (87)	0.65 *	1.1 *	0.2 *
HFIR ; hydraulic tube	4.4 (87)	6.5 *	11.9 *	3.4 (88)
Ratio: ORR / HFIR	0.11	0.10	0.09	0.06

*Values determined by flux wire, this study.

J. Experimental Errors

The possible errors associated with the measurements or estimates of (1) the fast neutron flux and fluence, (2) the foil thicknesses, from which were calculated the void concentration values, (3) the immersion densities, and (4) the microhardness are discussed in this section. The uncertainty in another important factor, (5) the irradiation temperature, has already been considered.

The procedures involved in determining the fast neutron flux are taken up in more detail in Appendix A. The error involved corresponds essentially to the uncertainty in knowing the effective neutron cross section of the flux wire material, Co-doped stainless steel. This uncertainty is on the order of 10-15%, so the flux and also fluence values are uncertain to a like degree (the irradiation time being known quite accurately). Good agreement (within 5%) was also obtained between these flux wire results and the computer-calculated flux values of Sims[89] which are felt to be of similar accuracy.

Several measurements subject to error are involved in the calculation of the void concentration and the swelling values. The former quantities were obtained by straightforward calculation using:

$$N = \frac{n}{(\ell/M \times w/M \times t)}$$

where

N = void number density,

n = number of voids observed in area ℓ x w on micrograph,

M = linear magnification of micrograph, and

t = foil thickness.

Uncertainties in $\underline{M}$ and $\underline{t}$ are frequently taken to be ± 5% and ± 20% respectively, and enough micrographs at one fluence (3×10^{20} neutrons/cm^2) were examined to obtain an estimate of ± 30% of the mean value as the standard deviation of $\underline{n}$. Combining these uncertainties by the rules of propagation of error yielded an uncertainty of ± 35% for both void concentration $\underline{N}$ and swelling $\Delta V/V$. Error bars on Figs. 26 and 28 reflect this uncertainty except for the lowest fluence where a ± 50% possible error is indicated.

The error bars for the immersion density measurements which also appear on Fig. 28 represent simply the range of values obtained in the testing. Unfortunately not enough repeated measurements were conducted to permit determination of standard deviations. An attempt to calculate an overall uncertainty, on the basis of the estimated weighing sensitivities combined by propagation of error methods, yielded extremely large error bars (e.g., an uncertainty of ± a factor of ten for the lowest immersion density data point). Nevertheless the immersion density values did appear to be consistent with the values obtained from electron microscopy observations.

The microhardness measurements were repeated five or ten times per specimen. Estimates of their standard deviations were obtained from the ranges of values using the small-sample conversion factors of Davies and Pearson;[90] these σ estimates comprise the error bars in Fig. 31.

IV. RESULTS

A. Fluence Effects

Examples of voids observed in 99.9999% aluminum, all at a magnification of 58,000x are presented in Fig. 4. The fluences on the figure are nominal values for the fast fluence (E > 0.82 MeV); see Table VI for the exact values (E > 0.82 or > 0.1 MeV). With increasing fluence the voids increase both in number and size, as shown by the statistical information collected in Table VIII.

No voids were observed at fluences of 10^{17} and 10^{18} neutrons/cm^2. Low densities of dislocation loops were found--about 2 x 10^{12} and 5 x 10^{12} loops/cm^3 for the 10^{17} and 10^{18} irradiations, respectively. A low concentration of "grown-in" loops (about 10^{12} loops/cm^3--one or two per plate at the standard magnification) was observed in the unirradiated control material. This "background" level has been subtracted from the data in arriving at the above approximate figures.

At a fluence of nominally 1 x 10^{19} neutrons/cm^2, widely dispersed small voids were observed. The voids were only found upon subsequent close inspection of micrograph plates or prints and were not visible on the electron microscope screen at the standard magnification employed. Only rarely was more than one void seen on the same plate, and many times no voids were detected on plates in which the focus (on other features) was judged adequate to reveal voids if present. Therefore the void concentration value given in Table VIII is quite approximate. An interesting exception to the general rule of widely isolated voids is seen in Fig. 5. Seven voids are present, four of which are located apparently in close pairs (the voids' separation in depth is not known but

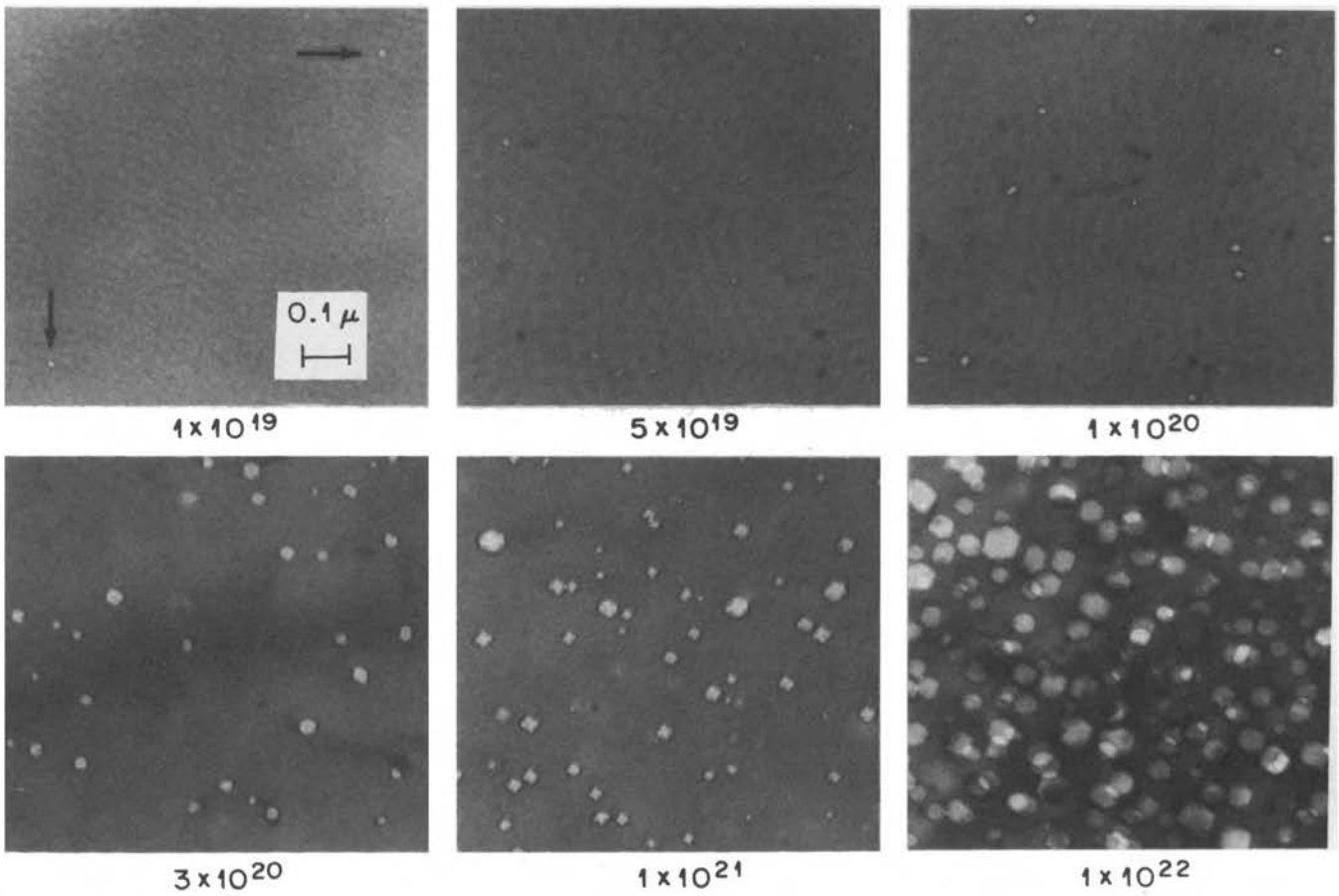

Fig. 4. Examples of voids produced over the range of fluence studied.

Table VIII. Collected Statistics on the Observed Void Populations

Capsule Ident.	Nominal Fluence (neutrons/cm^2, E > 0.82 MeV)	Void Max. Size (Å)	Void Mean Size (Å)	Number of Voids/cm^3	Calc. Total Void Volume (%)	Number of Loops/cm^3
RC	1×10^{19}	238	161	$\approx 1 \times 10^{12}$	---	2×10^{13}
RJ	5×10^{19}	320	201	2.1×10^{13}	0.01	8×10^{13}
RD	1×10^{20}	401	244	3.8×10^{13}	0.03	1×10^{14}
RE	3×10^{20}	583	299	1.1×10^{14}	0.19	3×10^{14}
RF	1×10^{21}	712	329	3.9×10^{14}	0.86	$\approx 2 \times 10^{14}$
RH	1×10^{22}	1020	495	5.9×10^{14}	7.4	---
ORR L939	1×10^{20}	609	323	1.9×10^{13}	0.04	5×10^{13}
RRE-2	3×10^{20}	320	226	2.6×10^{13}	0.17	---
DG-E	3×10^{20}	532	279	1.0×10^{13}	0.15	---

Fig. 5. Possible void-pairs after irradiation to 10^{19} neutrons/cm^2.

presumably small). It is plausible that these void pairs may be the precursors of elongated voids found especially at the next higher fluence.

At the 5×10^{19} and 1×10^{20} neutrons/cm^2 fluences, a considerable proportion of the voids were elongated. Close examination of such voids often revealed transverse indentations or striations suggesting that these voids had formed from the merger of adjacent, small, equiaxed voids and that the coalescence was not yet complete. Some of these features can faintly be seen in the second picture of Fig. 4. Also at these lower fluences, the voids were distributed rather heterogeneously within the material.

At 3×10^{20} neutrons/cm^2, there was a considerable increase in the average void size (see Table VIII) and the overall spatial distribution was less heterogeneous. Nearly all voids were equiaxed. By 1×10^{21} neutrons/cm^2, the average size was still larger, the distribution was approximately homogeneous, and the void shapes displayed greater symmetry and more well-developed facets. At 1×10^{22} neutrons/cm^2, the void sizes and numbers increased further; the total void volume fraction was about 7.4% as determined by immersion density measurements. This is as high a void volume fraction as has been reported for any irradiated material to date, and certainly the highest for aluminum.

In various cases the projected void shapes took the form of squares, rectangles, hexagons, and rhombs. All of these projected shapes are consistent with different views of an octahedron as illustrated in Fig. 6. In several cases discussed in Appendix B, this interpretation was checked by analyzing selected area diffraction (S.A.D.) patterns corresponding

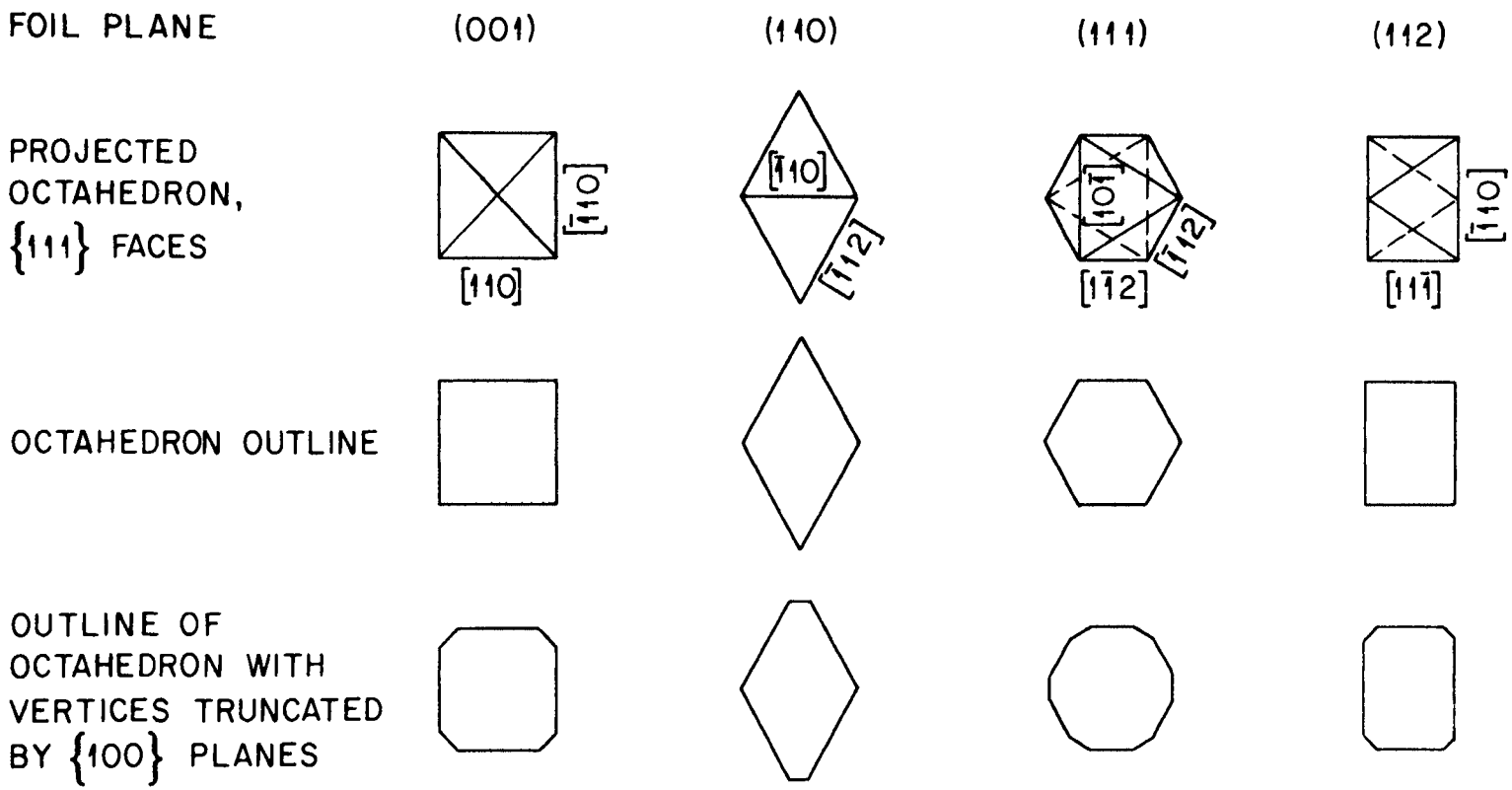

Fig. 6. Differing views of an octahedral void bounded by {111} planes.

to void-containing micrographs. In each case the crystallographic orientation was consistent with octahedral voids bounded by {111} planes, sometimes having the corners truncated by {100} planes. Similar conclusions have been reached for quenched-in voids in aluminum.[91]

Voids were never observed to lie upon grain boundaries; rather there always existed a region clear of voids on each side of a grain boundary. Not many grain boundaries were seen in this study because of the large grain size of this high purity material. Still, the available observations suggest that there was little or no influence of neutron fluence upon the width of the denuded zones, at least up to 1×10^{21} neutrons/cm^2. No boundaries at all were observed in the thinned regions of specimens irradiated to the highest fluence. The denuded zone widths were on the order of 0.3 microns.

Void size data obtained by the use of the Zeiss Particle Size Analyzer was initially used to obtain an individual size distribution histogram for each irradiation; the histogram for the 1×10^{21} neutrons/cm^2 irradiation is shown (Fig. 7). The ordinate is simply the percent of voids found in each size range (i.e., in each counter of the Zeiss Analyzer--approximately 30 Å size increments for the micrograph enlargements employed). From these histograms such information as the peak (most frequently observed) and the maximum observed void sizes could be obtained. Relatively speaking, these histograms were narrow and high (up to 33%) for the low fluence irradiations, and lower but much wider for the high fluences; the area underneath each was unity.

To compare the void size distributions from different irradiations, it was felt preferable to substitute as the ordinate the number of voids/cm^3 in the size range. The void size distribution curves for five of

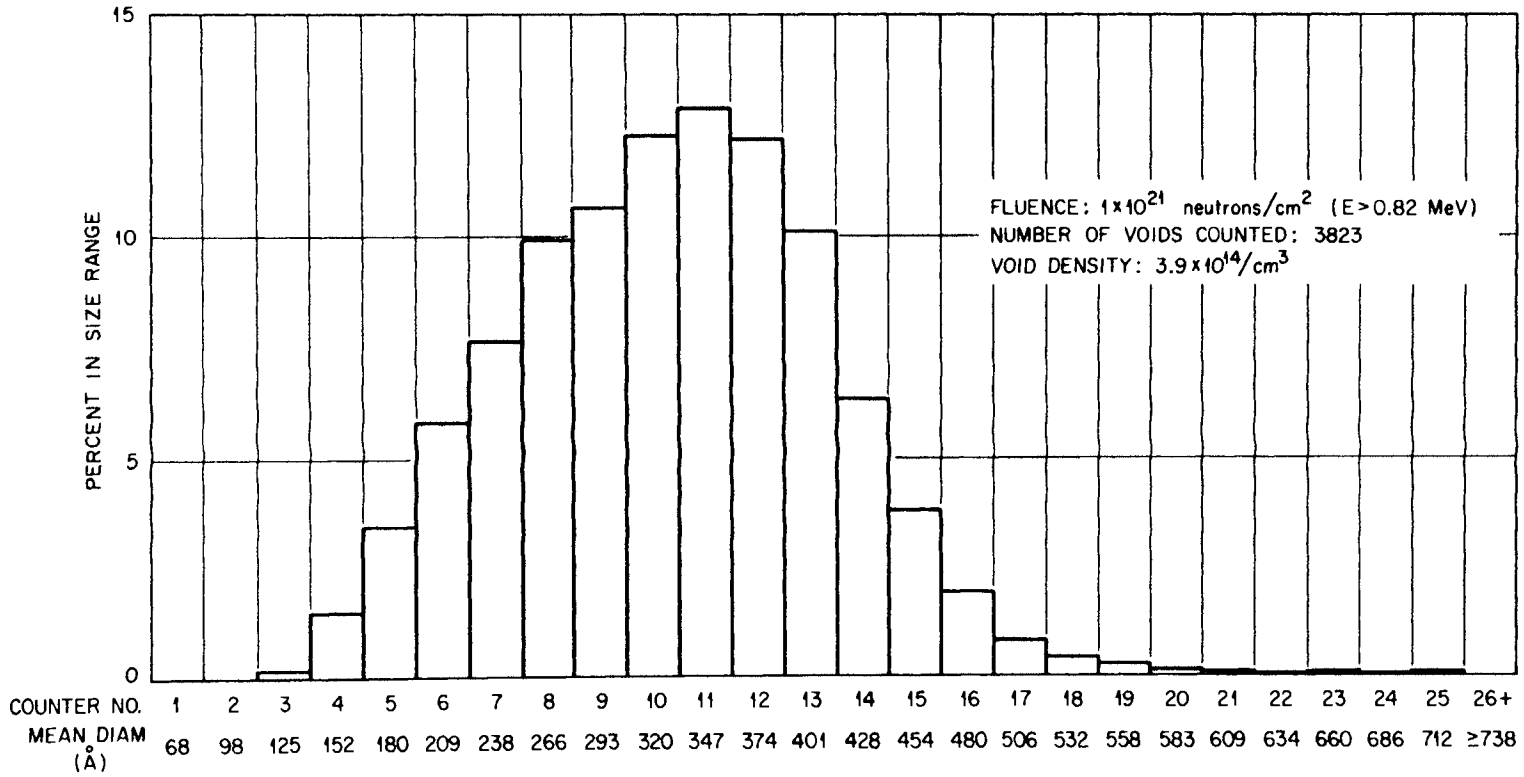

Fig. 7. Example of a void size distribution histogram.

the irradiations are plotted this way in Fig. 8, and for the lowest three void-producing irradiations in Fig. 9. The areas under these curves represent the relative void concentrations resulting from the different irradiations. It is evident that both the most common and the maximum void sizes increase continuously with increasing fluence. The shapes of the curves, which for the smallest observable void sizes all begin at low values, imply that not very many voids must have been present which were too small to detect. Only 58 (widely scattered) voids were measured for the 10^{19} irradiation and about 300 each were measured for the next two higher fluences. Considerably larger numbers of voids (1800-3800) were measured in obtaining void size distributions for the 3×10^{20}, 10^{21}, and 10^{22} irradiations; the greater numbers resulted from the higher void concentrations in these cases.

With the void size distribution and void concentration data, a value for the total void volume fraction resulting from each irradiation was calculated. The results are included in Table VIII and are also plotted as a function of fluence in Fig. 28, assuming spherical void shapes. The total void volume was also calculated assuming octahedral and cubic void shapes, generating for these cases void volume figures uniformly a factor of two to three lower than those shown for the spherical case. The lower values agree less well, however, with the immersion density results than do the spherical assumption values. The arithmethic mean void diameter was also calculated for each irradiation, and the resulting values are listed in Table VIII.

The density-decrease values obtained from immersion density measurements on the same irradiated material are also plotted on

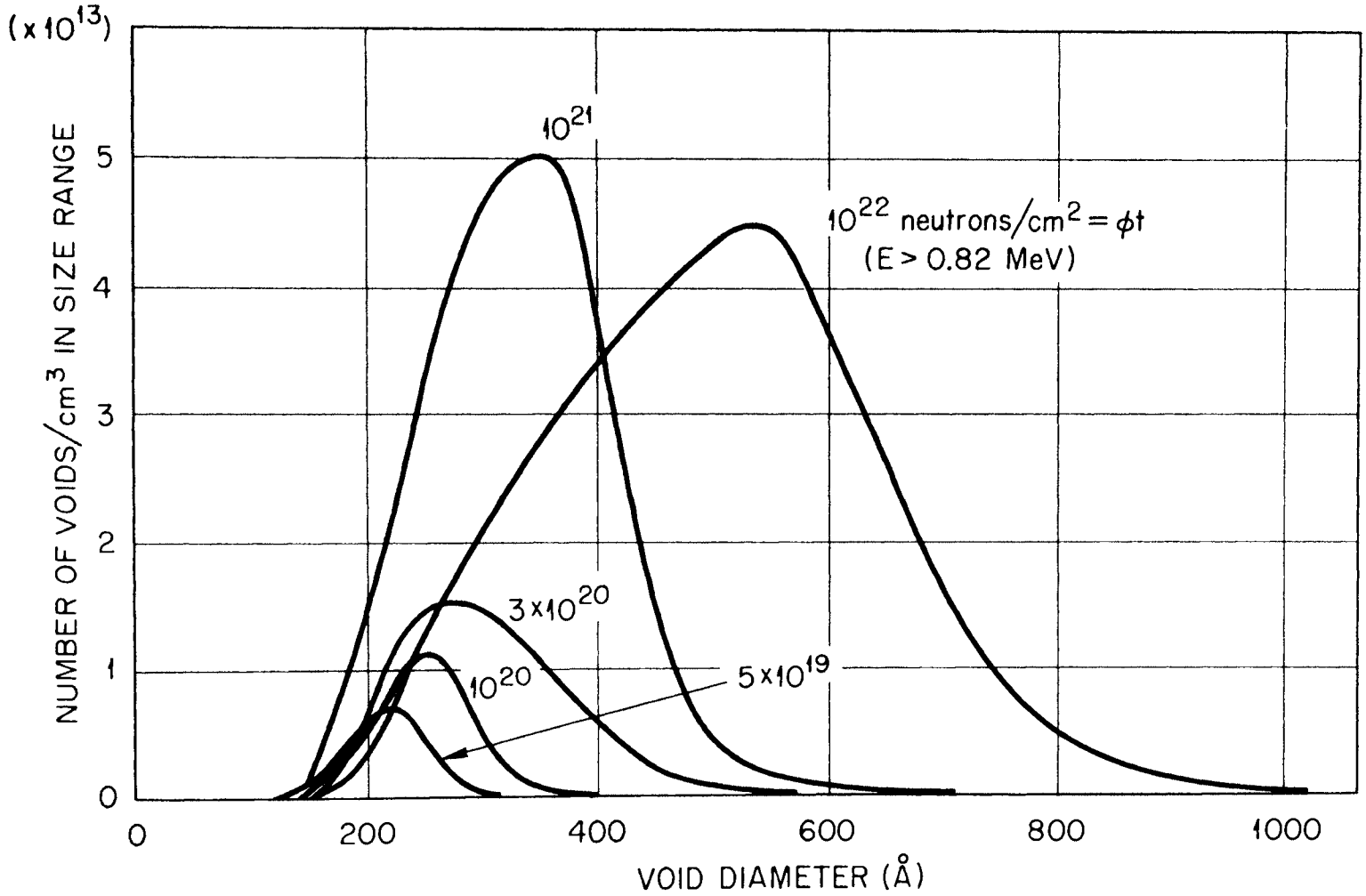

Fig. 8. Void size distribution curves for all except the lowest fluence.

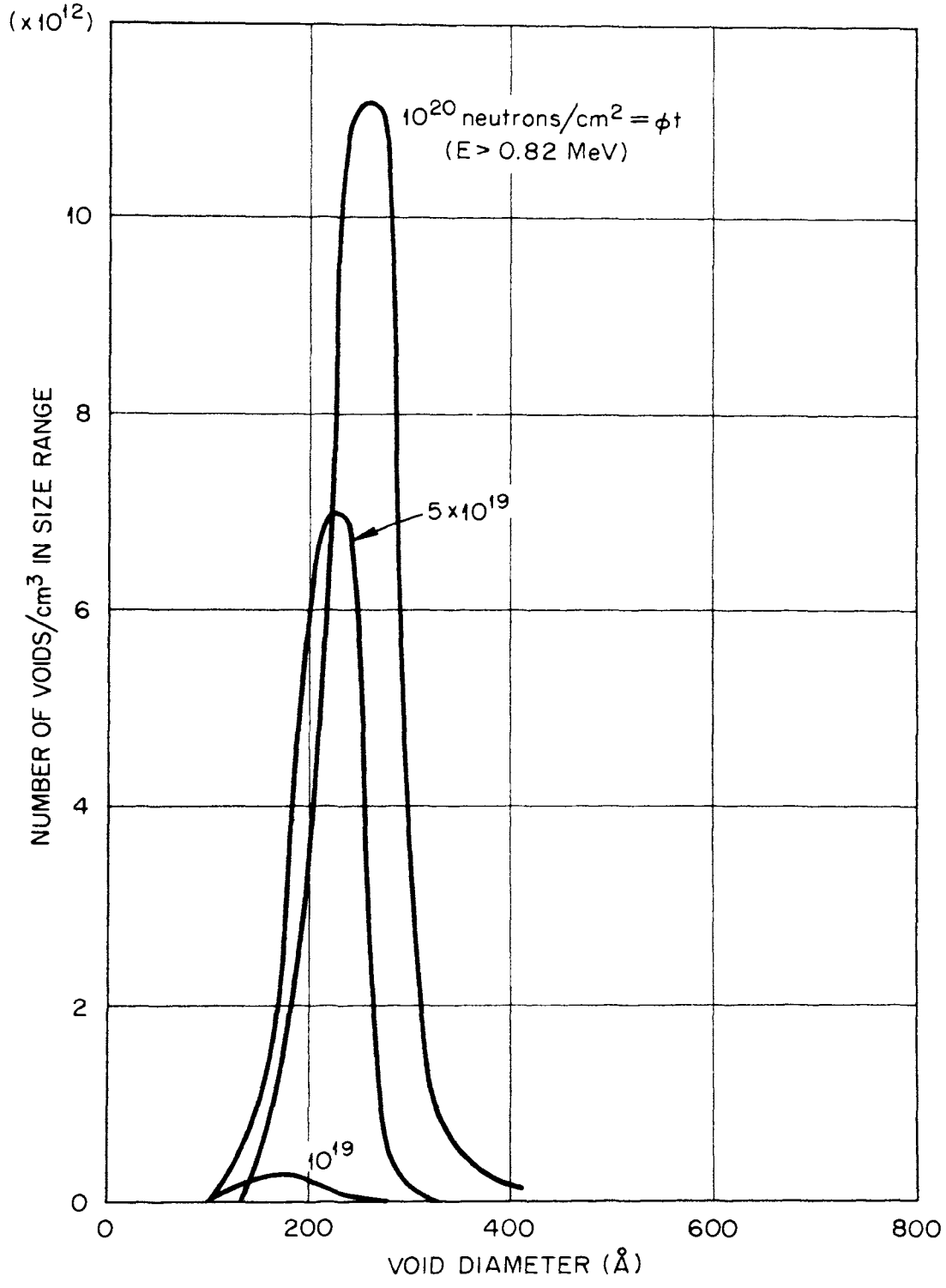

Fig. 9. Void size distribution curves for the lower three fluences.

Fig. 28. While the agreement between the two techniques is relatively good, better utilization of the data results from allowing each set to complement the other. At the highest fluence where swelling exceeds 5%, the immersion density figure is certainly the more reliable, considering the very small overall volume of material that is examined in the electron microscopy technique. However, for the irradiations which yielded volume changes approaching 0.1%, the immersion density measurements are less reliable; the technique is at the limit of its application. Taken together, the best swelling data include the lower five calculated (from microscopy) values plus the immersion density result for the 10^{22} irradiation.

It was extremely difficult to obtain any reproducible information about the concentration of dislocation loops in the irradiated materials. However approximate values of the loop concentration are listed in Table VIII and are plotted with uncertainty indicated in Fig. 26. At the lower fluences, the loops appeared as black dots, often exhibiting a line of no contrast down the middle, or occasionally in a closed loop form. Their size increased somewhat at intermediate fluences. In the material irradiated to 10^{21} neutrons/cm^2 (shown in Fig. 10), in addition to some smaller loops, there appeared a large number of dislocation segments which may have been segments of larger loops that had grown to intersect the foil. If this previously proposed hypothesis[5] is correct, then a wide range of loop sizes (perhaps from 10^2 to 10^4 Å) resulted from this irradiation. Upon a fluence increase to 10^{22} neutrons/cm^2, the loop structure appeared to consist primarily of similar "large loop" segments; no meaningful value for the loop concentration was obtained. Whether

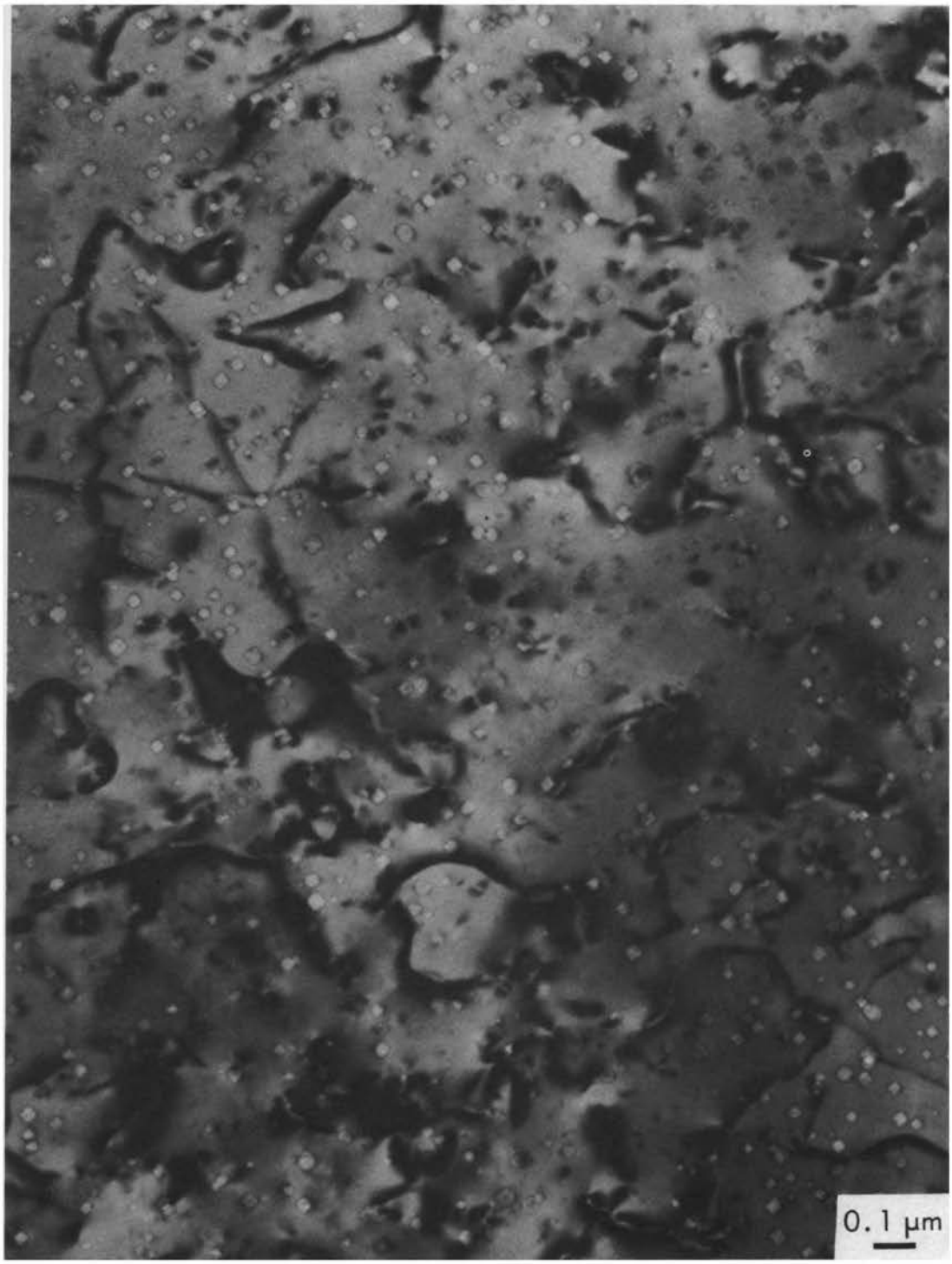

Fig. 10. Dislocation loops and segments after irradiation to 10^{21} neutrons/cm^2.

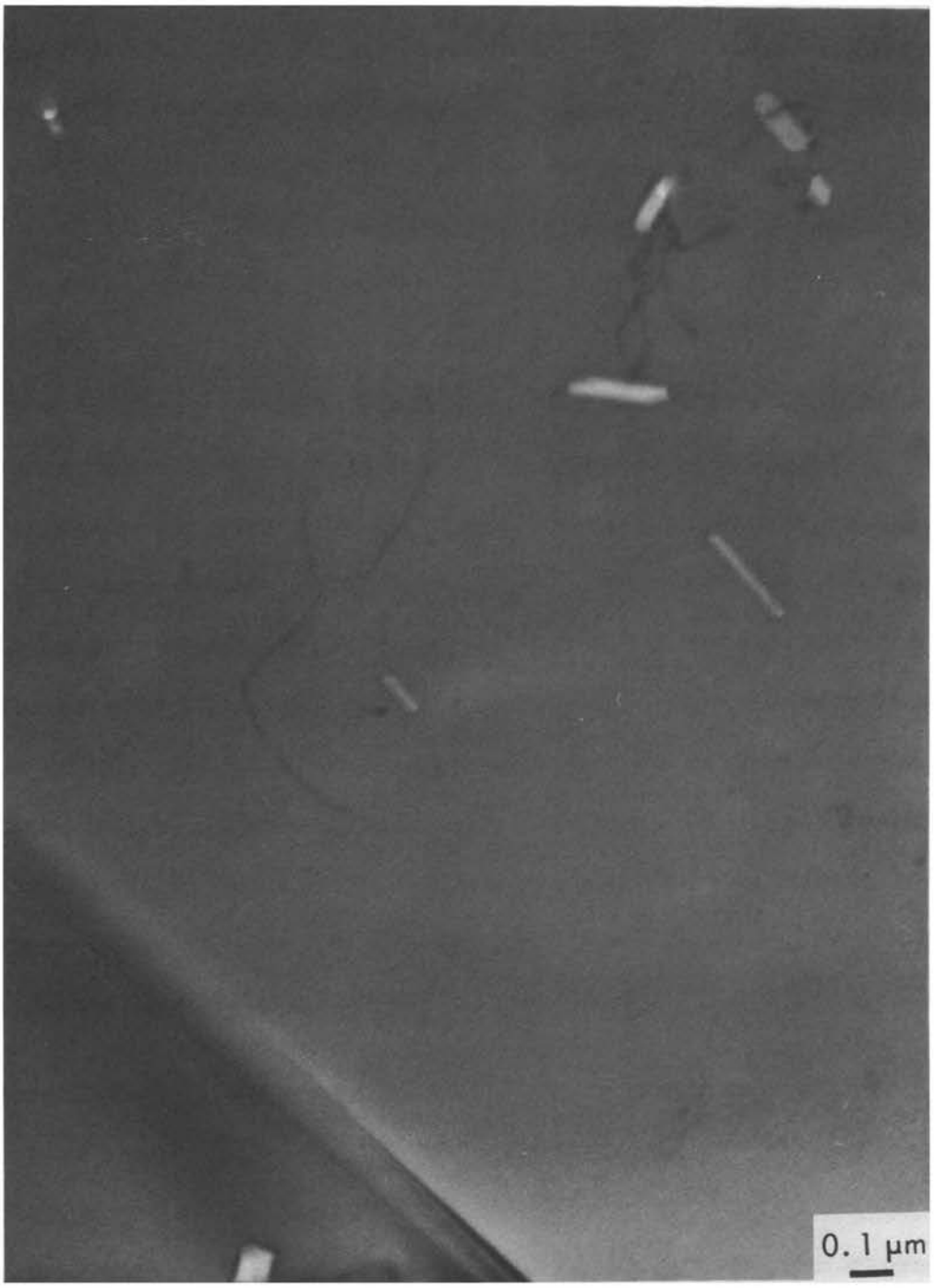

Fig. 11. Voids resulting from irradiation at a temperature of ≈ 100° C.

the dislocation loops were vacancy or interstitial was not determined. The interstitials produced by the irradiation may be represented in dislocation loops and segments and/or may be in an unobservable form.

Results of microhardness measurements made on the irradiated material are shown in Table IX. The hardness is seen to increase continuously with increasing fluence.

B. Flux Effects

As mentioned earlier, some irradiations were conducted in facilities other than the HFIR hydraulic tube in an attempt to distinguish the effect of neutron flux upon void formation. However two of these irradiations were subsequently found to have been carried out at temperatures significantly higher than that of samples irradiated in the HFIR hydraulic tube. Since the irradiation temperature itself is known to have a profound influence upon void formation, any effects resulting from these irradiations' lower flux would have been masked.

The voids resulting from irradiation in the ORR 209 experimental assembly in fact show the marked changes in morphology associated with irradiation at a higher temperature. The temperature in the vicinity of the specimen rods was about 103°C, the flux and the fluence were 3.0×10^{13} neutrons/cm^2/sec and 1.1×10^{20} neutrons/cm^2 ($E > 0.1$ MeV) as determined by a flux monitor wire, and the resulting voids were relatively few in number but extremely large and often greatly elongated (Fig. 11). Similar but larger so-called "supervoids" were observed[64] in the same material irradiated to a fluence of 4×10^{20} neutrons/cm^2 ($E > 0.82$ MeV) at irradiation temperatures of 150 and 125°C.

Table IX. Variation of the Microhardness with Fluence

Sample Ident.	Lot No.	Nominal Fluence (E > 0.82 MeV)	Hardness (DPH)	Percent Increase
C-3 (Control)	7767	unirradiated	17.9	---
C-4 (Control)	6353	unirradiated	17.1	---
C-6 (Control)	5719	unirradiated	18.6	---
RA	6353	1×10^{17}	17.1	0.0
RB	6353	1×10^{18}	18.2	6.4
RC	6353	1×10^{19}	18.1	5.9
RJ	7767	5×10^{19}	21.0	17.3
RD	7767	1×10^{20}	22.6	25.7
RE	5719	3×10^{20}	27.4	47.3
RF	6353	1×10^{21}	35.5	107.6
RH	5719	1×10^{22}	48.3	160.0
RRE-2	5719	3×10^{20}	39.6	112.9

For the specimen rods irradiated in a perforated capsule (ORR L939) in a hydraulic facility of the ORR, however, the irradiation temperature was about 55°C, the same temperature as that of specimens irradiated in HFIR. For this irradiation the neutron fluence of $7.7 \pm 0.2 \times 10^{19}$ neutrons/cm^2 (E > 0.82 MeV), determined by a flux monitor were included in the capsule, was quite close to the fluence of 8.5×10^{19} neutrons/cm^2 (E > 0.82 MeV) received by the RD capsule of the main study. With temperature and fluence roughly equalized, it was possible to look for differences in void morphology caused by the order of magnitude difference in flux. Micrographs of specimens from both irradiations are shown in Fig. 12, the respective void size distributions in Fig. 13, and statistical comparisons in Table VIII. The material irradiated at a ten times slower rate contained half as many voids, but they were larger so that the total void volume was comparable to that produced at the higher rate. Some of the low-flux voids were more elongated than any observed in the higher flux irradiations. Also the low-flux voids were considerably more heterogeneous in spatial distribution; occurrence in patches or strings was more the rule than the exception.

C. Reirradiation Experiment

Another experiment involved the reirradiation of material which had previously been irradiated and then annealed to remove structural damage including voids. Though the second irradiation matched the fluence and conditions of the first irradiation, the resulting voids were markedly different. Electron micrographs showing voids present after the first and second irradiations are presented in Fig. 14, and the void size distributions appear in Fig. 15. A much wider range of void sizes was

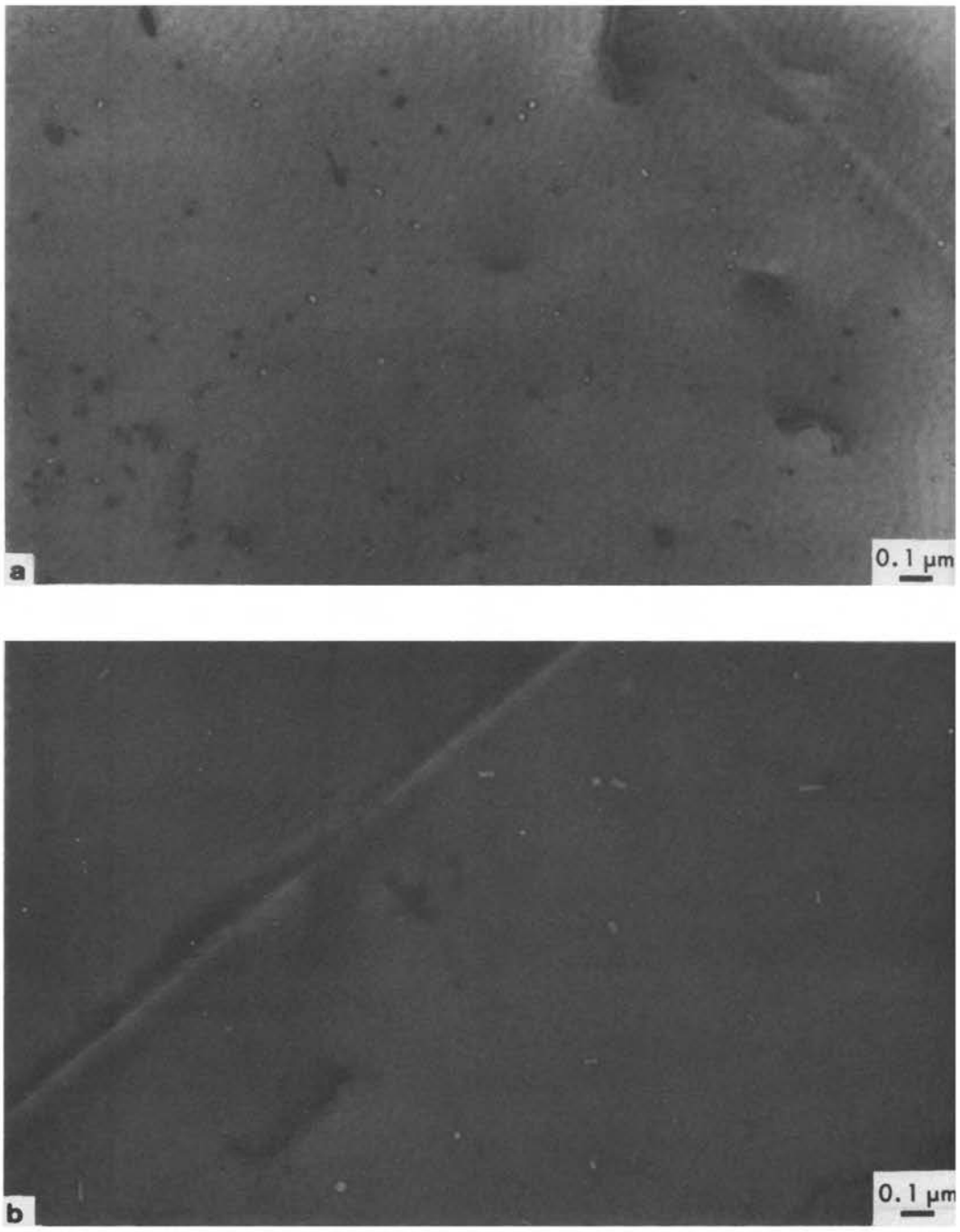

Fig. 12. Voids resulting from irradiation to 10^{20} neutrons/cm^2 at (a) high flux and (b) low flux.

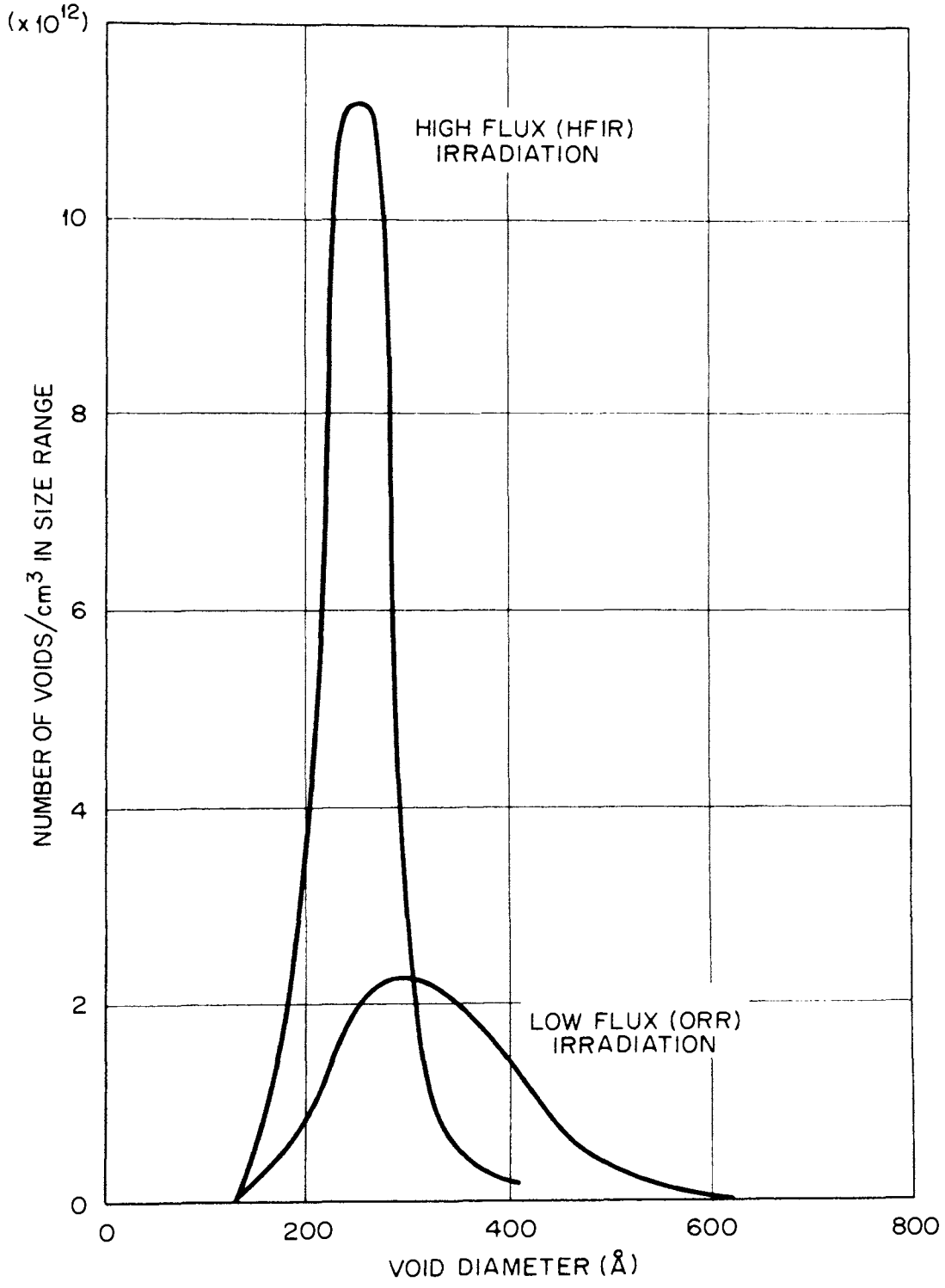

Fig. 13. Void size distributions for the high and low flux irradiations.

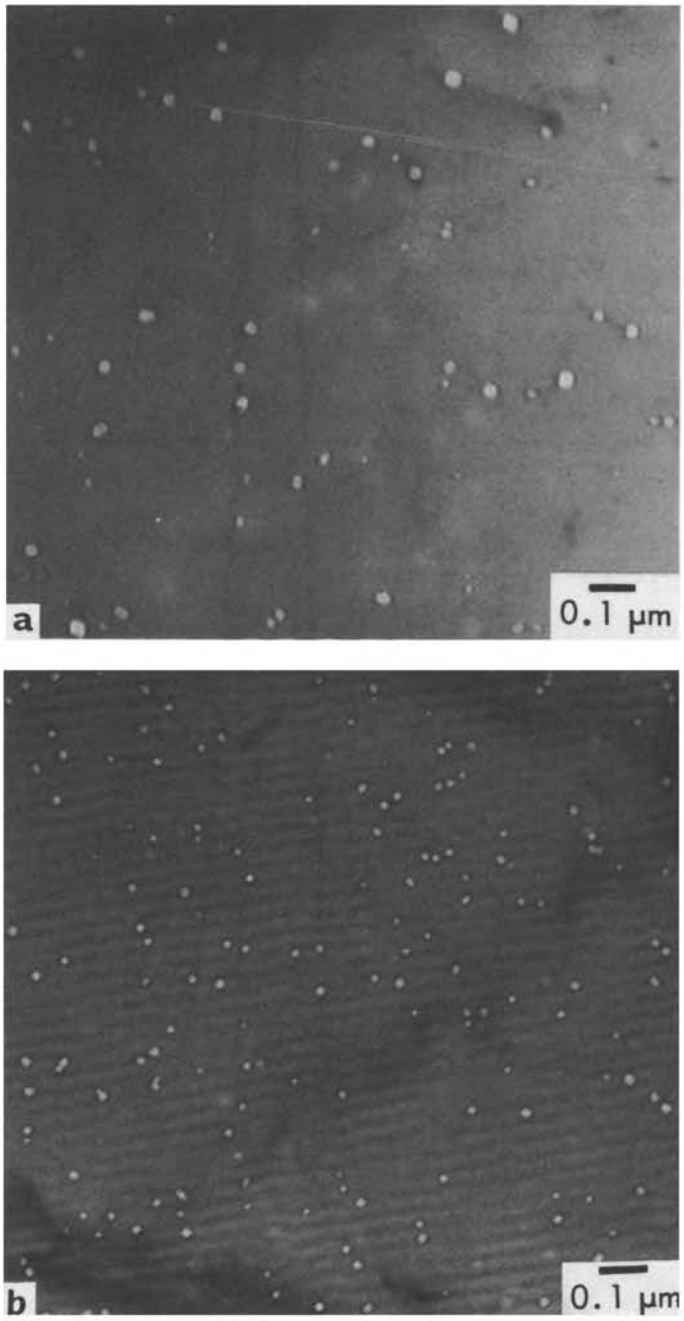

Fig. 14. Voids resulting from (a) original irradiation and (b) reirradiation (striations visible are polishing effects on the foil surface).

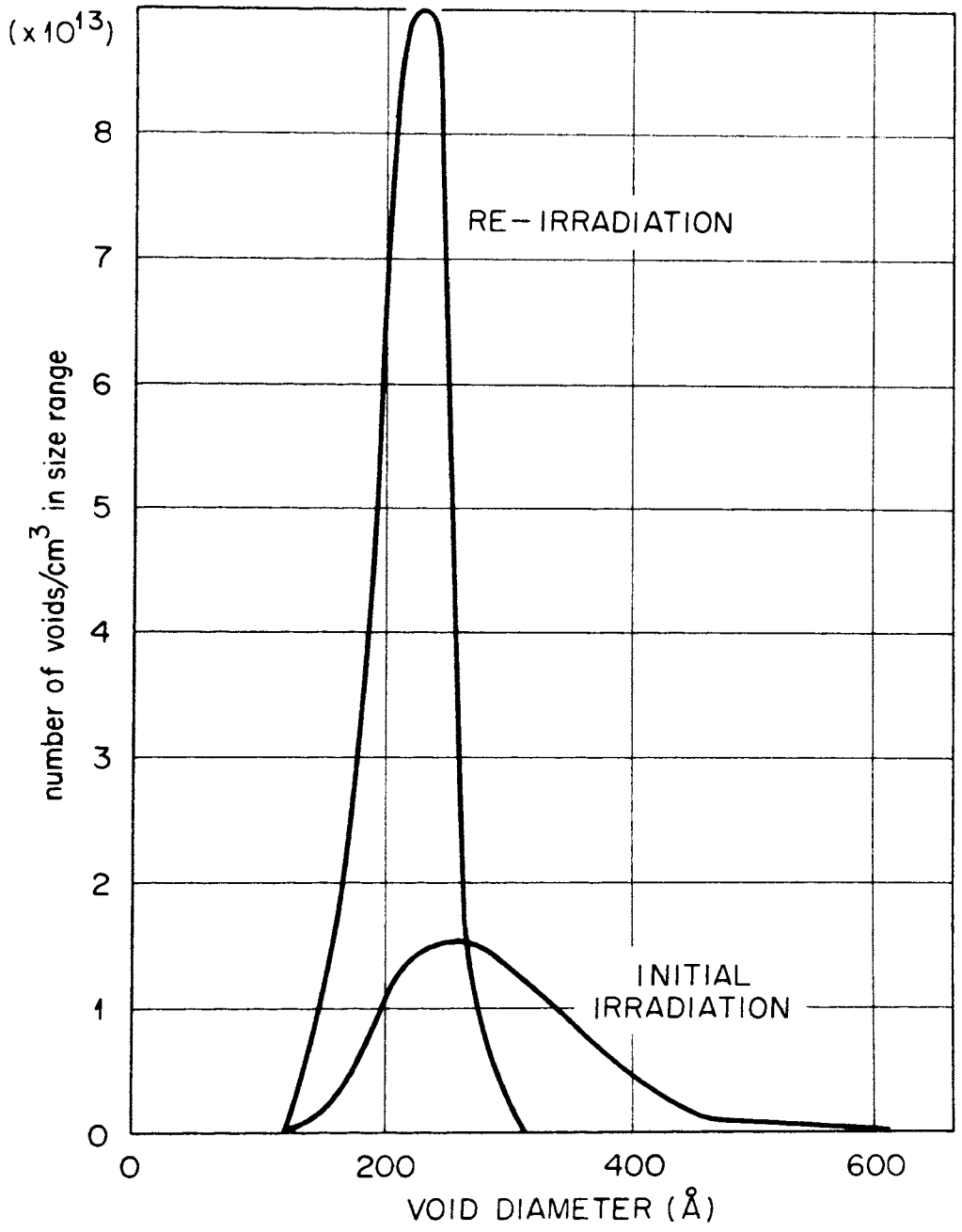

Fig. 15. Void size distributions for original irradiation and reirradiation.

produced by the original irradiation than by the reirradiation; however, the reirradiation voids were more than twice as numerous. As in the previous experiment, the calculated total void volume fractions were found to be the same within the limits of experimental error (compare capsules RE and RRE-2, Table VIII). Both the dislocation loop concentrations and sizes were comparable in the two irradiations. However there was a significant change in the microhardness (see Table IX); the hardness increase over the unirradiated control value for the reirradiated material was more than twice that for the original irradiation.

D. Impurity Influences

The results of the reirradiation experiment are most readily interpreted as a demonstration of the effects of irradiation-produced transmutation impurities, which in this case must have survived the void-removing anneal and influenced void formation during the reirradiation. The only direct observation of any such impurities was made in the examination of material irradiated to 10^{22} neutrons/cm^2. Small black precipitate particles could be seen in stereo both on the surfaces and within the foil in close association with voids. The precipitate sizes were on the order of 100 Å. The particles seen on the surfaces may have been released into the solution during the polish operation and then clung to the foil surfaces when the thinned specimen was removed from the polish bath. Similar particles have been observed[5] in 1100 aluminum irradiated to 1.5×10^{22} neutrons/cm^2 ($E > 0.82$ MeV). Postirradiation annealing of that material coarsened the particles to thin plates which could be identified as silicon by electron diffraction techniques. The present particles are therefore thought to be precipitates of transmutation-produced

silicon. Some of these particles, in the form of small black dots, can be seen attached to several voids in the "1 x 10^{22}" picture of Fig. 4 (e.g., a void in the lower right corner).

In Table X are given the estimated concentrations of transmutation-produced impurities at several fluences, calculated with the aid of a computer program and cross section data from the literature.[92] The calculated silicon concentration of 0.43 atomic percent after the 10^{22} neutrons/cm^2 irradiation is well in excess of the solubility limit, estimated to be less than 0.05 at.% at 250°C.[93]

For all except the highest fluence irradiation, the hydrogen content present in the as-received material (about 15-20 atomic ppm, Table V) exceeded the amount introduced by transmutation reactions during irradiation. It was therefore of interest to determine whether this level of preexisting gas had any effect on void formation. As described in the previous chapter, gas extraction was performed on several Cominco Grade 69 samples sent to Alcoa Research Laboratory, and the "degassed" material was returned by them. Therefore a feasible experiment was to irradiate this material to the same amount experienced by a previous capsule. Comparative statistics on the voids produced in the two irradiations are presented in Table XI, and the void size distribution curves are shown in Fig. 16. The concentrations and size distributions of the voids resulting from both irradiations are quite comparable. The best available knowledge of the diffusion of hydrogen into aluminum,[94] confirmed by vacuum fusion gas analyses carried out at ORNL, indicate that the degassed aluminum did not significantly regas prior to being included in the experiment. Therefore the experiment indicates little effect of

Table X. Calculated Concentrations of Transmutation-Produced Impurities

Capsule Ident.	Actual Fluence (neutrons/cm^2, E > 0.82 MeV)	Helium concentration (atomic ppm)	Hydrogen concentration (atomic ppm)	Silicon concentration (atomic ppm)
RC	0.84×10^{19}	0.006	0.04	4
RJ	0.42×10^{20}	0.03	0.2	20
RD	0.85×10^{20}	0.07	0.4	42
RE	2.8×10^{20}	0.2	1.2	140
RF	0.87×10^{21}	0.7	3.7	420
RH	0.88×10^{22}	6.7	38.	4300

Table XI. Comparison of Irradiation-Produced Voids in As-Received Versus Degassed Cominco Grade 69 Aluminum (Lot 5719)

Capsule Ident.	Actual Fluence (neutrons/cm^2, E > 0.82 MeV)	Pre-irrad. Hydrogen Content (at. ppm)	Void Max. Diam. (Å)	Void Mean Diam. (Å)	Number of Voids/cm^3 (10^{13})	Calc. Total Void Volume (%)
RE	5.2×10^{20}	14.5	583	299	1.1 ± 0.4	0.19 ± 0.07
DG-E	5.3×10^{20}	2.2	532	279	1.0 ± 0.2	0.15 ± 0.04

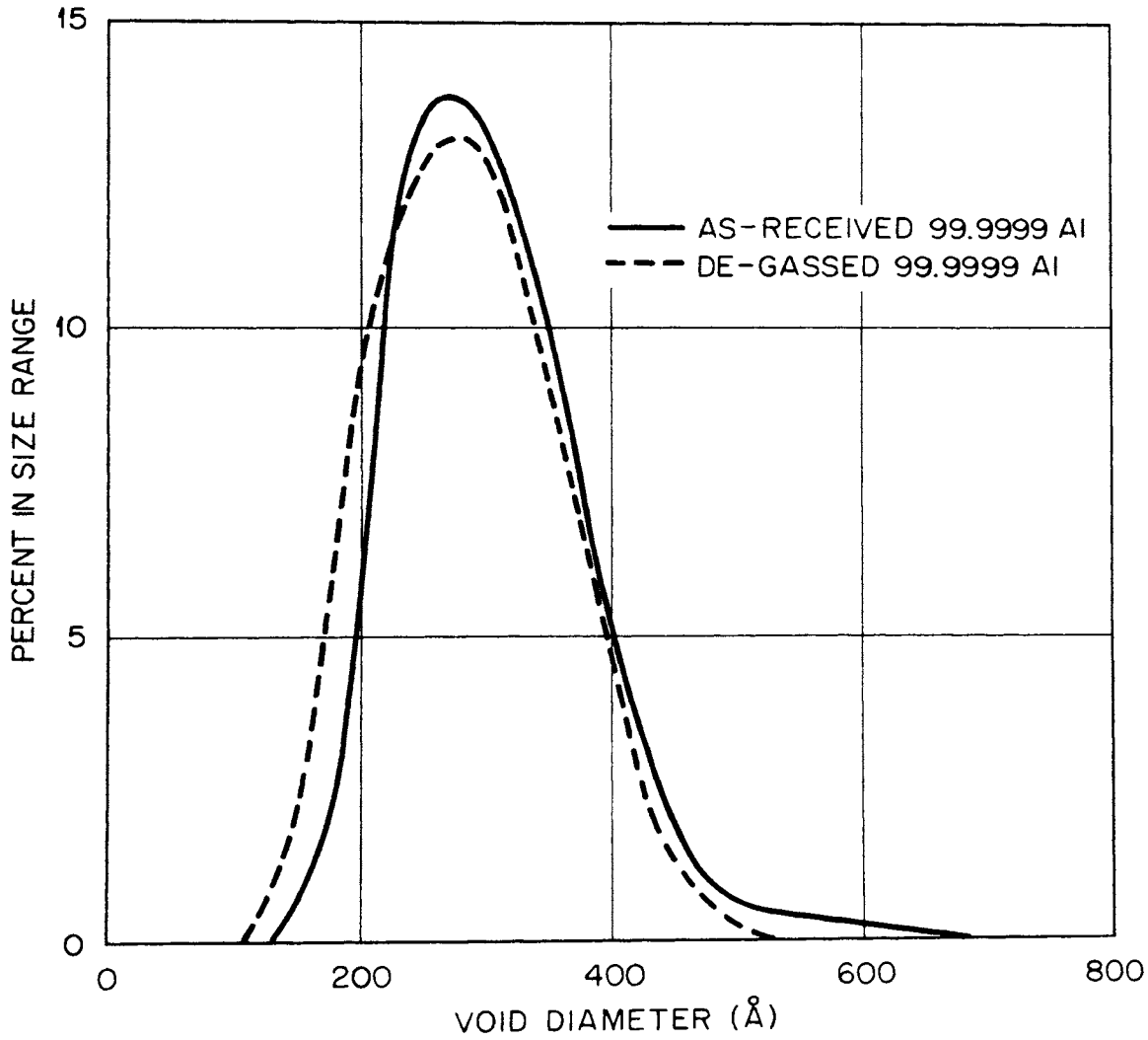

Fig. 16. Size distributions of voids produced by irradiation in as-received and degassed high purity aluminum.

an initial ≈ 15 atomic ppm hydrogen content upon void formation.

E. Void Annealing Studies

Studies of the annealing behavior of voids in an ultrahigh vacuum electron microscope were carried out initially on aluminum alloy 8001 (98.5 Al, 1.0 Ni, 0.5 Fe) irradiated to 1.0×10^{22} neutrons/cm^2 (E > 0.82 MeV), and subsequently on the irradiated 99.9999% aluminum. Quite similar results were obtained for both materials. As described in Chapter III, the technique involved following the annealing kinetics of a relatively small number of individual voids. A typical annealing sequence is shown in Fig. 17. Only 6 of the 18 plates taken are included and each photograph shows only a small portion of the actual plate. It should be noted that voids which appear to be close together may in fact be widely separated in the direction parallel to the electron beam. Measured void diameters were plotted as a function of annealing time to produce a shrinkage curve for each void. Some examples of the shrinkage curves showing the individual measurements and their estimated error are given in Fig. 18.

Some voids either failed to shrink or appeared to increase slightly in size during the course of an anneal. At the same time the images of many of them became much less distinct, suggesting that they had intersected the surface of the foil and were being smoothed by surface diffusion. Figure 19 shows a region containing some surviving voids and some "pits" after a 3-hr anneal at 150°C.

Curves depicting the 150°C annealing behavior of sixteen voids produced by the 3×10^{20} neutrons/cm^2 irradiation are shown in Fig. 20. Voids annealed in thin foils exhibit a wide variety of shrinkage rates.

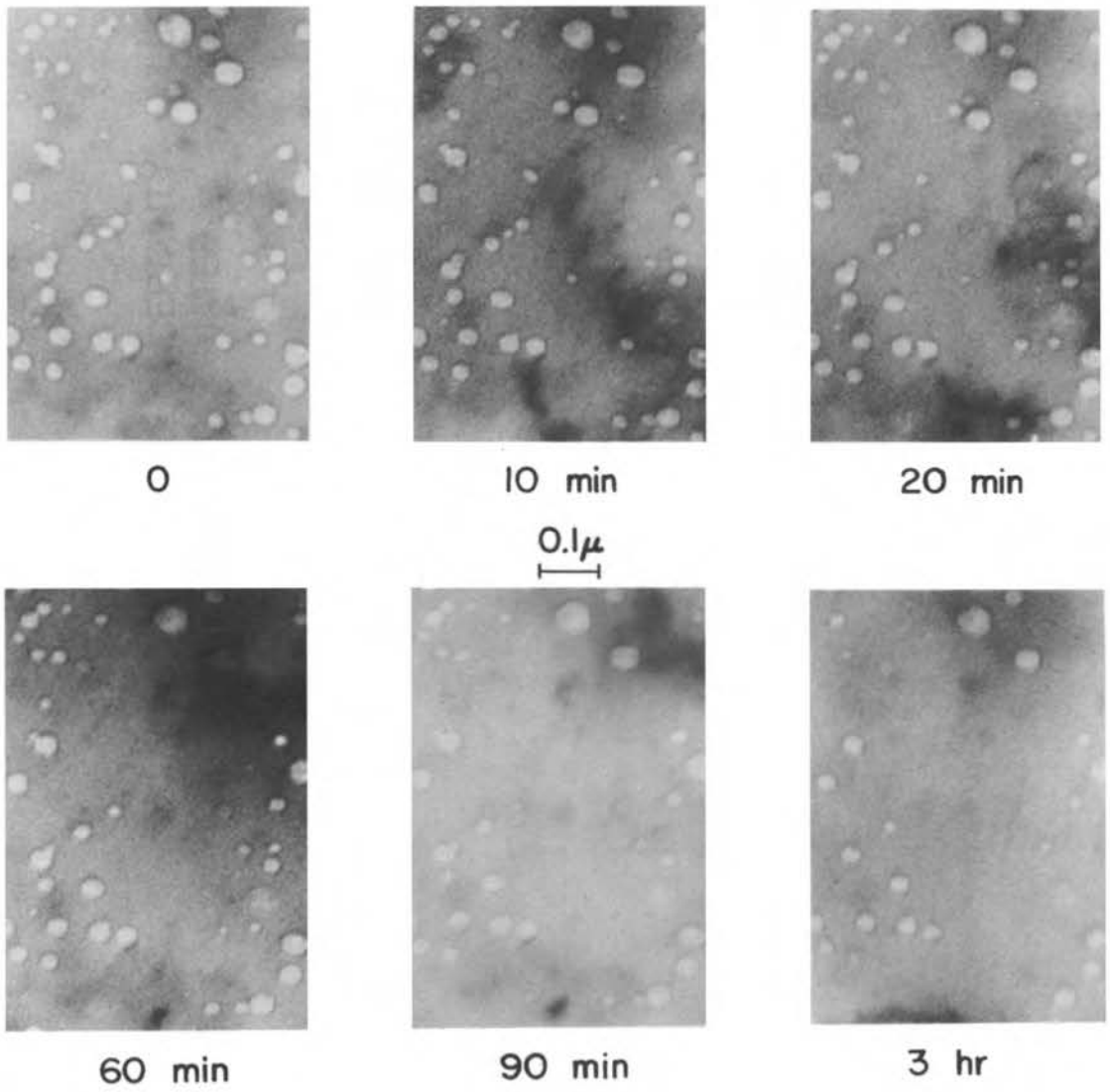

Fig. 17. Sequence of micrographs depicting void annealing at 150 ° C.

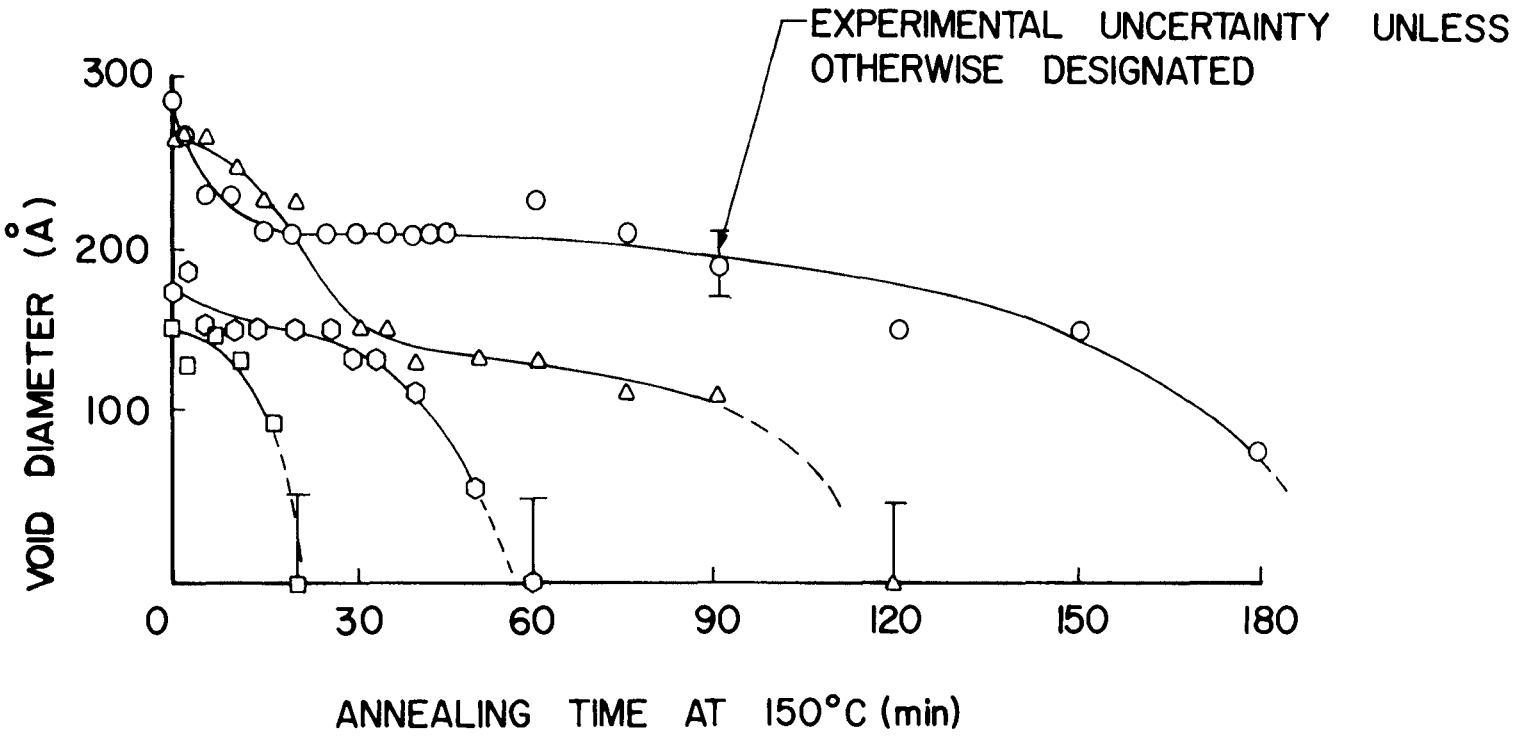

Fig. 18. Examples of void annealing curves, including all data points.

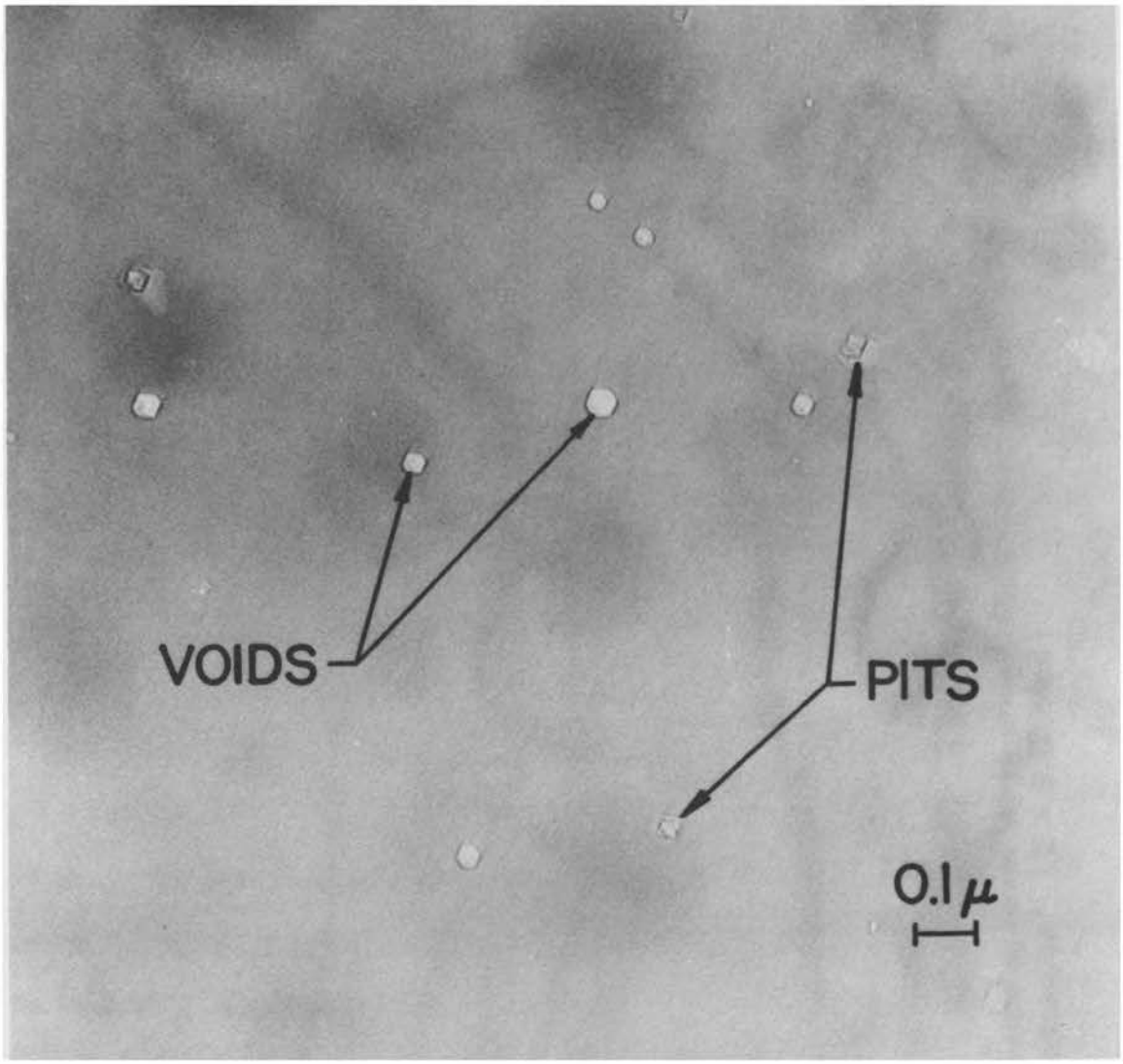

Fig. 19. Voids and "pits" after a 3-hr anneal at 150° C.

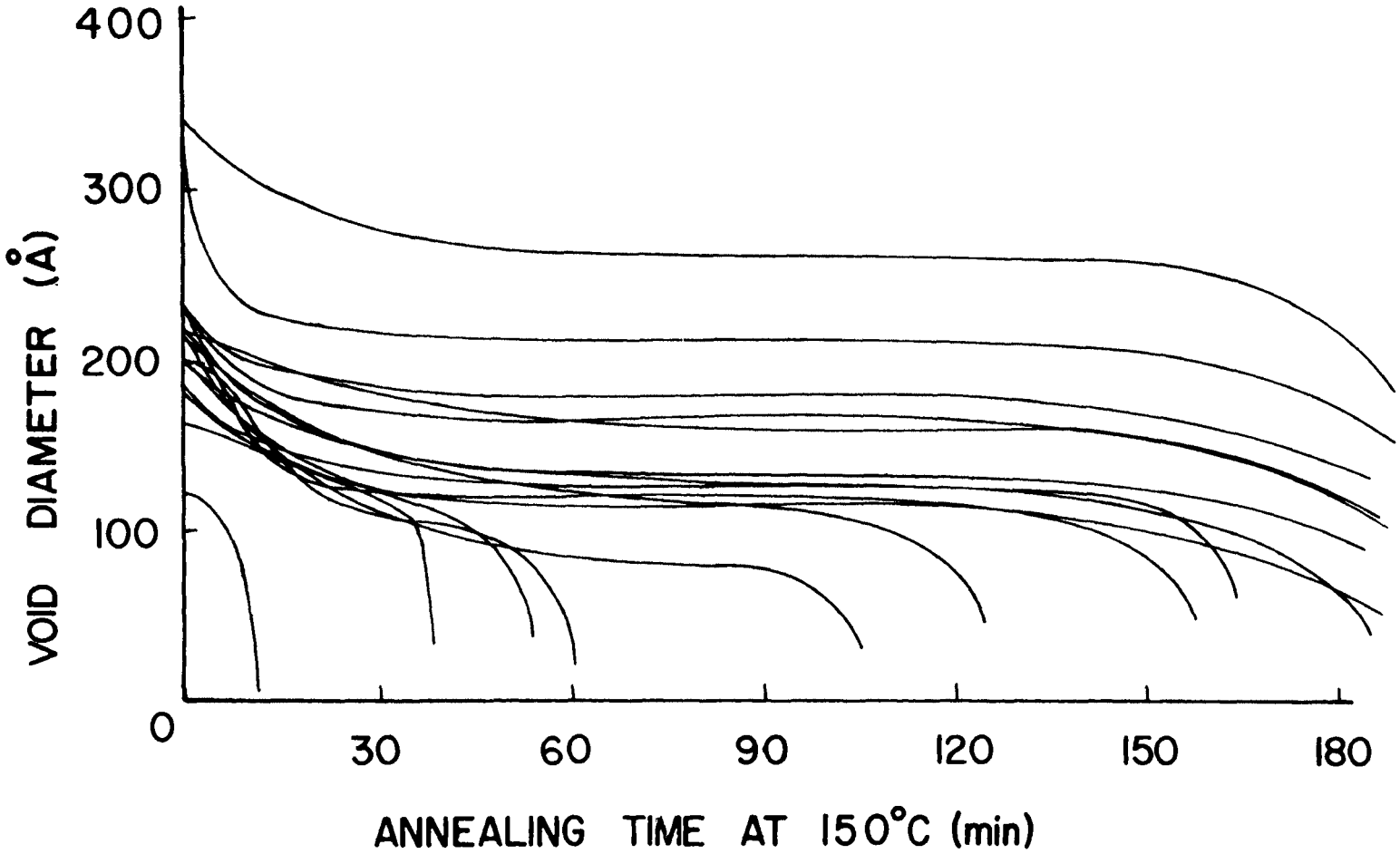

Fig. 20. Annealing curves for 16 voids in the specimen material irradiated to 3×10^{20} neutrons/cm^2 (E > 0.82 MeV).

As a general rule, initially larger voids usually take a longer time to anneal out than do smaller ones. This behavior is in agreement with observations in irradiated stainless steel.[36] However numerous exceptions to this rule are observed, and for any given value of void size, there is a considerable variation in the slopes of the curves.

To determine whether variations in shrinkage behavior were related to the locations of voids within the foil, a stereo-pair of electron micrographs was taken prior to one annealing run. Voids located close to the surfaces usually shrank at a relatively rapid rate while many of those situated deeper in the foil shrank more slowly. However, about half of the voids in the central third of the foil were also found to shrink quite quickly. It is plausible that these voids lost their vacancies to local sinks, such as dislocation loops, other voids, or gas bubbles, rather than to the foil surface.

The annealing of specimens inside an electron microscope permitted the taking of many micrographs over a short time interval. When attention was thus concentrated on the early part of an anneal (note the spacing of the data points in Fig. 18), a brief initial high-shrinkage rate was very frequently observed. This effect usually lasted for the first 10 to 20 min of the anneal, and is revealed by most of the void shrinkage curves in Fig. 20. In order to determine whether temperature changes were causing this high shrinkage rate, the original temperature of 150°C was increased to 170°C during one run and a second high shrinkage rate was observed (Fig. 21). When the temperature was decreased from 150 to 100°C, the opposite effect on the voids was noticed; there was a slight increase in void size (Fig. 22). An additional run was

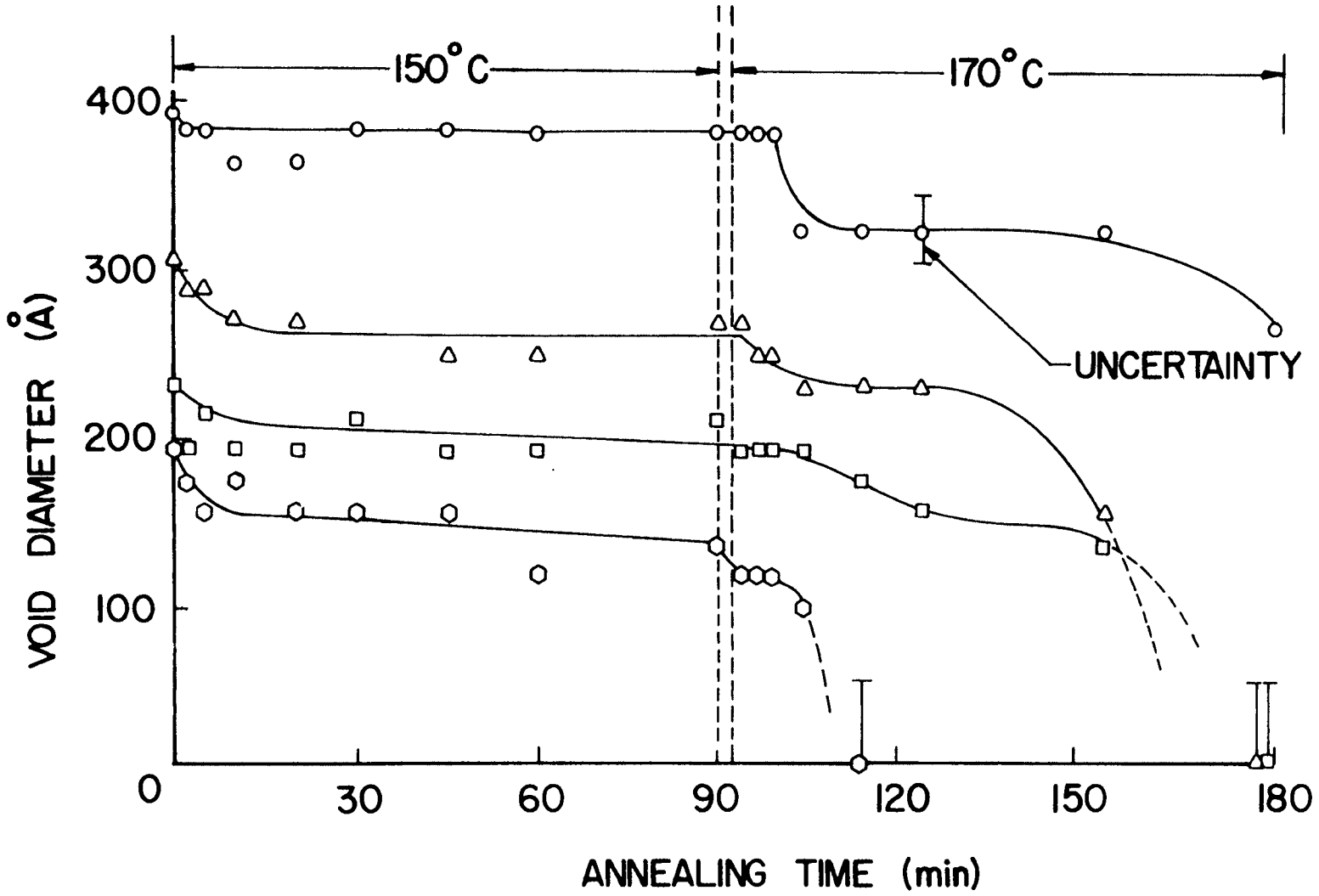

Fig. 21. Void annealing behavior upon raising the temperature from 150° to 170°C in the middle of the run.

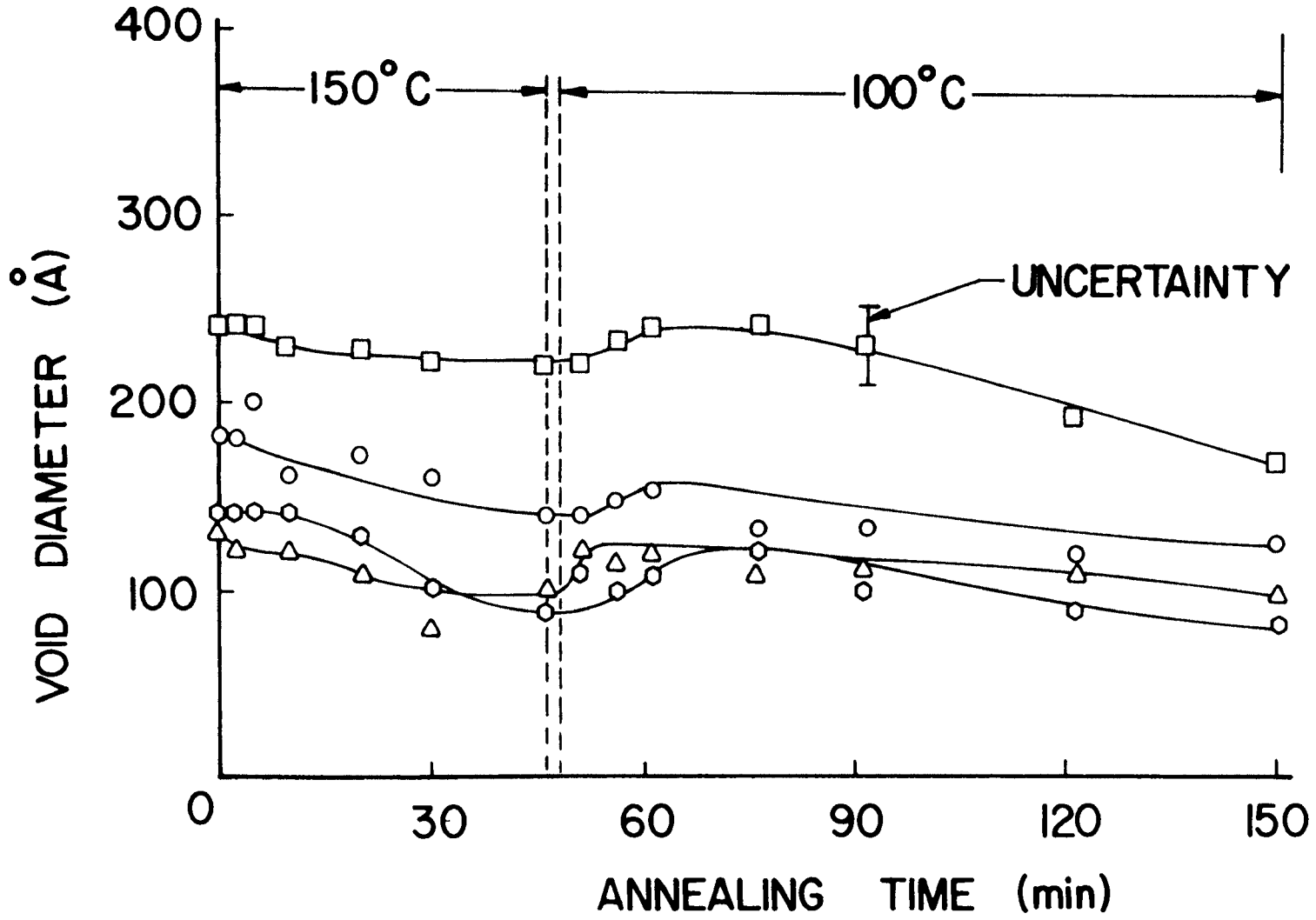

Fig. 22. Void annealing behavior upon dropping the temperature in midrun from 150° to 100°C.

made to determine whether any heating from the electron beam could have caused the initial high shrinkage rate. The beam was turned on for 10 min during the middle of a run, but no change in shrinkage rate was observed during this period. The observations therefore indicate the existence of a transient temperature effect in the annealing of voids in a thin foil specimen.

Brief annealing studies on voids from other irradiations (10^{20}, 10^{21}, and 10^{22} neutrons/cm^2) indicated little consistent influence of the fluence upon void annealing characteristics. Rather, the variability of annealing behavior among individual voids remained a dominating factor. The magnitude of the initial transient effect increased somewhat with increasing fluence, but this may simply reflect the increasing average void size with fluence. Larger voids tended to exhibit larger initial size changes, in absolute measure, although again numerous exceptions were noted.

V. DISCUSSION

A. Discussion of the Observations

1. Effects of Neutron Fluence

One of the few investigations which have included a specific examination of the effects of fluence upon void formation is the recent one by Bloom[95] on type 304 stainless steel. Some of his results, and some preliminary findings of Stiegler[96] on Nickel 270 (≈ 99.98% pure), will be contrasted with those from the present aluminum study. It will be quite apparent that void formation occurs in a wide variety of ways, making any single description of the process extremely difficult.

Size distributions of voids irradiated to several indicated fluences (E > 0.1 MeV) in type 304 stainless steel are shown in Fig. 23 for the two irradiation temperatures examined by Bloom. The effect of temperature is quite noticeable. At all fluences the most frequently observed void size is larger at the higher temperature. But for either irradiation temperature it is significant that the size distribution curves are simply displaced upward (toward greater void concentrations) with increasing fluence. The curves maintain essentially the same shapes, and neither the maximum nor the modal void sizes shift significantly with changing fluence. This behavior is quite unlike the corresponding results of this study, presented in Fig. 8 and Table VIII, in which the maximum and the modal void sizes increased continuously with increasing fluence. The shapes of the latter curves changed too, with the distribution width at half height likewise increasing monotonically with fluence. A more detailed look at void growth processes is needed to explain these disparities.

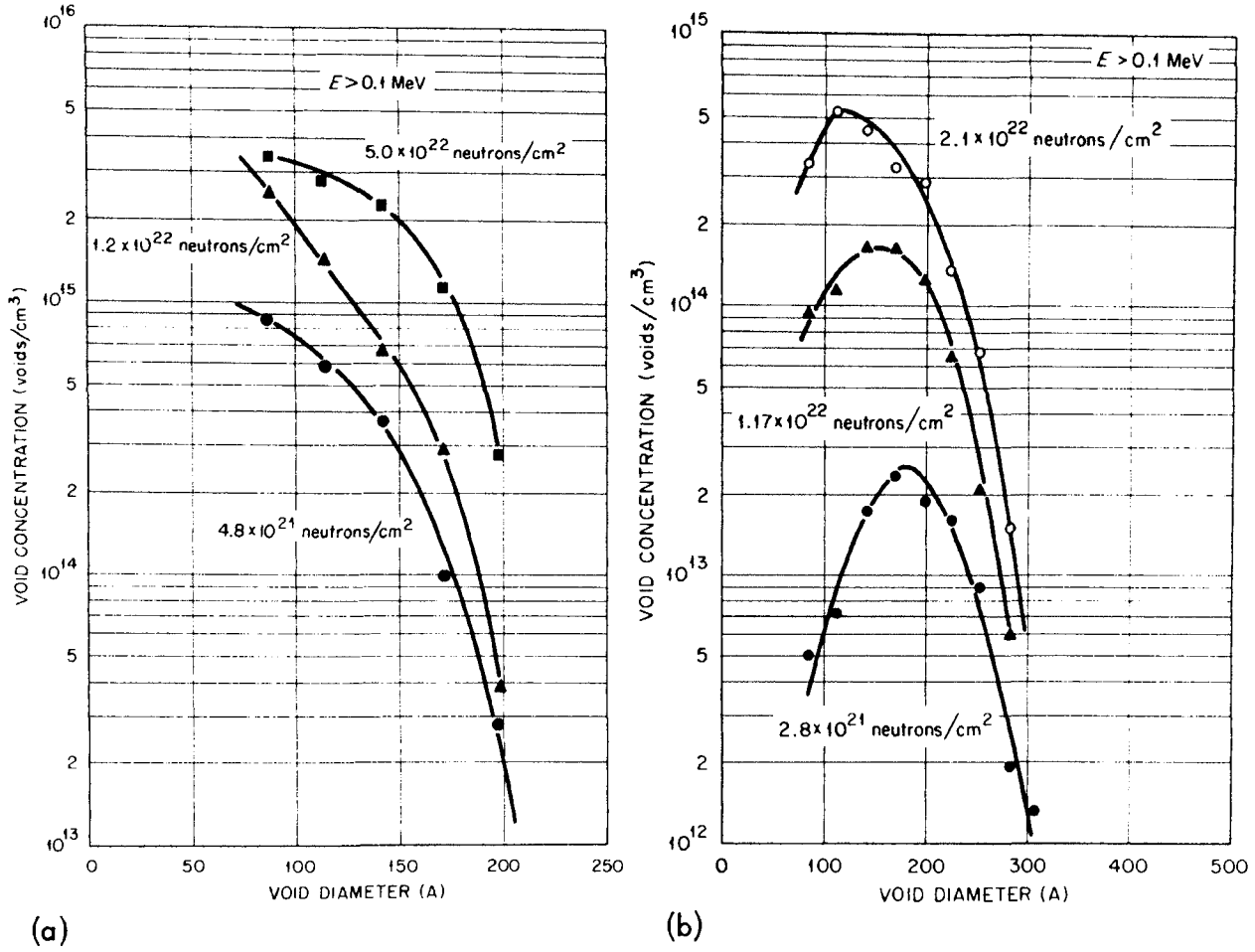

Fig. 23. Void size distributions in type 304 stainless steel irradiated at (a) 370–380 ° C and (b) 460–470 ° C.

E. E. Bloom, "An Investigation of Fast Neutron Radiation Damage in an Austenitic Stainless Steel," Oak Ridge National Laboratory report ORNL–4580 (1970).

In Fig. 24, both the maximum and the mean observed sizes of voids in this study are plotted versus fluence. Both sets of data can be fitted to the general relation: $r \sim t^{m}$. A first-order least-squares fit yielded values for the slope $\underline{m}$ of 0.22 and 0.16 for the maximum and mean size data, respectively. Either quantity is a measure of the void growth rate, but according to Woodhead[97] the change in mean size is the more useful of the two. Thus it is concluded that voids in this study grew according to the relation:

$$r \sim t^{0.16} \text{ or } \sim t^{1/6}, \text{ approximately.} \qquad (6)$$

In Bloom's type 304 stainless steel, on the other hand, the void maximum size reached the limiting values shown in Fig. 25. Bloom explained his observed limiting size as an alloying effect. Since growth by diffusion of vacancies into a void corresponds to atomic diffusion away from the void, alloying elements with high mobility would leave the vicinity of the void more rapidly than slowly diffusing constituents. Thus a shell of low mobility elements would form around the void, inhibiting its further growth and leading to the restricted maximum size observed. Such an alloying effect would not be expected and was not seen in either the high purity aluminum of this study or the Nickel 270 examined by Stiegler.[96]

In Fig. 26 is shown the fluence dependence of the observed void concentration. (The void concentration will be employed as the best available measure of void nucleation behavior, even though strictly it represents only the nucleated voids which have survived to observable size. The validity of this approximation cannot presently be assessed.)

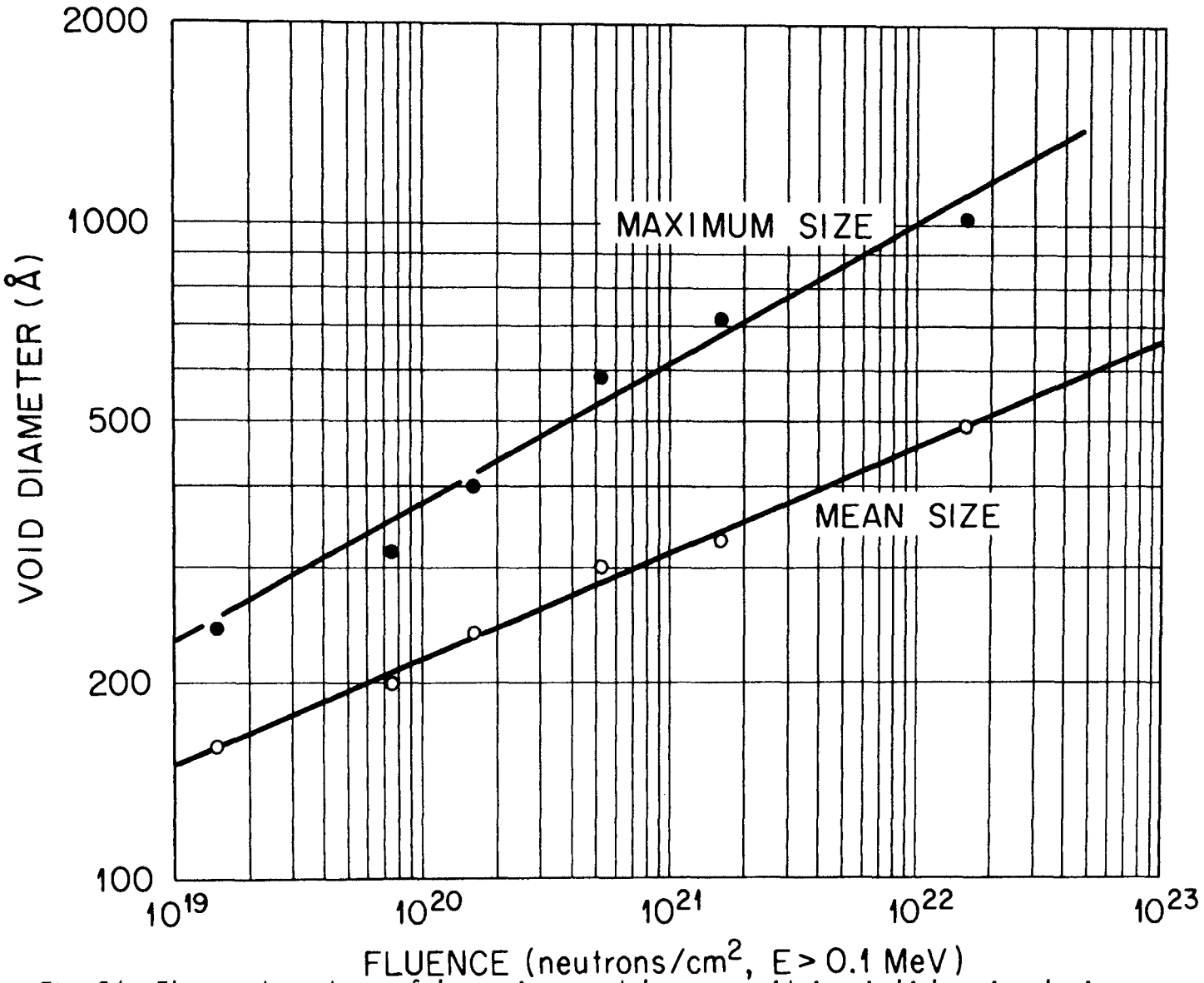

Fig. 24. Fluence dependence of the maximum and the mean void sizes in high purity aluminum.

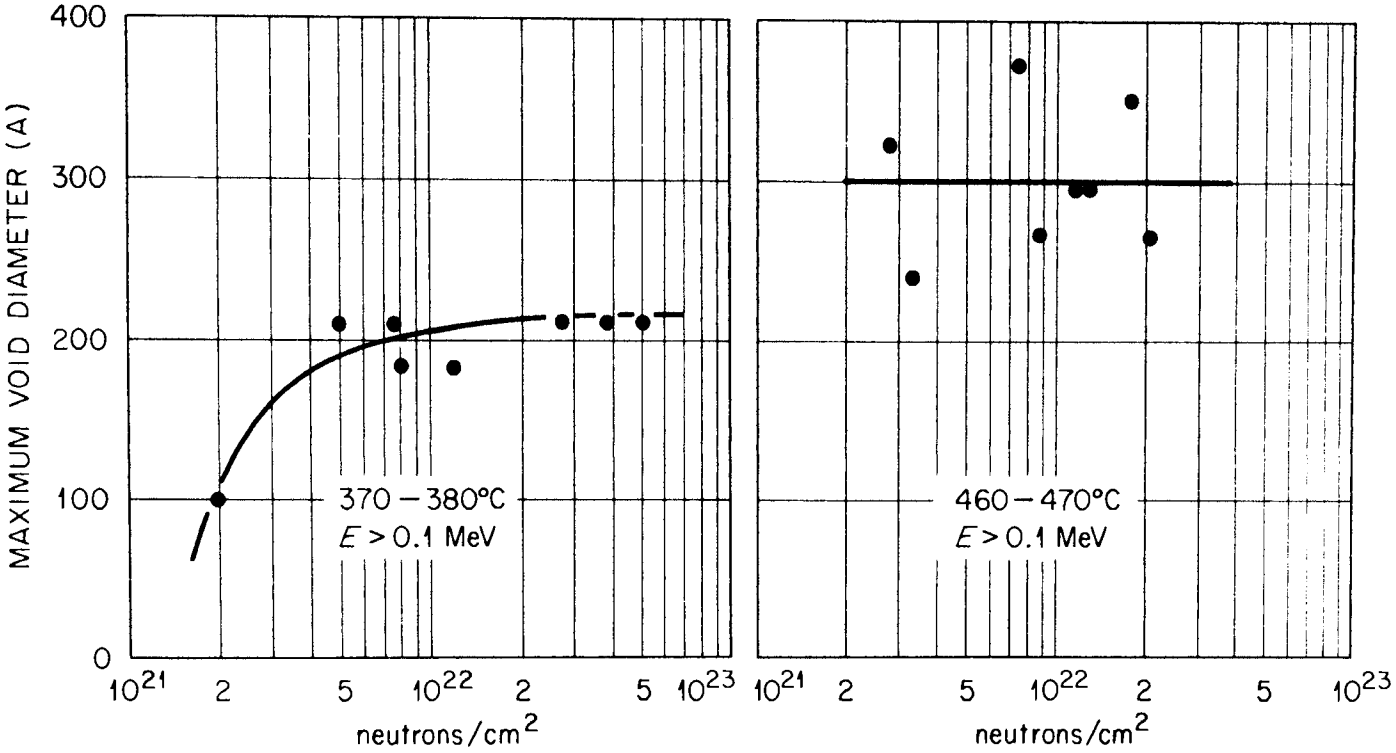

Fig. 25. Fluence dependence of the maximum void size in type 304 stainless steel.

E. E. Bloom, "An Investigation of Fast Neutron Radiation Damage in an Austenitic Stainless Steel," Oak Ridge National Laboratory report ORNL-4580 (1970).

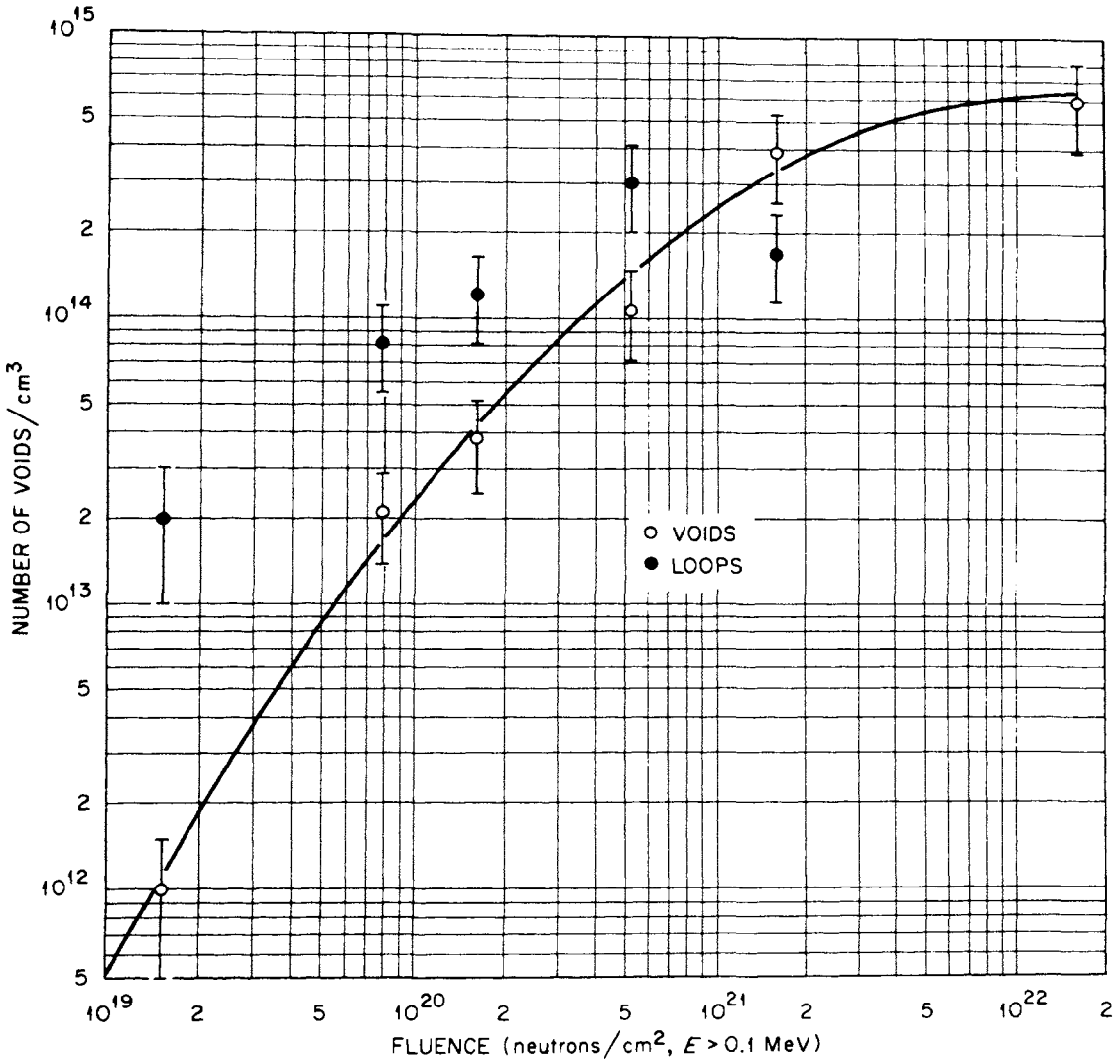

Fig. 26. Void concentration as a function of neutron fluence in high purity aluminum.

Unlike void growth, the "nucleation" is seen to diminish and almost cease over the range of fluence studied. The line through the data points represents a second-order least-squares fit; tangents to it have slopes ranging from 2.0 at 10^{19} neutrons/cm^2 down to 0.1 at 10^{22} neutrons/cm^2. It appears unsatisfactory to attempt to fit a single straight line of slope a, obeying a power law $N \sim (\phi t)^a$, through this data. The diminishing nucleation rate itself is the significant result, again in contrast to observations in stainless steel, and in nickel as well. In the type 304 stainless steel, Bloom obtains a uniform increase in void nucleation with fluence (Fig. 27). The rate is lower at the lower irradiation temperature, yet both sets of data are well represented by the power law expression over the range of fluence investigated--with values for the exponent a of 0.66 and 1.66 for the 370 and 470°C temperatures respectively.

Quite the opposite result has been found by Stiegler,[96] in Nickel 270, however. Above the very low fluence of $\approx 10^{18}$ neutrons/cm^2, essentially no change was observed in the void concentration of 2-3 x 10^{14} voids/cm^3. As fluence increased to 1.5 x 10^{22} neutrons/cm^2, rather, they grew from barely detectable size to as large as 2000 Å diam., with void coalescence occurring in the later stages. Surprisingly, even irradiation temperature seemed to have little effect on nucleation, for at a common fluence of 1.4 x 10^{20} neutrons/cm^2, the void concentration did not vary significantly over the range 375 to 525°C (0.37 to 0.46 T_m). These results are consistent with a model of void nucleation only at preexisting sites. Nucleation by such a mechanism would be very sensitive to the specific impurity content of the specimens actually irradiated, so it is not particularly surprising that Straalsund[98] has

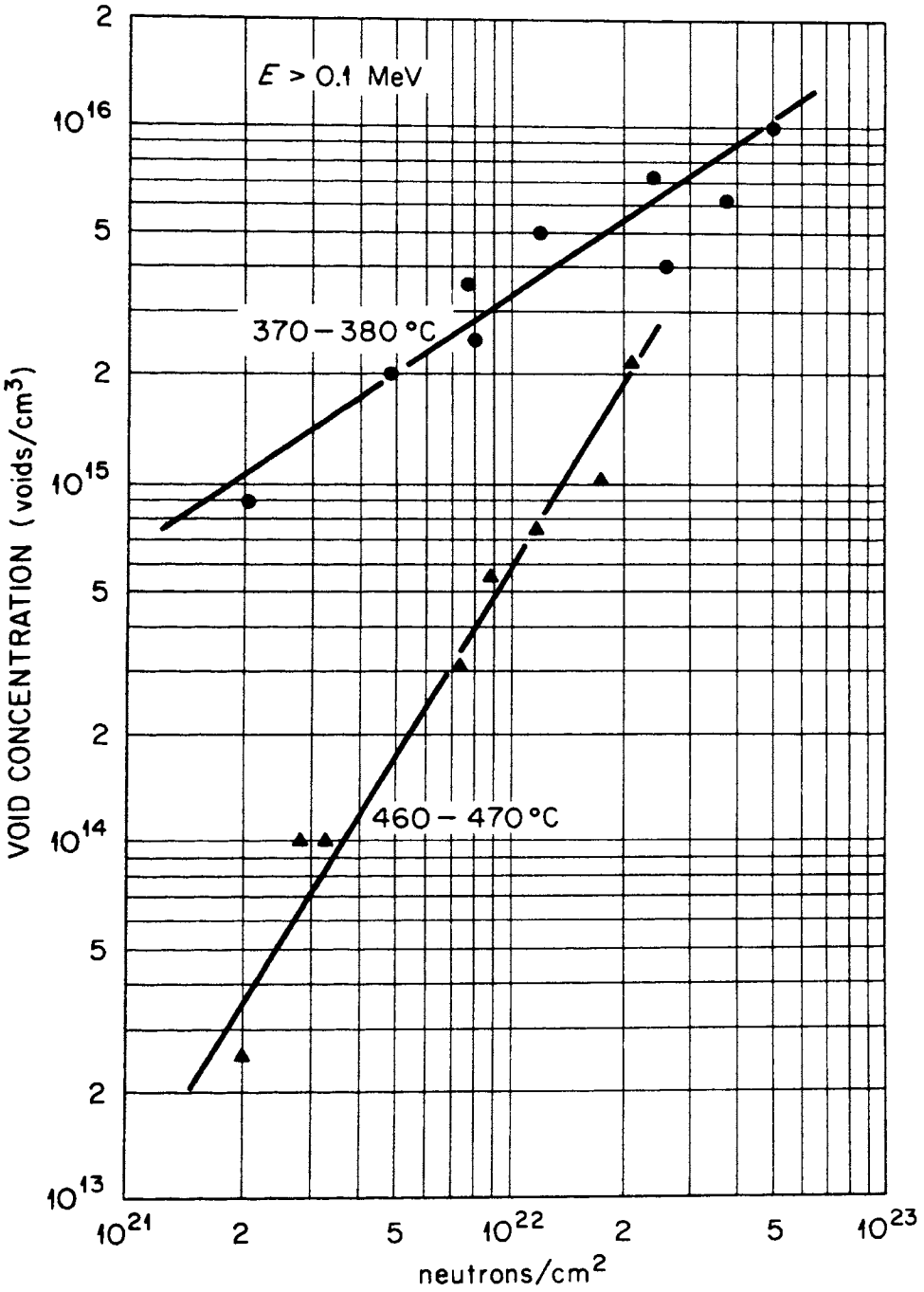

Fig. 27. Void concentration as a function of neutron fluence in type 304 stainless steel.

E. E. Bloom, "An Investigation of Fast Neutron Radiation Damage in an Austenitic Stainless Steel," Oak Ridge National Laboratory report ORNL-4580 (1970).

obtained differing results for Nickel 270. He found the void concentration to increase by more than an order of magnitude as fluence increased from 10^{20} to 10^{21} neutrons/cm^2, though the concentration did not reach the higher, static value of Stiegler's material. What is important here is that void nucleation processes, like growth processes, vary from one material to another and cometimes even within the same material, depending upon its source or history.

The dislocation loop concentrations for this aluminum study are also plotted in Fig. 26 as a function of fluence. They were found in sparce numbers at the 10^{17} and 10^{18} neutrons/cm^2 fluences where voids were not observed, and they greatly outnumber the voids during the early stages of void formation. Yet they increase in concentration at a slower rate than do the voids. Above 10^{20} neutrons/cm^2, many of the loops apparently grow to sizes comparable to that of the foil thickness and the determination of their concentration becomes increasingly difficult and uncertain, as already noted. However the results available do seem to indicate a declining nucleation rate for the loops, similar to the behavior seen for the voids, with increasing fluence.

Voids did not form within denuded zones adjacent to grain boundaries, and the widths of these zones were found to be independent of the fluence. This result is in agreement with similar predictions[99] for dislocation loop denuded zones, and is understandable in that the effective range of grain boundaries as vacancy sinks should not depend upon the amount of damage but rather upon diffusion processes which are chiefly temperature dependent.

Void concentrations and size distributions yield data on the total void volume fraction; in Fig. 28 the "swelling" or percent volume change

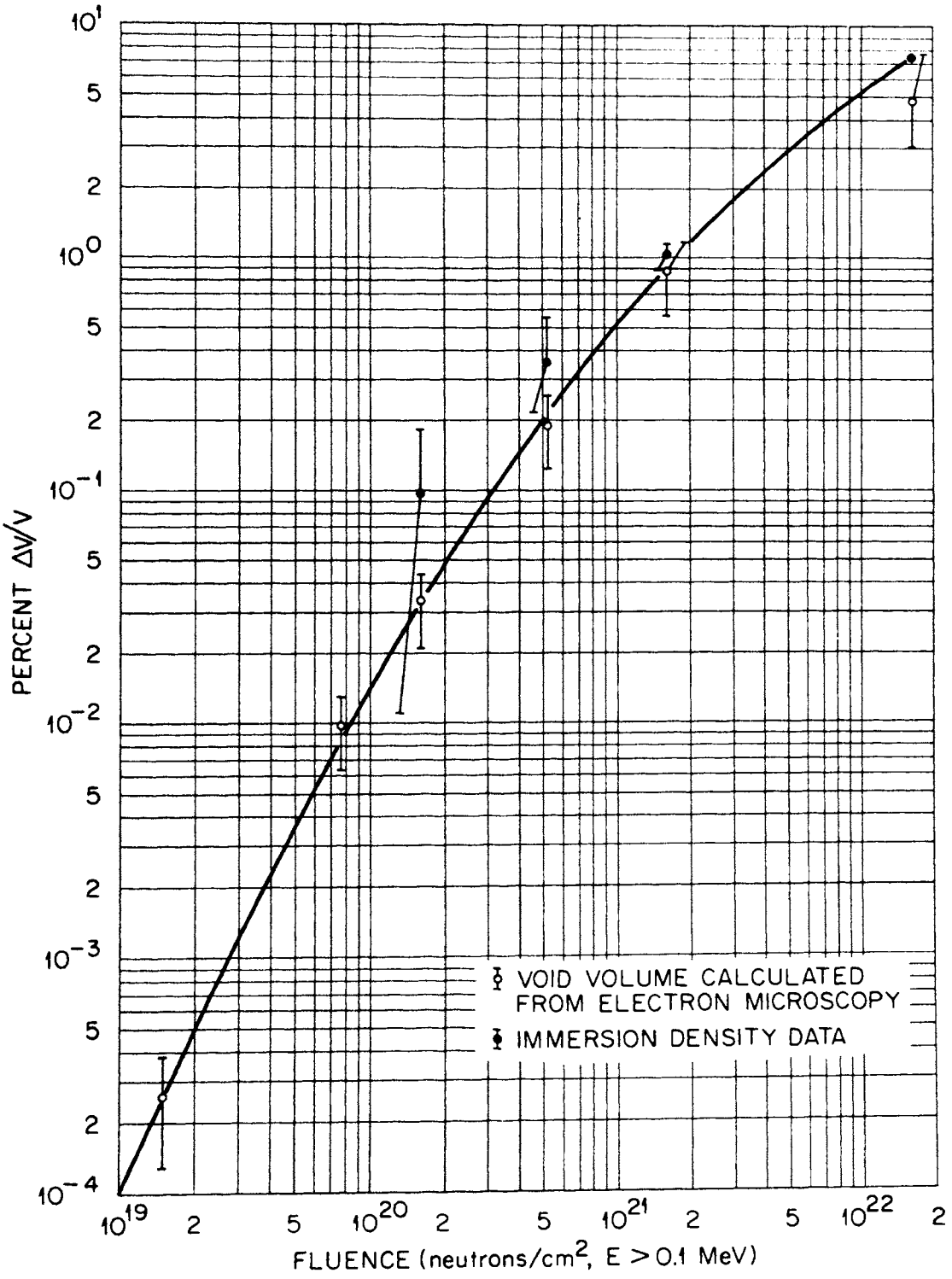

Fig. 28. Variation of the total void volume with fluence in high purity aluminum.

$\Delta V/V$ is shown as a function of fluence. As in the similar plot of void nucleation versus fluence (Fig. 26), a least-squares straight line of slope $\underline{b}$ relating swelling to some constant power of fluence, $\Delta V/V \sim (\phi t)^b$, is not a good representation. (If carried out, a first-order least-squares analysis yields a value for $\underline{b}$ of 1.45.) Taking a fragmented approach, the data can be broken into stages and straight lines fitted to each. Thus the first two data points (the lowest fluence values) might be considered in the "early void formation" stage with a power law exponent of $b = 2.25$, the second through fifth points taken as defining "mainstream" swelling with a slope of 1.5, while the fifth and sixth points could represent the onset of "saturation effects," with the exponent dropping to 0.9. But there are no obvious breaks in the data to justify such an approach. The best approach again is to represent the data with a smooth curve, even though this dispenses with a unique swelling exponent which could be compared to other experimental results or theoretical models. A second-order least-squares curve is fitted through the data. Tangents to it have slopes ranging from 2.4 (at 10^{19} neutrons/cm^2) to 0.75 (at 10^{22} neutrons/cm^2). Slight extrapolation of the curve to cover the fluence range from 6×10^{18} to 2.5×10^{22} neutrons/cm^2 permits the results to be expressed more generally as

$$\frac{\Delta V}{V} \sim (\phi t)^b, \quad 0.5 < b < 2.5 \quad . \tag{7}$$

In Bloom's work on stainless steel, straight lines were fitted to the swelling data at 370 and 470°C (Fig. 29) with slopes of 0.84 and 1.60 respectively. The data for the lower irradiation temperature might

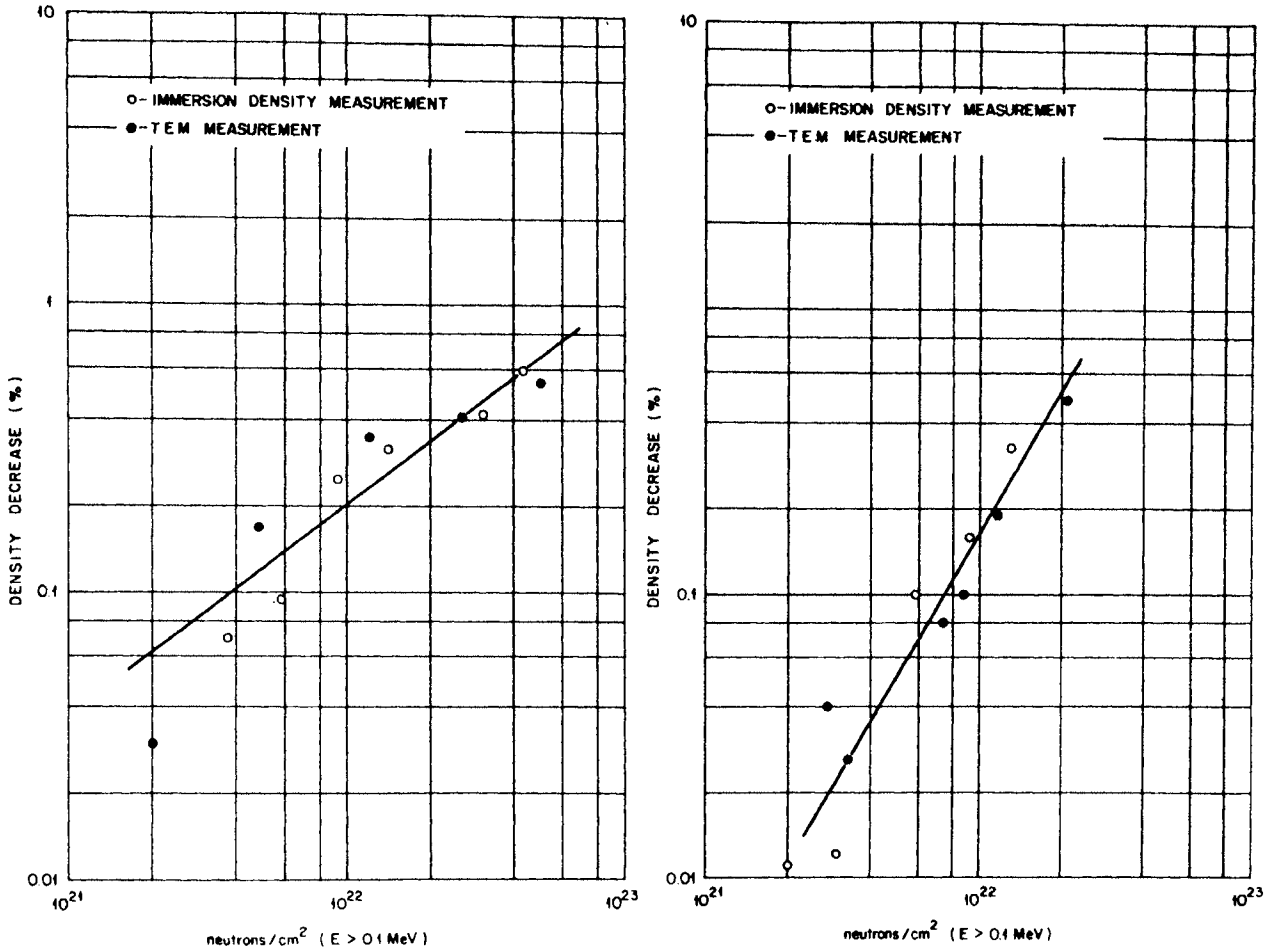

Fig. 29. Density decrease (void volume) versus neutron fluence for type 304 stainless steel.

E. E. Bloom, "An Investigation of Fast Neutron Radiation Damage in an Austenitic Stainless Steel," Oak Ridge National Laboratory report ORNL-4580 (1970).

better have been fitted by a curve. Nevertheless void nucleation in Bloom's study did follow the basic power law relation, and his swelling data is reasonably described by a similar relation. In the present study, on the other hand, both nucleation and overall volume can be best expressed by a power relation only with a continuously changing exponent.

The present results combined with immersion density measurements[100] of 1100 aluminum (99% Al) and 8001 aluminum demonstrate that increasing the purity in aluminum enhances swelling, but the shapes and slopes of the swelling curves are all quite similar (Fig. 30). All were irradiated at essentially the same temperature, approximately 50°C. Apparently the similarities in basic material (aluminum) and irradiation temperature are reflected in the common slope of the swelling versus fluence curves, even though purity variations cause large lateral shifts of the curves. It is hard to say whether the data for the impure aluminum materials would also show a significant curvature if extended to both higher and lower fluences, or whether the curvature found in the present study is rather a peculiarity of the high purity aluminum.

The last aspect of the fluence-effect investigation, that of microhardness changes, is interpreted along the lines suggested recently by Kulcinski et al.[67,101] From the work of Coulomb,[37] it was shown that the increase in yield stress $\Delta\sigma_v$ caused by the presence of voids of concentration $\underline{N}$ and average diameter $\underline{d}$ should be given by:

$$\Delta\sigma_v = 2Gb(Nd)^{1/2} \tag{8}$$

where

G = shear modulus, and

b = principal Burgers vector in the material.

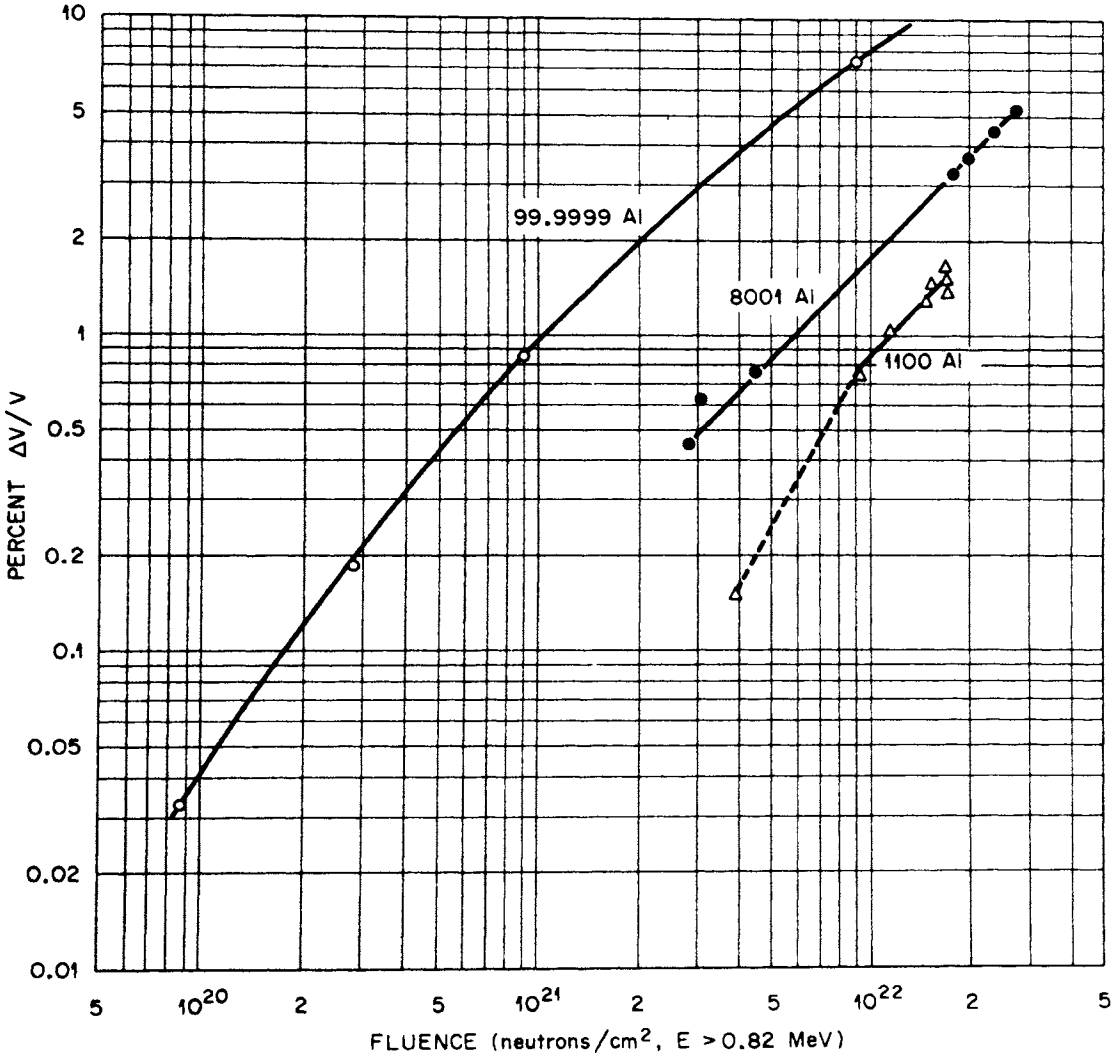

Fig. 30. Density decrease versus fluence for high purity aluminum (this study) and for two aluminum alloys (reference 100).

Tabor[102] and others have demonstrated that the increase in Vickers hardness (or microhardness) ΔH for a number of metals and alloys is proportional to the yield stress expressed in kg/mm^2, with the proportionality constant averaging about 3 from various studies. Combining these, Kulcinski found that the expression:

$$\Delta H = 6Gb(Nd)^{1/2} \tag{9}$$

was well obeyed by microhardness tests (and checked by electron microscopy observations of the void content) on irradiated nickel specimens given various postirradiation annealing treatments. They have therefore suggested that microhardness testing could serve as a rapid preview or screening test in assessing the relative void contents of irradiated materials.

However the nickel specimens examined by Kulcinski contained few or no dislocation loops, since these had been removed by annealing. Before applying Eq. (9) to the present data, an estimate of the loop contribution to the hardening must be made. Westmacott,[103] quoted in Holmes et al.,[36] obtained for the loop contribution:

$$\Delta\sigma_l = \frac{2Gb(dN^{2/3})}{\beta} \tag{10}$$

where β is a parameter with values taken variously between 3 and 16. The combined change in yield stress arising from both loops and voids was shown by Koppenaal and Kuhlmann-Wilsdorf[104] to be given by:

$$\Delta\sigma_{tot} = (\Delta\sigma_v^2 + \Delta\sigma_l^2)^{1/2} . \tag{11}$$

If either hardness component is much larger than the other, it will be dominant.

Equation (10) was used with loop number density data from Fig. 26, $\beta = 10$, and assumed mean loop diameters ranging from roughly 200 Å at low fluences to 400 Å at 10^{21} neutrons/cm^2. The resulting $\Delta\sigma_l$ values were compared with values for $\Delta\sigma_v$ obtained using Eq. (8) and the measured void concentrations and average sizes. For all fluences except 10^{19} and 10^{22} neutrons/cm^2, $\Delta\sigma_v$ was found to be greater than $\Delta\sigma_l$ by factors ranging from 7 to 16. Taking the smallest of these ratios still yields $(\Delta\sigma_v)^2 \approx 50(\Delta\sigma_l)^2$ so the loop contribution is indeed small compared with the void contribution to hardening. At 10^{19} neutrons/cm^2, the void contribution was only $(2.5)^2 = 6$ times that of the loops, but the void concentration is known very poorly here; while at the highest fluence as already noted, no meaningful value could be obtained for the loop numbers or sizes.

If the loop influence is small, then the factor $(Nd)^{1/2}$ should be proportional to ΔH expressed in units of kg/mm^2. Figure 31 is a graph of $(Nd)^{1/2}$ vs. ΔH, and a least squares straight line has the slope 5.2×10^4 dynes/cm. The quantity $6Gb$ in aluminum, by comparison, has an approximate value of 4.3×10^4 dynes/cm. Considering the approximations made in deriving the expressions and the uncertainty of the data the agreement is quite good. Expression (9) is apparently obeyed in this aluminum study as it was in the nickel work.

2. Effects of Neutron Flux

As described in the last chapter, some of the specimen material was irradiated in a different reactor at a temperature and fluence close to

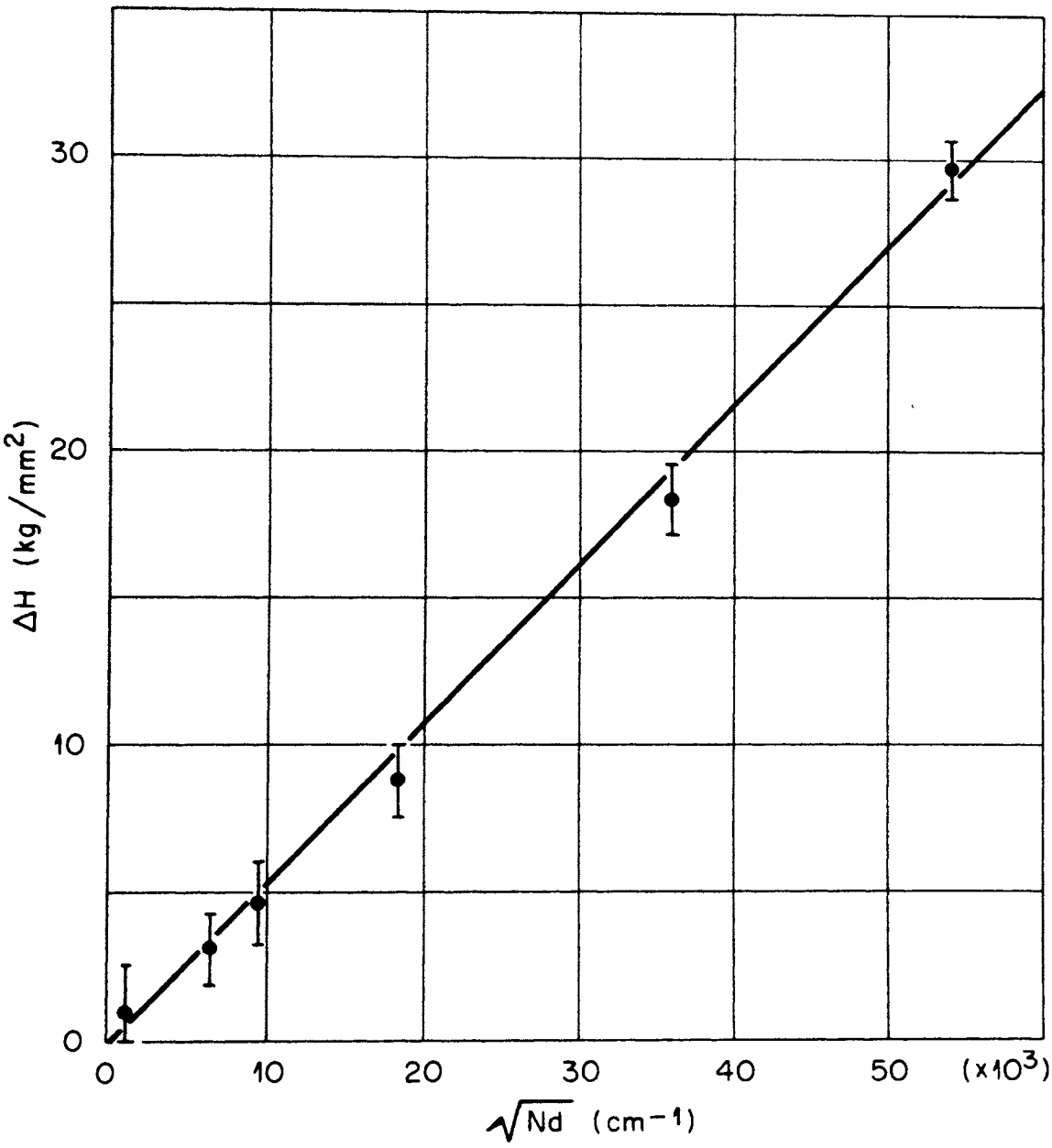

Fig. 31. Hardness increase ΔH versus $(N d)^{\frac{1}{2}}$, with N the void concentration and d the average void diameter.

that of a HFIR-irradiated capsule, but at a factor-of-ten lower neutron flux. The resulting voids were found to be larger (particularly in comparing maximum observed sizes) but only half as numerous, such that the aggregate void volume in each case was about the same. The voids formed in the lower flux irradiation tended more often to be elongated, to have greater length-to-width ratios, and to be less homogeneous in spatial distribution than voids formed during the higher flux irradiation. All of these changes parallel those which result from irradiating at a higher homologous temperature, the extreme case being the huge, nonuniformly distributed, and very elongated "supervoids" reported by Farrell.[64] The common condition which should result from either higher temperature or lower flux irradiation is a lower vacancy supersaturation relative to the thermal equilibrium concentration.

3. Reirradiation and Degassed Aluminum Experiments

The reirradiation experiment involved the annealing out of voids in previously irradiated material and reirradiating it under the same conditions to the same fluence, producing a significant change in the void morphology. Relative to the voids produced by the first irradiation, those generated in the second were smaller but over twice as numerous. It is suggested that the additional void nucleating sites may have been remnants of the voids from the first irradiation.

The earlier voids may have contained some gas. During the anneal these voids would have shrunk until they became submicroscopic gas-stabilized bubbles that could be effective void nuclei. Additional void nuclei would have been generated in the normal fashion during the second irradiation. The same effect could also have been caused by dissolved

gases, or other transmutation-produced impurities (e.g., silicon) from the first irradiation, enhancing nucleation in the reirradiation, but this alternative provides no obvious explanation for the fact that the increase in void concentration was approximately two-fold.

If preexisting void nuclei of some sort were present at the start of the reirradiation, they appear to have grown at nearly the same rate, as indicated by the resulting narrow void size distribution and lack of large voids. The growth of voids from new nuclei would have been similarly restricted as a result of the increased competition for vacancies. The absence of any significant difference in the total void volume resulting from each irradiation confirms that approximately the same number of vacancies was created by displacements in each case, and moreover implies that the residual nuclei from the first irradiation present at the beginning of the second indeed must have been quite small in size. The results of this reirradiation experiment reinforce those models which give irradiation-generated impurities a major role in void nucleation. By the same token, these results are extremely difficult to explain by any void model that relies upon homogeneous nucleation from the vacancy supersaturation.

The negative results from the experiment using degassed material, on the other hand, indicate that the simple presence of gaseous impurities does not necessarily have a profound influence upon void formation. Since the irradiation of as-received material containing up to 20 ppm H and the same lot of material degassed to approximately 2 ppm H yielded identical void numbers as well as sizes, apparently the presence of even relatively large quantities of hydrogen in as-received material has

little influence upon void formation. This fortunately removes the as-received hydrogen content from contention as a major influence upon the results obtained in this work, at least under these irradiation conditions. Such provisos are necessary, for Farrell et al.[66] found a significant increase in void nucleation in 99.9999% aluminum which had only 9 ppm H injected by cyclotron bombardment prior to neutron irradiation at 150°C (a much smaller effect resulted from irradiation at 125°C). The contrasts with the present work were the injection of hydrogen and the higher irradiation temperature; together these may have introduced and agglomerated the hydrogen into a form suitable to alter void nucleation, perhaps tiny bubbles.

4. Void Annealing Studies

Investigations of the annealing behavior of voids in thin foil specimens, using the ultrahigh vacuum electron microscope, resulted in the observation of two effects not previously reported. A great diversity in the annealing behavior of individual voids was always noted. While larger voids and voids located more deeply within the foil generally took relatively long times to anneal out, there were many examples of contrary behavior. Previous in situ annealing studies of voids produced by quenching[105-6] have found relatively uniform void annealing behavior, and postulated vacancy migration from voids to the outer foil surfaces to be the only significant annealing mechanism. However a more recent study in copper[107] did note an appreciable void-to-void variation in the shrinkage rates at constant void radius which could not be explained according to the surface sink mechanism. The variable annealing behavior observed in the current work seems to be best ascribed to

the influence of local sinks or imperfections, such as dislocations, other voids, or possibly small gas bubbles of the type discussed below.

The second phenomenon observed was transient temperature effect displayed by a majority of the voids at the beginning of an anneal, or following a later change in annealing temperature. The effect consisted of a sharp change in the shrinkage rate which decayed within 10 to 20 minutes following the temperature change. To explain such an effect, one must account for a relatively large number of vacancies leaving a void in a short time. Approximately 10^5 vacancies are removed when a 200-Å-diameter void shrinks to 160 Å. Since there were about 10^{14} voids/cm^3 present in the material, a total emission of 10^{18} - 10^{19} vacancies/cm^3 must be accounted for. The explanation must also permit a void to acquire vacancies when the annealing temperature is suddenly lowered. Considering the matrix as the controlling sink cannot account for the magnitude of the transient effect, since the equilibrium concentration of thermal vacancies at 150°C in aluminum is only about $10^{14}/cm^3$ (calculated, taking the vacancy energy of formation in aluminum as 17.3 kcal/mole[108]). Defects such as dislocation loops would serve as effective sinks for vacancies, but would not be expected to release them upon a decrease in annealing temperature.

A physical model that could fulfill these requirements consists of a large number of submicroscopic gas bubbles uniformly distributed in the matrix. With an increase in temperature, the gas pressure in the bubbles would increase and they would grow to a new stabilized size by absorbing vacancies. Rough calculations, using a value for surface tension[107] of 1140 erg/cm^2 and assuming ideal behavior, indicate that when the

temperature is raised from room temperature to 150°C, a 20-Å-diameter bubble could absorb about 100 vacancies in this manner, presumably obtained from voids. Upon a temperature decrease the reverse would occur, releasing vacancies to the voids. A density of 10^{16}-10^{17} such bubbles per cubic centimeter would be required to account for the entire transient effect. Possible evidence[61,109] for this model was offered when bulk specimens of the 8001 aluminum alloy were annealed at 400°C for 1 hour. All the voids were removed, but homogeneously distributed bubbles in concentrations higher than $10^{15}/cm^3$ became visible. Since the solubility of gases decreases rapidly with decreasing temperature, considerably greater numbers of submicroscopic gas bubbles should be present in the as-irradiated material at 150°C. There may be a sufficient number to account for the reversible transient size changes of the voids.

Recalling some of the theoretical considerations of void nucleation, the existence of such a large population of submicroscopic gas bubbles is not inconsistent with the models proposed by Bullough[76] or Bloom.[65,95] In the former work, only voids greater than some critical size were assumed to grow to visible sizes while those smaller had to shrink. But if a void or potential void contained any gas at all, it was stable against total disappearance, and so the establishment of a sizeable population of small void-bubbles would not be surprising. In the void nucleation mechanism suggested by Bloom, helium bubbles may in fact be the principal nuclei for voids. If so, a large number of helium bubble-void nuclei might again coexist along with the visible voids. In either case, the transient temperature effect observed in this void annealing experiment could be a manifestation of the presence of such a bubble population.

B. Evaluation of Proposed Void Nucleation and Growth Models

The results of this study of void formation will now be compared with the available models. The proposed mechanisms for void nucleation will be considered first, followed by those for void growth, and then for overall swelling behavior. Finally a selection will be made of the description most in harmony with these experimental results.

1. Nucleation Models

The principal model employing homogeneous nucleation theory, that of Harkness and Li,[56] assumes that spike cores are the nucleating sites for voids, but beyond this assumption uses the concept of a critical size for nuclei, an activation energy for void formation, and other aspects of classical nucleation theory. This model was discussed in Chapter II; the nucleation rate was found to be proportional to the flux ϕ (Eq. 1), so the void concentration was predicted to increase linearly with fluence: $N \sim \phi t$. A recent modification[110] of the theory now predicts a very early saturation in nucleation resulting from the buildup in the microstructure of vacancy and interstitial sinks (voids and loops) which act to lower the vacancy supersaturation. In this study void nucleation in aluminum was observed to decrease as the irradiation progressed. But in contrast to the revised Harkness model which predicts the void nucleation $\underline{N}$ to be proportional to $(\phi t)^{\underline{a}}$ with $\underline{a}$ decreasing from 1 to 0, we here observe $N \sim (\phi t)^{\underline{a}}$ with $\underline{a}$ decreasing from 2 to ≈ 0. The model cannot explain the much higher observed rate of early nucleation. Such a model also predicts a strictly homogeneous distribution of voids throughout the material and ignores the presence of impurities, including helium. Yet voids generated in many of these irradiations were notably

inhomogeneous in their spatial distributions (e.g., Figs. 4, 5), and apparently quite sensitive to impurities in their nucleation behavior. The results of the reirradiation experiment and perhaps the void annealing experiments cannot be rationalized on the basis of this model. The nucleation part of Claudson's eclectic model[55] is essentially the same as that of Harkness and therefore shares the latter's inability to explain a number of this study's significant results.

The mechanism of void nucleation in overlapping spikes, which was supported by Beeler's damage-simulation computer studies,[70] is a model which should strongly depend upon the flux; the higher the flux, the more likely will be overlaps of the short-lived spikes. Such a model should show the dependence $N \sim (\phi)^x$ where $\underline{x}$ is the number of overlapping spikes required to produce a void nucleus above the critical size. Since a flux dependence was observed in the current study, a value for $\underline{x}$ can be calculated using the following results from the flux effect experiment:

$$\phi_1 t_1 \cong \phi_2 t_2, \qquad \phi_1 \cong 10\phi_2, \qquad N_1 \cong 2N_2$$

Now if $$N \sim \phi^x t = (\phi^{x-1})(\phi t)$$

then $$\frac{(10\phi_2)^{x-1}(\phi_1 t_1)}{\phi_2^{x-1}(\phi_2 t_2)} \cong \frac{N_1}{N_2} = \frac{2N_2}{N_2}$$

$$(x-1)\ln 10 \cong \ln 2$$

$$x \cong 1 + 0.3$$

Thus only about 1.3 or essentially one spike per void (i.e., no overlap) is apparently required to yield the observed flux dependence, and a mechanism of overlapping spikes is not necessary.

However the helium-stabilized (single) spike concept of void nucleation put forth by Shively[73] shows more promise of successfully describing the current results. Here the author postulated that the nucleation rate $\dot{N}$ should depend upon both spikes and helium generation, so that $\dot{N} \sim \phi(\phi t)$ and $N \sim (\phi t)^2$, initially. But the voids were assumed to increasingly act as sinks for the helium, causing the nucleation rate to decline and eventually cease and the exponent in the nucleation expression to diminish from 2 to 0. Essentially this dependence of nucleation upon fluence was actually observed in these studies. Further, the model employs single spikes which were shown above to give rise to a flux dependence similar to that observed. Moreover, it utilizes helium in an important role; thus the observed void heterogeneities and the results of the reirradiation experiment can be rationalized. The main problem with this model is that the existence of a true displacement spike in such a light metal as aluminum has been questioned. According to Nelson[111] displacement spikes in aluminum are thought to be large and diffuse, with relatively little dynamic separation of the interstitials from the vacancies. Recombination would then be more complete and would not leave much of a nucleus to be stabilized by the helium.

The last nucleation model to be considered, that suggested originally by Cawthorne and Fulton[34] and more recently reasserted by Bloom[95] and Stiegler,[96] proposes that tiny gas bubbles may be the nuclei for voids. This model in its present form is qualitative rather than analytic in

its approach, but it is still in good agreement with many of the results of this study. According to this model, the earliest helium bubbles (void nuclei) should form at structural irregularities that absorb a few transmutation-produced helium atoms. The bubbles would be stable and capable of absorbing vacancies as well as gas atoms, especially after they exceeded the critical radius for unrestricted void growth proposed by Bullough.[76] Early voids should therefore be inhomogeneously distributed (as observed). Several voids could perhaps nucleate from one helium-trapping impurity and join to form elongated voids. The apparent void pairs shown in Fig. 5 may have formed in this manner. But early voids should also be seen in association with dislocation lines, a prediction fulfilled in stainless steel[95] but not in these observations of aluminum.

With increasing fluence and resulting increasing helium concentration, bubbles and voids could begin to form away from impurities and a more homogeneous void distribution would develop. At still higher fluences, saturation effects similar to those postulated by Shively (i.e., helium draining into voids from the matrix) would depress further nucleation. The model is in good qualitative agreement with the observed behavior of void nucleation as a function of fluence, although it provides no quantitative predictions. It should readily be able to explain the reirradiation results, and even the observed flux effect may be found consistent with the gas bubble model. Bullough[76] not only obtained a critical size for stable void growth but also demonstrated that this size depended upon the vacancy supersaturation. A lower supersaturation, as in the low-flux irradiation, would raise the critical size with the

result that fewer voids would attain stable growth and these could grow to larger sizes (as observed).

2. Growth Models

There are fewer void growth models to be considered, because many of the authors (Harkness, Shively, Murley,[74] and Gulden and Kaae[77]) have selected the same mechanism, that of growth controlled by the rate of vacancy diffusion through the matrix to the void. The treatment outlined in Chapter II was that of Harkness, but the others have obtained the same result:

$$\frac{dr}{dt} \sim \frac{1}{r}$$

which integrates to: $r \sim t^{1/2}$. This study yielded a much lower value, namely $r \sim t^{1/6}$.

The growth model of Bullough[76] defined the growth-controlling step to be that of the absorption of vacancies onto any part of a void's surface. This mechanism unfortunately has an even higher time dependence: $r \sim t$. The changes in the void size distribution curves with fluence (Fig. 8) also are inconsistent with the Bullough analysis, which would predict the curves to simply translate to the right with increasing fluence, obeying the relation dr/dt = constant.

Claudson[55] obtained the lowest exponent, $r \sim t^{1/3}$, by taking the controlling step to be the absorption of vacancies onto only the tips of voids, but even this mechanism yields a power twice that observed.

The problem with all these growth models, as Claudson et al.[112] have recently pointed out, is that each has concerned itself with the growth of only a single void in an infinite matrix. Proper consideration

of the competition for vacancies among voids, possible void-loop interactions, and the varying vacancy supersaturation with irradiation time should tend to reduce the exponent from the higher values predicted above.

3. Swelling Models

Four of the models propose both nucleation and growth mechanisms and combine them to obtain a prediction of swelling as a function of fluence: $\Delta V/V \sim (\phi t)^b$. The highest value for the exponent, b = 5/2, was obtained by Murley[74] and by the older Harkness model.[56] Claudson's model ranks next, with b = 2. In a new formulation which takes into account the buildup of voids and loops and the manner in which they lower the point defect supersaturations, Harkness[110] obtains a much lower, but still constant, value for the exponent of $b \approx 1$. The model of Shively[73] is the only one which features a variable exponent, reflecting the variable void nucleation already discussed. His value for b ranges from 7/2 (at early stages) down to 3/2 (or even 0 eventually, when even void growth is postulated - without explanation - to cease).

The current study yielded a nonconstant b, varying from 2.4 at low fluences down to 0.75 at 10^{22} neutrons/cm^2, or roughly between 5/2 and 1/2 as obtained in Eq. (7). The agreement is best with Shively's similarly varying model, particularly if his nucleation mechanism is retained but his growth component ($r \sim t^{1/2}$, $v \sim t^{3/2}$) replaced by the present experimentally observed value: $r \sim t^{1/6}$, $v \sim t^{1/2}$. With this modification, the Shively helium-spike model predicts the observed values for the swelling exponent: $1/2 < b < 5/2$.

4. Preferred Models for High Purity Aluminum

In selecting the void nucleation mechanism which best represents this study in high purity aluminum, several can be eliminated but two essentially similar models remain. Both assign a key role to the transmutation-generated helium--stabilizing spikes in the Shively model and forming bubble nuclei in the Bloom proposal. Each predicts a decline in the nucleation rate with increasing fluence and for the same reason--the progressive draining of helium from the matrix into the voids. The Shively model is more quantitative and it provides a more precise explanation for the observed flux effect. But it relies upon displacement spikes which are features of questionable effectiveness in aluminum. The Bloom model, on the other hand, is more clear in characterizing the inhomogeneous void distributions and possible impurity effects frequently noted here. Since it is in no way quantitatively inconsistent with the observations, it is the most satisfactory interpretation of these results.

All of the published growth models for voids seem to be oversimplified and all greatly overestimate the power dependence of time with respect to void radius. A more complex approach taking into account interactions with other defect clusters would probably reduce the power dependence to better agreement with the observed value.

VI. CONCLUSIONS

An investigation was made of void formation in 99.9999% aluminum irradiated at a temperature of 55°C (0.35 T_m), examining the effects of fast neutron fluence, flux, and both preexisting and irradiation-generated impurities. The principal experimental observations were as follows:

1. The presence of a low concentration (about $10^{12}/cm^3$) of irradiation-produced voids averaging 160 Å in diameter was first noted in specimens irradiated to only 1.5×10^{19} neutrons/cm^2 ($E > 0.1$ MeV). This is one of the lowest fluences at which voids have been observed in any material. On the other hand, specimens irradiated to the maximum fluence studied, 1.6×10^{22} neutrons/cm^2 ($E > 0.1$ MeV), contained voids up to 1000 Å in diameter and comprising 7.4% total volume, which is one of the highest swelling values obtained for any material. Thus this study spanned a wide range of void formation, and was the first to investigate fluence dependence.

2. Voids created in low fluence irradiations were frequently seen to be elongated, and some appeared to exhibit transverse constrictions. Such voids may have coalesced from void pairs, two examples of which were observed at the lowest fluence.

3. Voids were distributed nonuniformly after low fluence irradiations, but they appeared to become more homogeneous in distribution as fluence increased. Zones were observed along grain boundaries which were denuded of voids. The zone widths did not vary significantly with fluence.

4. All observed void shapes were consistent with those of octahedra bounded by {111} planes, occasionally having the corners truncated by {100} planes.

5. Void size distributions were determined over the range of fluence studied. A continuous increase in both the maximum and the mean void sizes was observed with increasing fluence. Void growth followed the power law relation of $r \sim t^{1/6}$ with no discernable deviation through 1.6×10^{22} neutrons/cm^2 ($E > 0.1$ MeV).

6. The void concentration grew rapidly at first but eventually approached saturation. If this behavior of nucleation with fluence is expressed as a power law: $N \sim (\phi t)^a$, then the exponent was observed to vary from $a = 2$ at the lowest fluence down to $a = 0.1$ at the highest fluence studied.

7. The total void volume, which reflects both the void sizes and concentrations, also was found to be proportional to the fluence raised to a variable power, whose value decreased from 5/2 to 1/2 over the studied range of fluence. The rate of swelling increase at intermediate swelling values was approximately the same as that previously determined for several alloys of aluminum.

8. Variations of the microhardness with fluence, ascribable to the increasingly numerous voids acting as obstacles to dislocation movement, agreed well with the previously proposed relation: $\Delta H = 6Gb(Nd)^{1/2}$.

9. Irradiation at a flux which was lower by an order of magnitude yielded half as many, but larger, voids compared with irradiation to a like fluence at the normal higher flux. The voids in the specimens irradiated to a lower flux were less homogeneously distributed and

frequently more elongated. Quite similar effects are known, and were found, to result from irradiation at a higher temperature.

10. Irradiation, annealing to remove the damage, and reirradiation resulted in a twofold increase in void concentration compared to the original irradiation alone, but the reirradiation voids were smaller and restricted to a much narrower range of sizes.

11. No difference was evident between voids in material which had been degassed prior to irradiation when compared with as-received material after a like irradiation.

12. Void annealing experiments performed inside an ultrahigh vacuum electron microscope resulted in the observation of two unusual effects: a marked variability in the shrinkage behavior of individual voids, and a transient high rate of shrinkage or growth which was associated with abrupt changes in the annealing temperature.

These observations have led to the following interpretations and conclusions:

1. Voids in neutron-irradiated high purity aluminum appear to initially nucleate at impurities and/or inhomogeneities in the material.

2. Void nucleation in this material is consistent with a previously proposed void model featuring helium-stabilized spikes and also is qualitatively consistent with a model which treats gas bubbles as the void nuclei.

3. Void growth, although showing no saturation tendencies, exhibited a smaller power law dependence than the values predicted by all current models. It is felt that the current void growth models may agree with the experimental evidence when more consideration is given to the complex environment of a population of growing voids.

4. Of the current swelling models, the best explanation for the observed fluence dependence is provided by helium-stabilized spikes, especially if the void growth rate observed here is substituted for that assumed in the model. The salient feature of this model is the dominant though progressively changing role played by the helium gas in void nucleation.

5. Similar effects observed to result from either lower flux or higher temperature irradiations probably both stem from the lowering of the in-pile vacancy supersaturation. It is worth noting that the flux effect seen here was not insignificant, but neither was it as intense an effect as might be expected on the basis of some of the void nucleation models (homogeneous nucleation, for example).

6. The experiments involving reirradiation and void annealing both produced effects most readily explained by postulating the presence of submicroscopic gas bubbles. In the former case, the twofold increase in void concentration was suggested to result from the survival of remnants of the first irradiation voids, quite possibly in the form of submicroscopic gas-stabilized bubbles. These entities could have served as preexisting nuclei at the start of the reirradiation. In the annealing studies, the observed effects may have been caused by a high density of tiny gas bubbles acting as reversible vacancy sinks. Such bubbles have been coarsened to detectable size in previous higher temperature bulk anneals. However, the lack of any observed effect of the as-received hydrogen content upon void morphology cautions that the influence of gaseous impurities upon void formation is as complicated as it is significant.

VII. APPENDICES

Appendix A: Determination of Fast Neutron Flux and Fluence Values

Flux monitor wires, type 302 stainless steel doped with cobalt, were included in one HFIR capsule (DG-E) and in two ORR experiments to experimentally determine the corresponding fast-neutron flux levels. After irradiation the Mn^{54} activity was measured by the Analytical Chemistry Division of ORNL. The reaction Fe^{54} (n,p) Mn^{54} has a threshold at about 4 MeV; its cross-section was taken to be 0.613 barns with an estimated uncertainty of 10-15%.

Measurements by Kam and Swanks[88] of the 4 MeV flux profile down the HFIR centerline were used to transform the experimental flux value of 6.60×10^{13} neutrons/cm^2/sec (E > 4 MeV), obtained by irradiation in hydraulic tube position #7, to a reactor midplane (position #5) value. Then, using a midplane centerline neutron spectrum obtained by T. M. Sims[89] from multi-group diffusion theory calculations, the 4 MeV flux value was converted to yield midplane flux values of 6.46×10^{14} (E > 0.82 MeV) or 11.92×10^{14} (E > 0.1 MeV) neutrons/cm^2/sec.

Either of these flux values was then employed in the determination of the actual fluence received by a HFIR capsule--after giving consideration to several variables. The midplane flux above had to be reduced by a correction factor to yield the flux in the particular capsule's irradiation position. Values for this axial position factor, determined from T. M. Sims' calculated 0.2 MeV flux profile,[89] followed a slightly skewed cosine dependence, falling from a maximum of 1.00 at position #5 to 0.64 and 0.54 at positions #2 and #8 respectively. The time-in-cycle factor, resulting from a systematic change noted by Kam and Swanks[88] in the flux during each HFIR cycle, was much less significant but still

taken into account. This factor only varied from 1.00 for the first half of a cycle down to 0.97 at its end, however. The fluence value for a given capsule was taken to be the product of four quantities: mid-plane flux (either E > 0.82 or 0.1 MeV), axial position factor, time-in-cycle factor, and irradiation duration in seconds. The results were presented in Table VI.

Flux determinations in the ORR were handled in an analogous fashion although without the correction factors; in these cases the flux calculation was only performed for the specific capsule which contained the flux wire.

Appendix B: Establishment of the Void Morphology by Transmission Electron Microscopy and Electron Diffraction Techniques

Shown in Fig. 32 are voids in the reirradiated specimen material, and in Fig. 33 the selected area diffraction (S.A.D.) pattern corresponding to the same region. Indexing the diffraction pattern permits identification of the lattice planes which bound the voids.

By comparing an observed S.A.D. pattern with the collection of indexed patterns given by Hirsch,[113] a tentative identification of the pattern is often made possible. In such fashion the pattern of Fig. 33 was found to closely resemble that resulting from diffraction by {110} planes in an f.c.c. material. In confirmation one can measure the distances, from the center, of several spots and compute the ratios of these distances to one another. It can be readily shown (using trigonometry and Bragg's Law) that:

$$r\,d = L\,\lambda \quad \text{(the "camera constant")}$$

where

- r = distance of spot from center of pattern,
- d = lattice spacing of diffracting planes,
- L = distance from specimen to photographic plate, and
- λ = electron wavelength.

Therefore the radial distances of diffraction spots are related to the lattice spacings of the planes in the specimen that produced them. Since, in cubic crystals,

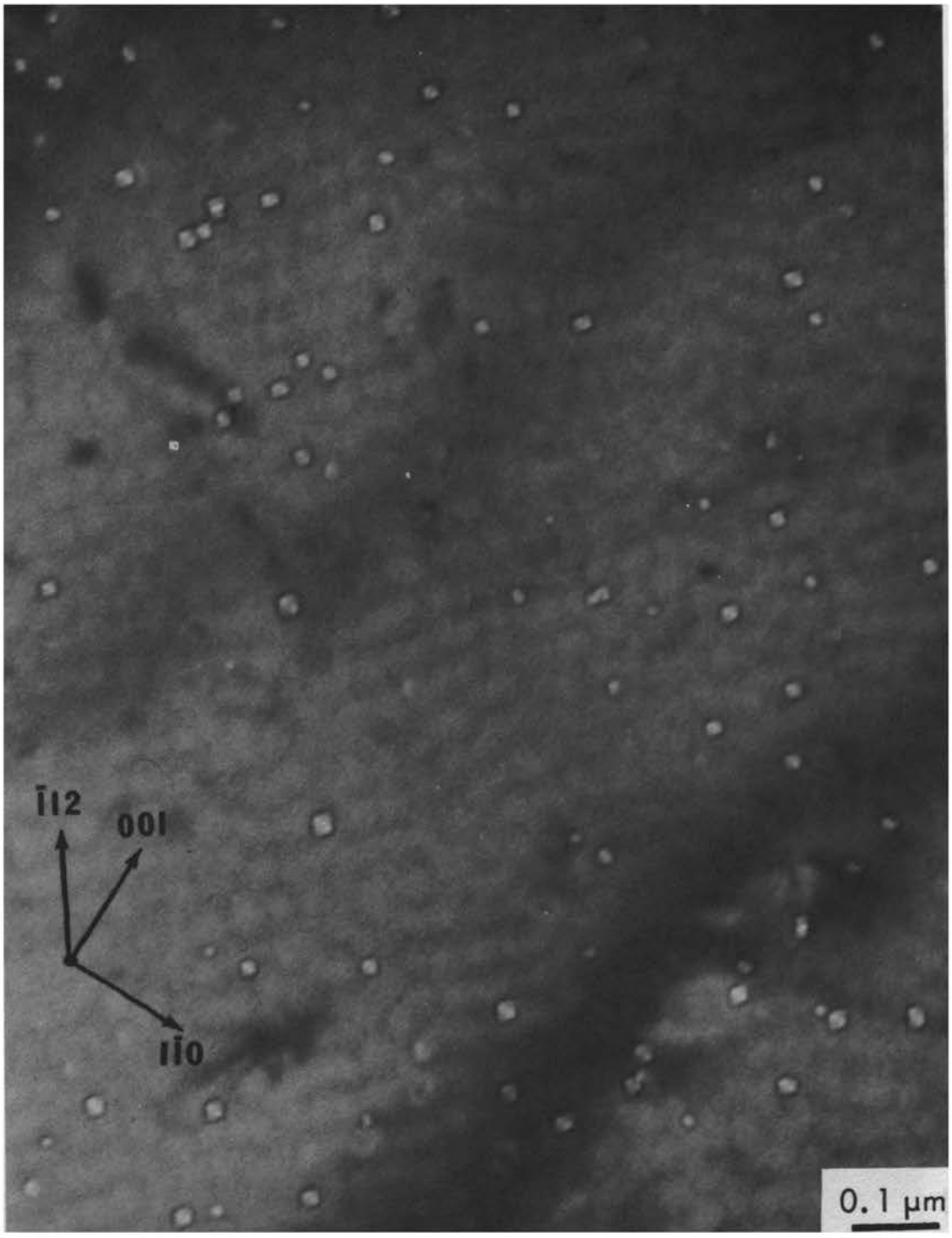

Fig. 32. Octahedral voids in irradiated high purity aluminum.

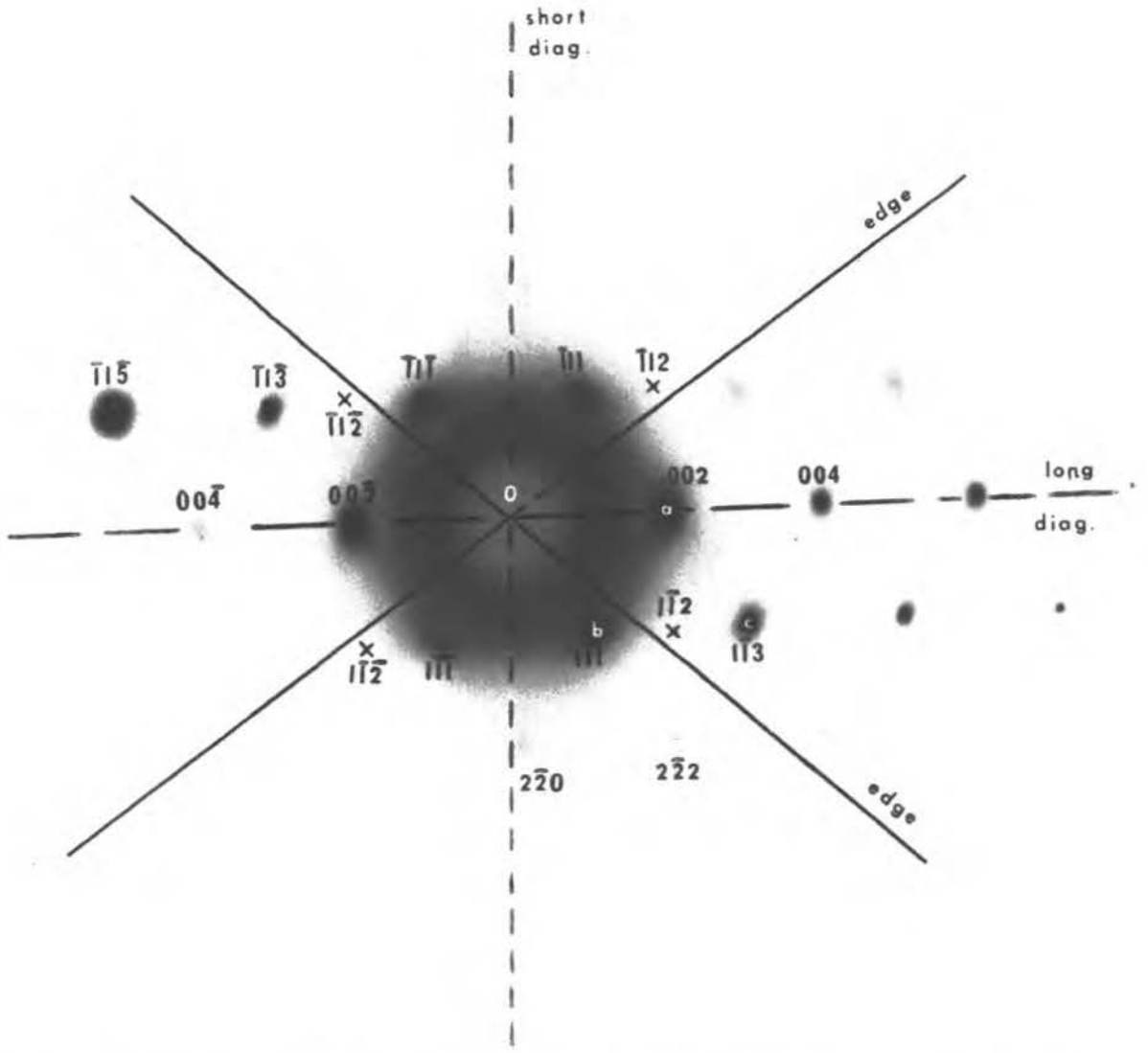

Fig. 33. Indexed selected area diffraction pattern corresponding to the region shown in Fig. 32.

$$d_{hk\ell} = \frac{a_o}{\sqrt{h^2 + k^2 + \ell^2}}$$

where

a_o = lattice parameter of material,

h,k,ℓ = Miller indices of the family of planes,

we can finally obtain a relation:

$$\frac{r_1}{r_2} = \frac{d_2}{d_1} = \frac{\sqrt{h_1^2 + k_1^2 + \ell_1^2}}{\sqrt{h_2^2 + k_2^2 + \ell_2^2}} \qquad (12)$$

with which the tentative indexing of pairs of spots can be verified for consistency with their measured radial positions.

If the (110) indexed pattern in Hirsch is assumed to match this one and the spot marked a in Fig. 33 is selected to be the (002) reflection, then spots b and c correspond to the $(1\bar{1}1)$ and $(1\bar{1}3)$ reflections respectively. The distances oa = 2.05 cm, ob = 1.80 cm, and oc = 3.40 cm were then measured. Forming ratios and using Eq. (12),

$$\frac{ob}{oa} = 0.877 \quad \text{compared with} \quad \frac{\sqrt{1^2 + 1^2 + 1^2}}{\sqrt{0^2 + 0^2 + 2^2}} = \frac{\sqrt{3}}{2} = 0.866$$

and

$$\frac{oc}{oa} = 1.658 \quad \text{compared with} \quad \frac{\sqrt{1^2 + 1^2 + 3^2}}{\sqrt{0^2 + 0^2 + 2^2}} = \frac{\sqrt{11}}{2} = 1.658 \ .$$

The agreement is relatively close, suggesting that the foil was indeed quite near to (110) in orientation.

Examining the voids in Fig. 32 reveals that a majority of them have similar shapes and are in a common orientation. The angles between the vertical in the micrograph and the directions of the edges and body diagonals of these voids were measured. Since S.A.D. patterns on the Hitachi electron microscopes can only be taken at a specific magnification which is much lower than that of Fig. 32, a rotation correction of 51° clockwise was added to each angle measured. Then the traces of the void edges and diagonals were plotted onto Fig. 33. The long and short body diagonals of the voids are seen to lie very close to the [001] and [110] crystallographic directions, respectively. The void edges are aligned along the <112> directions. The {112} planes give no allowed reflections in an f.c.c. lattice--hence they do not appear as diffraction spots and are indicated by crosses on the pattern. If comparison is made with Fig. 6, these directions are seen as precisely those to be expected in octahedral voids bounded by {111} planes and viewed along a [110] direction. Even the fine lighter and darker features visible within most of the voids of Fig. 32 are consistent with this description, the lightest portions appearing where an octahedron would be thickest when viewed as in the figure.

Several similar identifications were carried out with voids from other specimens irradiated to both higher and lower fluences. A number of different foil planes, such as (310) and $(11\bar{4})$, were determined in these trials but the void shapes consistently turned out to be octahedra, as in the present example.

VIII. LIST OF REFERENCES

LIST OF REFERENCES

1. C. Cawthorne and E. J. Fulton, "The Influence of Irradiation Temperature on the Defect Structures in Stainless Steel," p. 446 in The Nature of Small Defect Clusters, Vol. II, Ed. by M. J. Mahin, AERE-R-5269 (1966).

2. J. E. Cunningham, "Severe Radiation Damage to Aluminum Alloys," Oak Ridge National Laboratory report ORNL-TM-2138 (1968).

3. J. L. Brimhall and B. Mastel, J. Nucl. Mat. 33 (1969) 186.

4. J. L. Brimhall and B. Mastel, J. Nucl. Mat. 29 (1969) 123.

5. J. O. Stiegler, K. Farrell, C. K. H. DuBose, and R. T. King, "High Fluence Neutron-Irradiation Damage in Aluminum," p. 215 in Radiation Damage in Reactor Materials, Vol. 2, International Atomic Energy Agency, Vienna (1969).

6. R. E. Smallman and K. H. Westmacott, J. Appl. Phys. 30 (1959) 603.

7. J. Silcox and P. B. Hirsch, Phil. Mag. 4 (1959) 1356.

8. J. Silcox, "Radiation Damage in Face-Centered Cubic Metals," p. 362 in Proceedings of the European Regional Conference on Electron Microscopy 1, Delft (1960).

9. W. R. Thomas and J. L. Whitton, Acta Met. 9 (1961) 1075.

10. R. S. Barnes and D. J. Mazey, Phil. Mag. 5 (1960) 1247.

11. M. Rühle and M. Wilkins, Phil. Mag. 15 (1967) 1075.

12. K. G. McIntyre, Phil. Mag. 15 (1967) 205.

13. J. C. Crump III, Bul. Am. Phys. Soc. 13 (1968) 462.

14. D. I. R. Norris, Phil. Mag. 19 (1969) 527.

15. M. Wilkens, "Studies of Point Defect Clusters by Transmission Electron Microscopy," p. 485 in Vacancies and Interstitials in Metals, A. Seeger, B. Schumacher, and W. Schilling, eds., North-Holland Publ. Co., Amsterdam (1969).

16. G. R. Piercy and J. L. Whitton, J. Instit. Metals 90 (1961-62) 386.

17. T. K. Bierlein and B. Mastel, J. Appl. Phys. 33 (1962) 2873.

18. D. Kuhlmann-Wilsdorf and H. G. F. Wilsdorf, J. Appl. Phys. 31 (1960) 516.

19. R. A. Johnson, Phil. Mag. 16 (1967) 553.

20. J. A. Sigler and D. Kuhlmann-Wilsdorf, Phys. Stat. Sol. 21 (1967) 545.

21. E. Ruedl, P. Delavignette, and S. Amelinckx, J. Nucl. Matls. 6 (1962) 46.

22. M. Kiritani and S. Yoshida, J. Phys. Soc. Japan 18 (1963) 915.

23. M. Kiritani, J. Phys. Soc. Japan 19 (1964) 618.

24. M. Kiritani, Y. Shimomura, and S. Yoshida, J. Phys. Soc. Japan 19 (1964) 1624.

25. M. Kiritani and S. Yoshida, Japan J. Appl. Phys. 4 (1965) 148.

26. Y. Shimomura, J. Phys. Soc. Japan 20 (1965) 965.

27. G. Das and J. Washburn, Phil. Mag. 11 (1965) 955.

28. Y. Shimomura and S. Yoshida, J. Phys. Soc. Japan 22 (1967) 319.

29. L. M. Clarebrough, P. Humble, and M. H. Loretto, Acta Met. 15 (1967) 1007.

30. J. J. Gilman and W. G. Johnston, J. Appl. Phys. 29 (1958) 877.

31. B. V. Budylin and Yu. F. Kozlov, Soviet Physics-Solid State 6 (1964) 1237.

32. C. S. Morgan and D. H. Bowen, Phil. Mag. 16 (1967) 165.

33. D. H. Bowen, "Cavity Formation in Neutron-Irradiated Magnesium Oxide," p. 461 in The Nature of Small Defect Clusters, Vol. II, ed. by M. J. Makin, AERE-R 5269 (1966).

34. C. Cawthorne and E. J. Fulton, Nature 216 (1967) 575.

35. E. E. Bloom, W. R. Martin, J. O. Stiegler, and J. R. Weir, J. Nucl. Matls. 22 (1967) 68.

36. J. J. Holmes, R. E. Robbins, J. L. Brimhall, and B. Mastel, Acta Met. 16 (1968) 955.

37. P. Coulomb, Acta Met. 7 (1959) 556.

38. J. J. Holmes, R. E. Robbins, and J. L. Brimhall, J. Nucl. Matls. 32 (1969) 330.

39. H. R. Brager and R. E. Robbins, Trans. Met. Soc. AIME 242 (1968) 2010.

40. R. E. Robbins, J. Nucl. Matls. 33 (1969) 101.

41. B. Mastel and J. L. Brimhall, J. Nucl. Matls. 28 (1968) 115.

42. H. E. Kissinger, J. Nucl. Matls. 28 (1968) 118.

43. J. J. Holmes, J. Nucl. Matls. 29 (1969) 241.

44. R. T. King and E. L. Long, Jr., J. Metals 20 (1968) 116A.

45. F. W. Wiffen and J. O. Stiegler, J. Metals 20 (1968) 117A.

46. F. W. Wiffen and J. O. Stiegler, Trans. Am. Nucl. Soc. 12 (1969) 119.

47. T. Lauritzen, A. Withop, and U. E. Wolff, Nucl. Eng. and Design 9 (1969) 265.

48. J. O. Stiegler and E. E. Bloom, J. Nucl. Matls. 33 (1969) 173.

49. A. Bourret and D. Dautreppe, Phys. Stat. Sol. 29 (1968) 283.

50. J. L. Straalsund, J. J. Holmes, H. R. Brager, and R. L. Fish, J. Metals 21 (1969) 44A.

51. R. C. Rau, R. L. Ladd, and J. Moteff, J. Nucl. Matls. 33 (1969) 324.

52. R. C. Rau, F. Secco d'Aragona, and R. L. Ladd, Phil. Mag. 21 (1970) 441.

53. J. W. Corbett, "Electron Radiation Damage in Semiconductors and Metals, Parts V and VI," General Electric Research Laboratory Report No. 65-RL-3782(C)M (1965).

54. R. S. Nelson and D. J. Mazey, "Void Formation in Stainless Steel During Charged-Particle Irradiation at Elevated Temperatures," p. 157 in Radiation Damage in Reactor Materials, Vol. 2, International Atomic Energy Agency, Vienna (1969).

55. T. T. Claudson, J. J. Holmes, J. L. Straalsund, and H. R. Brager, "Fast-Reactor Radiation-Induced Changes in Cladding and Structural Materials," p. 165 in Radiation Damage in Reactor Materials, Vol. 2, International Atomic Energy Agency, Vienna (1969).

56. S. D. Harkness and Che-Yu Li, "A Model for Void Formation in Metals Irradiated in a Fast-Neutron Environment," p. 189 in Radiation Damage in Reactor Materials, Vol. 2, International Atomic Energy Agency, Vienna (1969).

57. G. L. Kulcinski, B. Mastel, and J. L. Brimhall, Radiation Effects 2 (1969) 57.

58. J. J. Holmes, Trans. Am. Nucl. Soc. 12 (1969) 117.

59. J. L. Brimhall and B. Mastel, Scripta Met. 4 (1970) 51.

60. E. E. Bloom and J. O. Stiegler, Trans. Am. Nucl. Soc. 12 (1970) 589.

61. R. T. King, E. L. Long, Jr., J. O. Stiegler, and K. Farrell, J. Nucl. Matls. 35 (1970) 231.

62. N. H. Packan and D. N. Braski, J. Nucl. Matls. 34 (1970) 307.

63. K. Farrell and J. T. Houston, J. Nucl. Matls. 35 (1970) 352.

64. K. Farrell and R. T. King, Phys. Stat. Sol. (a) 2 (1970) K5.

65. E. E. Bloom and J. O. Stiegler, "The Effect of Helium on Void Formation in Irradiated Stainless Steel," to be publ. in J. Nucl. Matls.

66. K. Farrell, R. T. King, and A. Wolfenden, "Effect of Preinjected Gases on Irradiation-Produced Voids in Aluminum," paper presented at the Spring Meeting of the Met. Soc., A.I.M.E., Las Vegas, May 1970; abstract publ. in Abstract Bulletin of the Institute of Metals Division, A.I.M.E. 4 (1970) 176.

67. G. L. Kulcinski, H. E. Kissinger, and B. Mastel, "Postirradiation Annealing of Voids in Nickel," paper presented at the Spring Meeting of the Met. Soc., A.I.M.E., Las Vegas, May 1970; abstract publ. in Abstract Bulletin of the Institute of Metals Division, A.I.M.E. 4 (1970) 176.

68. G. L. Kulcinski, B. Mastel, and J. L. Brimhall, Trans. Am. Nucl. Soc. 13 (1970) 162.

69. G. Lück and R. Sizmann, Phys. Stat. Sol. 6 (1964) 263.

70. J. R. Beeler, Jr., "Computer Experiments to Predict Radiation Effects in Reactor Materials," p. 3 in Radiation Damage in Reactor Materials, Vol. 2, International Atomic Energy Agency, Vienna (1969).

71. G. W. Greenwood, A. J. E. Foreman, and D. E. Rimmer, J. Nucl. Matls. 4 (1959) 305.

72. W. A. Johnson and R. F. Mehl, Trans. A.I.M.E. 135 (1939) 416.

73. J. H. Shively, p. 253 in Radiation Damage in Reactor Materials, Vol. 2, International Atomic Energy Agency, Vienna (1969).

74. T. E. Murley, Trans. Am. Nucl. Soc. 12 (1969) 586.

75. R. Bullough, B. L. Eyre, and R. Perrin, Trans. Am. Nucl. Soc. 12 (1969) 523.

76. R. Bullough and R. C. Perrin, "Growth, Stability and Interactions of Voids and Gas Bubbles in Solids," p. 233 in Radiation Damage in Reactor Materials, Vol. 2, International Atomic Energy Agency, Vienna (1969).

77. T. D. Gulden and J. L. Kaae, J. Nucl. Matls. 32 (1969) 168.

78. J. J. Holmes, Trans. Am. Nucl. Soc. 12 (1969) 701.

79. D. L. Kinosz, Alcoa Research Laboratories, personal communication, September 1969.

80. K. Farrell, Oak Ridge National Laboratory, personal communication, January 1969.

81. A. F. Zulliger, Oak Ridge National Laboratory, personal communication, March 1969.

82. B. L. Corbett, Oak Ridge National Laboratory, personal communication, March 1969.

83. C. K. H. DuBose and J. O. Stiegler, "Semiautomatic Preparation of Specimens for Transmission Electron Microscopy," Oak Ridge National Laboratory report ORNL-4066 (1967).

84. J. O. Stiegler, Oak Ridge National Laboratory, personal communication, October 1969.

85. V. Levy, "Examen au Microscope Electronique en Transmission de Bulles de Gaz Rare dans les Metaux: Analyse des Effets de Contraste Observes," Centre Energie Atomique rapport No. 2431 (1964).

86. O. N. Braski, J. R. Gibson, and E. H. Kobisk, Rev. Sci. Instr. 39 (1968) 1806.

87. F. B. K. Kam, Oak Ridge National Laboratory, personal communication, March 1970.

88. F. B. K. Kam and J. H. Swanks, "Measurement of the Neutron Flux Within the HFIR Target Region," paper presented at the Conference on Reactor Operating Experience, San Juan, October 1969; abstract publ. in Trans. Am. Nucl. Soc., Supplement to Vol. 12 (1969) 8.

89. T. M. Sims, Oak Ridge National Laboratory, personal communication, March 1970.

90. O. L. Davies and E. S. Pearson, Suppl. J. Roy. Statistical Soc. 1 (1934) 76.

91. M. Kiritani, Y. Shimomura, and S. Yoshida, J. Phys. Soc. Japan 19 (1964) 1624.

92. J. Weitman and N. Daverhog, in National Bureau of Standards, Washington D.C., Special Publication No. 229 (1968) 125.

93. M. Hansen, Constitution of Binary Alloys, 2nd ed. New York: McGraw-Hill Book Company (1958) 131.

94. W. Eichenaur and A. Pebler, Z. Metallkunde 48 (1957) 373.

95. E. E. Bloom, "An Investigation of Fast Neutron Radiation Damage in an Austenitic Stainless Steel," Oak Ridge National Laboratory report ORNL-4580 (1970).

96. J. O. Stiegler, Oak Ridge National Laboratory, personal communication, June 1970.

97. J. H. Woodhead, Metallography 1 (1968) 35.

98. J. L. Straalsund, Battelle Pacific Northwest Laboratory, personal communication, June 1970.

99. J. L. Brimhall and B. Mastel, "Neutron Irradiated Molybdenum--Relationship of Microstructure to Irradiation Tempeature," submitted to Radiation Effects.

100. E. L. Long, Jr., Oak Ridge National Laboratory, personal communication, December 1968.

101. G. L. Kulcinski, B. Mastel, and H. E. Kissinger, "Characterization and Annealing Behavior of Voids in Neutron-Irradiated Nickel," submitted to Acta Met.

102. D. Tabor. The Hardness of Metals. Oxford: Oxford Press (1951).

103. K. H. Westmacott, Phil. Mag. 11 (1966) 239.

104. T. J. Koppenaal and D. Kuhlmann-Wilsdorf, Appl. Phys. Letters 4 (1964) 59.

105. T. E. Volin and R. W. Balluffi, Phys. Stat. Sol. 25 (1968) 163.

106. K. H. Westmacott, R. E. Smallman, and P. S. Dobson, Metal Sci. J. 2 (1968) 177.

107. H. G. Bowden and R. W. Balluffi, Phil. Mag. 19 (1969) 1001.

108. R. O. Simmons and R. W. Balluffi, Phys. Rev. 117 (1960) 52.

109. K. Farrell, Oak Ridge National Laboratory, personal communication, February 1969.

110. S. D. Harkness, J. A. Tesk, and Che-Yu Li, Nucl. Applics. and Tech. 9, 7 (1970) 24.

111. R. S. Nelson, p. 256 in Radiation Damage in Reactor Materials, Vol. 2, International Atomic Energy Agency, Vienna (1969).

112. T. T. Claudson, R. W. Barker, and R. L. Fish, Nucl. Applics. and Tech. 9, 7 (1970) 10.

113. P. B. Hirsch, A. Howie, R. B. Nicholson, D. W. Pashley, and M. J. Whalen. Electron Microscopy of Thin Crystals. London: Butterworths (1965) 499.

IX. VITA

Nicolas Hayes Packan was born on December 6, 1942, in Akron, Ohio. He received his primary and secondary education in Akron and Canton, Ohio, graduating from Glenwood High School, Canton, Ohio, in June 1960. He received the degree of Bachelor of Science in Physics from Case Institute of Technology, Cleveland, Ohio, in June 1964. He then took a year of graduate study in physics at Northwestern University, Evanston, Illinois.

He enrolled in the Graduate School of the University of Missouri-Rolla in September 1965. From September 1966 to June 1970, he held a National Science Foundation Graduate Traineeship administered through the U.M.R. Department of Metallurgical Engineering. Since September 1968 he has pursued the research for this thesis off-campus, using the facilities of the Metals and Ceramics Division of the Oak Ridge National Laboratory, Oak Ridge, Tennessee